A GAS CALORIMETER FOR HIGH ENERGY EXPERIMENT
AND
STUDY OF HIGH ENERGY CASCADE SHOWER

September 1984

Hitoshi Miyata

Submitted in partial fulfillment of the requirements
for the degree of Doctor of Science
in Doctoral Program in
University of Tsukuba

ABSTRACT

High energy behavior of the electromagnetic cascade shower has been studied. The high energy showers were created by electron and hadron beams with energies between 25 GeV and 150 GeV at Fermi National Accelerator Laboratory. The showers were observed by a shower detector consisting of multi-layer of lead plates and proportional chambers. The experimental results were analyzed with special emphasis on the fluctuation problem of the electromagnetic cascade shower.

A new type of proportional chamber for the shower detector has been developed for the present experiment. Carbon mixed plastic tubes with resistivity of about 3×10^3 Ωcm have been molded with an extrusion method and used for the dc cathode of a multi-wire proportional chamber (MWPC). The signal by gas multiplication was picked up from strip and pad rf cathode set outside the tube. The electromagnetic and the hadronic cascade shower detectors, so called "calorimeters", were constructed with these MWPC's interleaved with lead plates and iron plates, respectively. These calorimeters provide detailed information on the spatial development of the cascade shower. The measurement of particle energy and the identification of electrons and hadrons were done. A detailed study was made on performance of the electromagnetic calorimeter.

By analyzing data obtained with the electromagnetic calorimeter, we have studied high energy electromagnetic cascade shower phenomena up to 100 GeV. The correction function $\rho(s)$ which is to be multiplied to the average transition curve of the electromagnetic cascade shower (shower curve) $\Pi_A(t)$ derived by Rossi under Approximation A to reproduce the observed shower curve was obtained for energies from 25 GeV to 100 GeV, where s is the shower age. We compared our result with that obtained by Muller for energies $\leq$ 15 GeV. The $\rho(s)$ obtained from the present experiment roughly agrees with Muller's one for $s \leq 1$ but disagrees for $s > 1$. Muller used scintillator as the sensor of the cascade shower, while we used the gas proportional chamber for the present experiment. The disagreement seems to be caused by the difference of the sensor of the cascade shower.

One of the central subjects of this thesis is the study of the fluctuation of the electromagnetic cascade shower. For this study, we use pulse height deviation of a chamber (δ_i), which is defined event-by-event as the deviation of pulse height from the average. Then, we calculate for an ensemble of events a matrix called "correlation matrix", which represents the strength of the correlation between pulse height deviations at two depths. The formulation of the pulse height fluctuation is made in terms of the correlation matrix with two assumptions. The formulation leads to following consequences:

1) The distribution function of the pulse height deviation of a

chamber placed at certain depth of the cascade shower is approximately obtained from the correlation matrix C.

2) The orthogonal matrix T which diagonalizes the correlation matrix C transforms correlated pulse height deviation (δ_i) at each plane of proportional chamber to uncorrelated one ($\tilde{\delta}_i$).

3) With the knowledge of C-matrix, the total fluctuation (δ_i) is separated into the fluctuation caused by the stochastic nature of the shower development (δ_i^S) and the fluctuation originated from characteristics of the detector (δ_i^D).

4) The correlation matrix for the shower fluctuation (C^S) is universal in the sense that it includes only shower fluctuation. The C^S obtained from the present experimental result agreed well, after appropriate normalization, with that derived from liquid argon calorimeter by other authors.

5) The correlation matrix for the shower fluctuation (C^S) is generalized to the continuous correlation function $C^S(t,t')$. In the description of longitudinal shower development, the function $C^S(t,t')$ is as fundamental as average shower curve, an analytical expression ($\Pi_A(t)$) of which was obtained by Rossi. The $\Pi_A(t)$ gives the average number of shower electrons at a depth t, while the $C^S(t,t')$ provides the information on the deviation of the number of electrons from the average.

These points were checked by analysis of the present experimental results.

As a result of the study of cascade shower fluctuation, a method of particle identification by the use of segmented calorimetry is proposed. The pion rejection against electron is greatly improved by this method. The goodness of the assumptions made in the formulation is proved later by comparison of our results with those by other authors.

ACKNOWLEDGEMENTS

As with any contemporary high energy physics experiment, success depends upon a great number of people, each giving his or her unique contribution. I would like to acknowledge these efforts and the large debt I owe to the people who performed them.

The author is deeply indebted to his advisor Prof. Kunitaka Kondo, whose guidance, encouragement during their five years of association, have been invaluable and very much appreciated.

The experiment described in this thesis is the product of a collaboration between Profs. K. Kondo, S. Miyashita, Drs. S. Kim, Y. Takaiwa, Messrs. Y. Hayashide, M. Ito, T. Kamon, F. Sato, M. Shibata, M. Shimura, and A. Yamashita of the University of Tsukuba; Profs. S. Mikamo and M. Mishina of National Laboratory for High Energy Physics (KEK); Dr. Y. Muraki of Institute of Cosmic Ray Research of Tokyo University; Prof. A. Murakami of Saga University; Drs. M. Atac, J.E. Freeman, J. Yoh, Messrs. D.R. Hanssen and J.C. Urish of Fermi National Accelerator Laboratory; and the author. Thanks are due to the coworkers for their advices and collaboration in carrying out this experiment.

I wish to express my appreciation to Prof. K. Takikawa, Drs. F. Abe, I. Nakano, and K. Yasuoka for their guidances and advices. I would like to thank members of technical supporting group of Fermilab, Messrs. M. Hrycyk, W. Coleman, J. Layman, and W. Ewer for their skillful works. Without the hard work and dedication of people in the Accelerator Division and Meson Laboratory at Fermilab, the experiment would not have been possible. I wish to thank them for their work. I greatly appreciate Profs. W. Carithers, W. Chinowsky, R. Ely, K. Shinsky, Messrs. M. Gold and P. Rowson of Lawrence Berkeley Laboratory, University of California for making their experimental data obtained with a hadron calorimeter available to us.

The present work was carried out as a program of the Collider Detector Facility at Fermi National Accelerator Laboratory (CDF) under the accord of US-Japan collaboration in high energy physics. I wish to express my special thanks to Prof. R. Schwitters and Dr. A. Tollestrup (CDF leaders), Dr. P. Koehler (Head of Research Division) and Dr. L. Lederman (Director) of Fermilab.

Finally, I would like to thank my wife Noriko for typing this manuscript.

CONTENTS

	page
ABSTRACT	i
ACKNOWLEGEMENTS	v
CONTENTS	vii
I. INTRODUCTION	1
A. Calorimeter	1
B. Electromagnetic Cascade Shower	10
II. CONDUCTIVE PLASTIC TUBE CHAMBER	14
A. Conductive Plastic Tube	14
B. Characteristics of a Proportional Counter made with Conductive Plastic Tube	16
C. Multi-wire Proportional Chamber with Conductive Plastic Cathode	20
III. SHOWER DETECTOR CONFIGURATIONS	22
A. Electromagnetic Calorimeter	22
B. Hadron Calorimeter	24
IV. BEAM TEST	26
A. Beam Line	26
B. Signal Read Out of Calorimeters	27
C. Fast Electronics System	28
D. Data Taking	28
V. SHOWER DETECTOR PERFORMANCE	31
A. General Response	31
B. Linearity and Energy Resolution	32
C. Lateral Shower Profile and Position Resolution	34
D. Uniformity	35
E. π/e Separation	36
VI. HIGH ENERGY ELECTROMAGNETIC CASCADE SHOWER	40
A. Average Shower Curve	40
B. Longitudinal Shower Fluctuation	43
C. Application of Study of Longitudinal Shower Fluctuation to π/e Separation	79
VII. DISCUSSION OF RESULTS	84
A. Calorimeter Performance	84
B. Average Shower Curve	86
C. Longitudinal Shower Fluctuation	87
VIII. CONCLUSIONS	98
A. Detector Performance	98
B. High Energy Cascade Shower	99
APPENDIX A FORMULATION ABOUT THE π/e SEPARATION	102
APPENDIX B ANALYTIC EXPRESSION OF THE AVERAGE TRANSITION CURVE OF ELECTROMAGNETIC CASCADE SHOWER	105
APPENDIX C GAIN CALIBRATION OF CHAMBERS USING GAUSSIAN FIT	107
APPENDIX D CALCULATION OF THE PROBABILITY OF CHARGE EXCHANGE INTERACTION	110
REFERENCES	112
TABLE CAPTIONS	115
FIGURE CAPTIONS	116
TABLES	
FIGURES	

CHAPTER I

INTRODUCTION

This thesis came out from a continuing effort of prototyping the end plug gas calorimeters for the Collider Detector at Fermilab (CDF). There are two motivations for this thesis study. One is to find out the performance of the end plug electromagnetic gas calorimeter, and the other is to investigate the high energy electromagnetic cascade shower phenomena, with an emphasis on fluctuation problem.

A. Calorimeter

Conceptually, a calorimeter is a block of matter, which intercepts the primary particle and is of sufficient thickness to cause it to interact and deposit all its energy inside the detector volume in a subsequent cascade shower of increasingly lower energy particles. Eventually most of the incident energy is dissipated and appears finally in the form of heat. Some fraction of the deposited energy goes into the production of a more practical signal (e.g. scintillation light, Cherenkov light, or ionization charge) which is proportional to the initial energy. In principle, the uncertainty in the energy measurement is governed by statistical fluctuations in the shower development, and the fractional resolution σ_E/E improves with

increasing energy E as $1/\sqrt{E}$.

A-1. Calorimeter Capability

The first large-scale calorimetric detectors were used in cosmic-ray studies [MU 67]. Interest in calorimeters grew in the late 1960's and early 1970's in view of the coming machines (CERN-ISR, Fermi National Accelerator Laboratory, CERN-SPS) with their greatly changed experimental environments, which made, for example, magnetic momentum analysis in large solid-angle experiments increasingly difficult [AT 75].

At the outset it was noted that calorimeters offer many other attractive capabilities, aside from the energy response, all of which have since been exploited in varying degrees:

1) They are sensitive to neutral as well as charged particles.

2) The size of the detector scales logarithmically with particle energy E, whereas for magnetic spectrometers the size scales with p, for a given relative momentum resolution $\Delta p/p$.

3) with segmented detectors, information on the shower development allows precise measurements of position and angle of the incident particle.

4) The differences in response to electrons, muons, and hadrons can be exploited for particle identification.

5) Their fast time-response allows operation at high particle rates, and the patterns of energy deposition can be used for real-time event selection.

We are now entering an era in which high-energy colliding beam machines may reveal a "new" physics of super-massive particles [BA 82] in extremely rare and complex events. The signatures of the new physics include the production of very energetic leptons and the fragmentation of massive quarks. In these experiments the traditional momentum analysis of a few charged particles will be replaced by measurements of momentum and energy flow among multiple jets of particles. Calorimeters are uniquely suited to such tasks.

A-2. Classification of Electromagnetic Calorimeters

For practical electron-photon calorimetry, a detector must efficiently convert photons and efficiently measure the total ionization loss or track length of secondary electrons. One choice is a dense (high-Z) scintillator block like a NaI crystal, measuring the total intensity of scintillation light. A lead-loaded transparent glass, so called lead-glass, measures the weak Cherenkov light, emitted along electron tracks. A more economical alternative is to sample the shower energy in regular steps with sandwich-type detectors (sampling calorimeters). These three detectors differ considerably in performance, cost, and flexibility. The discussion here is mostly on the quality of energy information (the energy resolution).

(1) NaI(Tℓ) Crystal

A NaI crystal has a high scintillation efficiency, 5 times as large as that from a plastic scintillator at the wavelength around 4000 Å, and a short radiation length (r.l.) of 2.6 cm. Since it is a continuously sampling device with low cut-off energy, an excellent energy resolution was achieved:

$$\sigma_E/E = 0.85\{E(\mathrm{GeV})\}^{-1/4} \ \%$$

for a crystal 41 cm in diameter and 61 cm in length (23.6 r.l.) [HU 72]. This resolution corresponds to 1 % FWHM at 10 GeV and about 5 % even at 50 MeV.

(2) Lead-glass

The lead-glass is a transparent glass containing PbO (about 50 % in weight) and thus has a short radiation length (2.5 cm typically). It emits and transmits the Cherenkov light in response to the passage of a fast ($\beta \gtrsim 0.6$) charged particle, so that the light output is proportional to the total track length of shower electrons. Though much worse than NaI due to the much lower light intensity and the higher cut-off energy, its energy resolution is a factor of 2 to 3 better than that obtained by sampling calorimeters. The lead-glass is superior to NaI in flexibility of size, cost, and speed of response. The energy resolution of lead-glass satisfies the following formula:

$$\sigma_E/E = (4 \sim 5)/\sqrt{E(\mathrm{GeV})} \ \%$$

(3) Sampling Calorimeters

The energy deposited in massive absorbers of a sampling calorimeter is not only unmeasurable, but also fluctuate statistically. Thus the energy resolution is limited by the absorber thickness (i.e. the rate of sampling) and it will be poorer than that of non-sampling devices we have discussed. Having many choices in calorimeter construction, the performance differ considerably from detector to detector as listed in Table I-1. The energy resolution is parametrized as

$$\sigma_E/E = K/\sqrt{t(r.l.)/E(GeV)}\ \% \ ,$$

where $K \approx 30$ for gas sampling calorimeter [AT 81a].

A-3. Gas Sampling Calorimeter

Gas ionization sampling calorimeters have become popular in the last few years. MAC detector at SLAC [AN 78], CLEO at Cornell [MU 81], and the neutrino experiment [BO 78] at CERN have built detectors using proportional tubes for sampling energy produced by electromagnetic and hadronic cascades. The usage of proportional counters in calorimetry is an old idea [MU 67]. Proportional chambers or arrays of proportional tubes are sandwiched together generally with lead plates or iron plates to sample a small fraction of the total energy through electromagnetic cascades for electrons, positrons, and photons, and hadronic and electromagnetic cascades for hadrons.

Some of the reasons that make proportional drift tubes or chambers attractive for calorimetry are summarized in the following:

1) They are relatively insensitive to magnetic field as compared to photomultiplier tubes in detecting Cherenkov or scintillation light.

2) There is no Cherenkov light problem as occurs with wave-length shifter bars collecting light from scintillators.

3) It is easier to bring signals out using wires and cables than guiding light by light guides.

4) Projected detector geometry (projecting to target) can be conveniently provided by using cathode pads detecting induced signals. This is like a "tower" structure following the energy flow out of the target.

5) Transverse position of the electromagnetic cascade showers can be determined to a σ_{rms} of about 1 mm at 50 GeV [AT 81b].

6) A natural consequence of using wires, cathode strips, and pads is excellent unambiguous multi-shower resolution [GE 78] of 2-5 cm obtained depending on separation efficiency.

7) Gas ionization sampling calorimeters provide reasonably good energy resolution. Some test results of electromagnetic calorimeters and the references are given in Table I-1. In the table the gas sampling and the plastic scintillator and liquid argon devices are compared. The gas sampling calorimeter has about factor 2 worse energy resolution than plastic scintillator or liquid argon calorimeters. But this difference becomes

unimportant at high energies.

8) Pulse height calibration has been one of the difficulties of scintillation calorimeter. For the gas ionization calorimeters, it was conveniently achieved to 1-2 % by the Fermilab experiment [AT 81b] using the 22 KeV line of a few Cd^{109} sources positioned on certain chambers. Those few wires monitored the gain variations due to changes in atmospheric pressure, environments temperature, and the gas compositions. This worked out very well since these quantities change very slowly in time.

9) Cost of gas sampling calorimeter systems is reasonable since the extruded aluminum or plastic drift-tube detectors are inexpensively constructed, and wires are connected together in depth resulting in a manageable number of readout channels.

A-4. End Plug Electromagnetic Gas Calorimeter for CDF

We have developed conductive plastic tube chamber as a sampling medium of the end plug electromagnetic gas calorimeter for CDF.

In the development of the recent high energy physics, multi-wire proportional chambers which cover a large area of sensitivity are often required. In collider experiment where jets in production processes or showers in calorimeters are most common phenomena, a single event generally contains many particles hitting a chamber. For such an event, one has to make a pattern recognition of the energy deposit over the wide area of

the chamber. The situation has made the cathode readout of the signal more useful and in many cases indispensable.

A scheme [BA 78] in which the high voltage is applied to a resistive cathode and the signal is picked up by a metal cathode outside the resistive cathode has several advantages:

1) Two functions of the cathode, i.e. dc field formation and rf signal pickup, are separated into two physically different parts of the detector. This makes handling of both the high voltage and the signal simpler.

2) By the same reason as 1), the design of complicated patterns for cathode is made easily. For example, segmentation of cathode into cylindrical coordinate bins.

3) In case an anode wire is broken, the wire usually contacts with a resistive wall without causing any trouble to the other tubes or to the high voltage power supply.

4) The tube structure of cathode in multi-wire chambers has advantages in field configuration and mechanical strength over the plane cathode configuration. By extrusion of conductive plastics, the tube structure can be obtained less expensively than by extrusion of metals, e.g. aluminum.

The properties of conductive plastic tube chamber are described in Chapter II.

The Collider Detector at Fermilab (CDF) is now under construction as a detector system with 4π coverage for 2 TeV $\bar{p}p$ colliding beam experiment [DE 81]. According to the coverage of

the polar angle θ, this detector is divided into three parts, the central detector ($10° < \theta < 170°$), the forward detector ($2° < \theta < 10°$) and the backward detector ($170° < \theta < 178°$). The CDF end plug electromagnetic calorimeter is a component of the CDF central detector and covers the polar angular range of $10° < \theta < 36°$ and $144° < \theta < 170°$ as shown in Fig.I-1. As a prototype for the CDF end plug electromagnetic calorimeter, a 30° sector of the cylindrical calorimeter system has been constructed in full size in radius as sketched in Fig.I-2. Each proportional chamber consisted of a conductive plastic tube array sandwiched with copper-clad G-10 panels. The G-10 panels were clad with copper lamination which was etched to form pickup cathode of pad shape or strip shape. Each pad or strip formed a tower projected from the center of the interaction region. Not only the structure of the electromagnetic calorimeter but also that of the hadronic calorimeter which was the prototype for the CDF end plug hadron calorimeter are described in Chapter III.

Test of these calorimeters was made at Fermilab M4 beam line by using electron and hadron beams with energies up to 150 GeV. In Chapter IV, beam test arrangement is described.

One of the purposes of this thesis is to establish that the energy resolution, the position resolution, the response uniformity, and the π/e separation capability of the calorimeter meet the desired characteristics of the CDF end plug electromagnetic calorimeter. The desired values of the energy

resolution, the position resolution, and the π/e separation capability are 29 % $/\sqrt{E(GeV)}$, 3 mm at 40 GeV, and less than 10^{-2}, respectively [DE 81]. The results show that a conductive plastic chamber works for such a large gas sampling calorimeter. The characteristics of the calorimeter at high energy up to 150 GeV were found to be satisfactory. The analysis of calorimeter performance and the results using electron and hadron beams with energy range from 25 GeV to 150 GeV are given in Chapter V.

B. Electromagnetic Cascade Shower

The characteristic features of electromagnetic showers have been investigated with a variety of experimental techniques by using accelerator electron or photon beams at energies up to several ten GeV.

B-1. Average Cascade Shower

The property of average cascade shower was studied with following detectors: ionization chamber [BL 50], cloud chamber [TH 64], bubble chamber [LE 63], spark chamber [SO 73], scintillation counter [MU 72] or probe [CR 67], photographic film [YU 70], and thermoluminescent dosimetry [NE 66]. On the other hand, theoretical works have been extensively carried out by many authors [RO 41], [NI 67] under the proper approximations (e.g. Approximation A, B). In particular, the rapid progress of computer and Monte Carlo techniques has made it possible to

calculate in great detail the cascade shower development in close touch with the real conditions [ME 70], [FO 78], and the results are widely applicable to the design of the calorimeter used in high energy experiments. It is experimentally checked for low energy cascade shower less than about 10 GeV that the shower curve obtained by Rossi under Approximation A is roughly correct if we choose proper cut-off energy. But if we do more detail comparison between Rossi's shower curve (Approximation A) and experimental result, there are considerable discrepancies. These discrepancies can be compensated by multipling the correction factor ρ to the number of shower electrons Π_A of Approximation A. Muller [MU 72] obtained this correction factor $\rho(s)$ as a function of the shower age s for cascade energies equal to or less than 15 GeV. Recently, Mitsui [MI 81] obtained $\rho(s)$ function by compiling various authors' experimental results including his own for about the same energies as those of Muller.

In this thesis, the $\rho(s)$ function was obtained for higher energies up to 100 GeV by using a gas ionization sampling calorimeter.

B-2. Cascade Shower Fluctuation

One of the main subjects in this thesis is study of the electromagnetic shower fluctuation. There has been almost no experimental study made on this subject with enough statistics for energies above 50 GeV. No convincing theory for the shower

fluctuation phenomena has yet been proposed. Actually there were two articles which described about study of shower fluctuation. Bushnin et al. [BU 73] studied about the correlation in the lateral shower fluctuation in lead at the depth of 4 cm for 32 GeV electrons. Cerri et al. [CE 77] obtained the "correlation matrix" of longitudinal shower fluctuation in stainless steel for 25 GeV electrons.

The correlation matrix is derived in this thesis for electromagnetic cascade shower with energies up to 100 GeV by using a gas ionization sampling calorimeter. The formulation of the longitudinal shower fluctuation is made in terms of the correlation matrix. In the formulation, the correlation matrix is separated into two matrices. One is the correlation matrix C^S for shower fluctuation δ_i^S which is caused by the stochastic nature of the shower development and the other is the one C^D for detector fluctuation δ_i^D which is originated from characteristics of the detector. The parametrization of the correlation matrix C^S for shower fluctuation is made by the use of the two dimensional Fourier series fit.

A result of shower fluctuation study was applied to π/e separation. A new method which uses the correlation matrix was developed and used for the π/e separation. This method made remarkable improvement of the π/e separation performance of the calorimeter, which cannot be obtained by the conventional method used in high energy experiment. Recently, Engelmann et al. used

basically the same method as ours for their π/e separation analysis [EN 83]. They developed their method independently of ours.

High energy cascade shower analysis outlined here and its results are described in Chapter VI.

In Chapter VII, we make the discussion of results. Finally, we conclude this paper in Chapter VIII.

CHAPTER II

CONDUCTIVE PLASTIC TUBE CHAMBER

We summarize in this chapter the property of conductive plastic tube chamber. For the details, the reader is referred to References [HA 83a] and [KO 82].

A. Conductive Plastic Tube

A-1. Fabrication of Conductive Plastic Tube

We have developed, in cooperation with industry [CO], a method to extrude a plastic material mixed with carbon grains to tube in order to use it for MWPC's. The substratum plastics we have tried are high-impact polystyrene, ACS (polymer blend of acryl nitril-chlorinated polystyrene-styrene), and ABS. The size of the carbon grains is of the order of 3×10^{-8}m (30 milli-microns) in diameter. The cross section of the extruded tube is shown in Fig.II-1. The size and thickness of the wall were determined by considering several competing factors (e.g. granurality of the detector, dead space fraction, and mechanical strength). The tube size used for the prototype CDF end plug electromagnetic gas calorimeter was 7 mm high, 10 mm wide in the inner dimension, and 0.8 mm thick.

A-2. Resistivity of the Plastics

The resistivity of the plastic wall of the tube was measured on strips cut from the tube (Fig.II-2). The measurement of resistivity was made along the length of the strip. In the measurement, it was difficult to control the contact resistance of the sample with a metal lead wire. To achieve a good contact between them, the best way we have found is to put a conductive paint "GRAPHIT 33" on the surface of the conductive plastic strip and attach there a copper tape connected with the lead wire (Fig.II-3).

The samples of conductive tubes we have produced had a volume resistivity of 20 $\sim$ 5000 Ωcm. The measured samples are strips with a thickness of 0.8 mm, hence, in terms of plane resistivity, the range of resistivity is 200 $\sim$ 50,000 Ω/square.

A-3. Radiation Resistance of the Conductive Plastic

The strength against radiation is an important property for materials to be used in a particle detector. Two kinds of samples of the conductive plastics, a) 6 kΩ/sq with polystyrene and b) 200 Ω/sq with ABS, have been exposed to the dose of 10^8R, 10^7R and 10^6R of Co^{60} γ rays. Converting the exposure dose to the absorbed dose by assuming a conversion coefficient of 0.95 rad/R, the absorbed doses are 9.5×10^7 rad, 9.5×10^6 rad and 9.5×10^5 rad, respectively. For the type a) tube, the decrease

of resistivity to 1.7 KΩ/sq was observed on a sample irradiated with 10^8 R of γ rays. All other samples showed no change in the resistivity.

In comparison, teflon tubes and epoxy glue used to attach the wire holder at the end of the resistive tube were badly damaged by the exposure to 10^8R of the γ radiation.

A-4. Quality Control in the Production Line

The resistivity of the tube depends on the carbon concentration in carbon-plastic mixture, the extrusion speed, and the temperature of the various parts of the oven. Ajusting these conditions, the uniformity of the resistivity along the length of the tube was controlled to the level of ± 10 %. It was observed that the uniformity of the resistivity around the circumference of the tube cross section was rather difficult to control, fluctuating about ± 20 %.

B. Characteristics of a Proportional Counter made with Conductive Plastic Tube

In this section we describe about the proportional mode operation of conductive plastic tube counter [HA 83a]. For the limited streamer mode operation, the reader is referred to Reference [HA 83b].

B-1. Structure of Single Tube Counter

A Single tube proportional counter was made by using an extruded tube as dc cathode and a gold plated tungsten wire of 35 μm or 50 μm in diameter as anode. The structure is shown in Fig.II-4(a). Each end plug made of plastic by an injection mold method has a V-shape hole to set the anode wire in position, a copper tube with 1 mm inner diameter to solder the anode wire and an external lead wire, and another copper tube with 1.5 mm inner diameter for gas tube connection.

An rf cathode to pick up signals was made of aluminized mylar with the mylar surface attached to the tube (Fig.II-4(b)). The aluminum surface has a strip pattern typically with 1 cm width orthogonal to the wire direction to measure the signal distribution along the wire.

B-2. Anode and Cathode Strip Signals

In proportional counters, the ion drift causes current on the anode and the cathode. If the anode or the cathode is grounded through a resistance, the induced current causes the voltage difference across the resistance, which is observed as a signal of the counter.

The conductive plastic cathode has a dual electric characteristic. At low frequency it works as a conductor: it forms the dc field which causes the electron avalanche and

determines the ion drift, collects ions and drains them into the ground. At high frequency, it works as an insulator: it simply transmits electric lines of force or the displacement current originated from the ion charge to the pickup electrode to feed the conduction currents into the pickup cathode. If a pickup cathode with strip electrodes is set orthogonal to the wire, the induced charge distribution parallel to the anode wire can be observed on strips. Fig.II-5 shows typical observed signals on the anode and cathode with a gas of argon-isobutane mixture.

B-3. Induced Signal Spread

For the actual conductive plastic which has a finite conductivity, the ion drift causes the conduction current which flows through the conductive plastic. This causes the broadening of the spatial distribution of the cathode induced signal. If on the other hand, the resistivity is too high, the charge of the collected ions will pile up on the surface of the plastic, and may cause the high-voltage break down.

In order to find out the optimized resistivity, we prepared proportional counters made of cathode tubes with different resistivity. A typical example of the signal destribution on cathode strips for a single event is shown in Fig.II-6. The destribution around the peak can be fitted with a Gaussian function to a good approximation. The width of the distribution depends on the resistivity of the tube wall, and the relation is

shown in Fig.II-7. The figure shows that the resistivity above 30 kΩ/sq gives practically well localized signals.

B-4. The Gain Uniformity along the Tube

The gain uniformity of anode signal along the tube was measured for one meter long conductive plastic tube counter with 50 μm diameter wire. Fig. II-8 shows the peak channel number of pulse height analizer for Fe^{55} 5.9 KeV γ source with respect to the measured position. The gain uniformity σ_G/G obtained for the tube size of 7 mm high and 10 mm wide in the inner dimension was 2.8 %.

B-5. The Gain Stability against Tube Bend

Before making actual chamber with conductive plastic tubes, we have to know the effect of tube bend on the gain of chamber. For this purpose, we have measured the pulse height change of anode signal due to the bend of the tube. The one meter long tube was placed on the flat table and tightly attached to the table on both ends. Small mylar sheets (250 μm thickness) were inserted between the tube and the table at the center of the tube as the spacers to make tube bend.

The total thickness of spacers corresponded to the displacement of the wire (50 μm diameter) from the center of the tube whose size was 7 mm high and 10 mm wide in the inner

dimension. Fig. II-9 shows the pulse height of the anode signal with respect to the displacement of the wire. In this figure, the solid curve was drawn with the next formula which was obtained by the least squares fit.

$$\Delta G/G = 22.4(d/D)^{3.0}$$

where d = Wire displacement

D = Half gap width (3.5 mm)

The 250 μm wire displacement gives us the 1 % gain change.

B-6. The Edge Effect on the Gain

The electric field around the wire at the tube end is relatively weak due to the leak of electric lines of forth to outside of the tube. The gain of gas multiplication drops significantly at the tube end. The property of the gain degradation was measured for the proportional counter made with conductive plastic tube. The Fe^{55} 5.9 KeV γ source and 6 mm thick 1 mm wide Pb slit as the collimator were used for the measurement. The pulse height of anode signal versus the distance from the tube end is shown in Fig.II-10. The gain drop begins at the position 1.5 cm apart from the tube end.

C. Multi-wire Proportional Chamber with Conductive Plastic Cathode

By putting many proportional tubes in parallel on a plane, a multi-wire proportional chamber can be formed. The signals on the chamber can be read out from cathode planes attached to the plane via insulator. The proportional chamber we have developed for the CDF end plug electromagnetic gas calorimeter at Fermilab has this type of structure.

One of the important characteristics of such chambers is the spread of the signal induced on the cathode plane. To study the spread we built a chamber with 15 tubes in parallel. The electrical contact between walls of adjacent tubes was poor, and the contact resistance was much higher than the tube resistance. The same ends of tubes were connected together to the ground. A parallel strips read out cathode which was made of aluminized mylar was set with the strip direction at an angle θ with the anode direction (Fig.II-11(a)). Namely, the signal distribution from wire to wire is measured at $\theta = 90°$, and the distribution along the wire is measured at $\theta = 0°$. The observed spread of the signal is shown in Fig.II-11(b). The difference in the charge spread along the two directions, $\theta = 0°$ and $90°$, is probably due to the charge diffusion going along the tube direction.

CHAPTER III

SHOWER DETECTOR CONFIGULATIONS

In this thesis work, We have used two calorimeters. One was the electromagnetic calorimeter for detection of the elctromagnetic cascade shower, while the other was the hadron calorimeter for detection of the hadronic cascade shower. The configulations of these detectors are as follows.

A. Electromagnetic Calorimeter

The electromagnetic calorimeter consisted of 38 layers of proportional chamber planes interleaved with 3 mm thick calcium-loaded lead plates. The total thickness was 22.5 radiation lengths including the cover plate. Each proportional chamber had a structure of the conductive plastic tube array sandwiched with copper-clad G-10 panels. An array of 54 conductive plastic tubes were glued side by side to cover a 30° sector of a G-10 panel with pickup electrodes printed on the inner surface, and then another similar board was glued on the top as shown in Fig.III-1.

Each tube cell was 7 mm high and 10 mm wide in the inner dimension. The tube wall was 0.8 mm thick, had plane resistivity of about 30 KΩ/sq, made of polystyrene loaded with fine grain

carbon powder [HA 83a,CO]. The structure of a porportional tube was sketched in Fig.III-2. Anode wires were gold-plated tungsten with 50 μm diameter.

The radial dimension and the patterns of the G-10 panels were similar to those of the final module which is used in the CDF experiment. The three kinds of patterns, pads, θ-strips, and φ-strips (see Fig.III-3(a)-(c)) were used. Each pad covered an area of 5° in azimuthal angle (φ), and of 0.1 in pseudo-rapidity (η) for the η range from 1.6 to 2.3, and of 0.05 in η for the η range from 1.15 to 1.6. Each θ-strip covered an area of 0.02 in η and 30° in φ . Each φ-strip covered an area of the η range from 1.15 to 1.60 and of 1° in φ or an area of the η range from 1.60 to 2.30 and of 1° in φ . The pad G-10 panels were placed on one side of every chamber layer. The θ -strip and φ -strip panels were placed on the other side of the sixth through the twenty-fifth chamber layers. They were interleaved with each other. On the other side of the remaining chamber layers were G-10 boards clad with copper lamination which was electrically grounded.

All pads and strips were connected by strip lines to card edge connectors at the outer circumferences of the G-10 panels. The pads in the same tower were connected together directly by flat cables into three longitudinal segments. The first, second, and third segments had thickness of 2.8, 11.3, and 7.3 radiation length, respectively. The θ- and φ-strips were connected

together into two longitudinal segments. The configuration of pickup cathode panels is listed in Table III-1. Every anode wire in the same chamber layer was connected to a bus line through individual 100 Ω resistor, and further connected to a high voltage bus line through 100 KΩ resistor. The same point was branched to a read-out signal cable through a blocking capacitor of 0.01 μF.

B. Hadron Calorimeter

The hadron calorimeter [HAD] had a structure essentially identical to the electromagnetic calorimeter. It consisted of 20 layers of proportional chamber planes interleaved with 5.1 cm thick iron plates, total thickness of which is 5.9 absorption lengths. Each proportional chamber had a structure of a conductive plastic tube array sandwiched between two 30° sector copper-clad G-10 panels. Each tube cell was 9 mm high and 14 mm wide in the inner dimensions. The tube wall was 0.8 mm thick, had a plane resistivity of about 100 KΩ/sq Pad patterns were printed on the inner surface of G-10 panels forming the same projective tower geometry as the electromagnetic calorimeter pad towers. Each pad covered an area of 5° in azimuthal angle (φ), and of 0.1 in pseudo-rapidity (η) for the η range from 1.2 to 2.4. Pad G-10 panels were placed on one side of every chamber layer. On the other side of the chamber layers, there were G-10 boards clad with copper lamination grounded electrically. All

pads in the same tower in the hadron calorimeter were connected in depth. Anode wires were gold-plated tungsten of 50 μm diameter. Every anode wire in the same chamber layer was connected together, and further connected to a high voltage bus line through 100 KΩ resister. A 0.025 μF capacitor was used as a blocking capacitor to read the signal from chamber plane. The hadron calorimeter was placed immediately behind the electromagnetic calorimeter. The pad towers were aligned to those of the electromagnetic calorimeter.

The photograph of this combined set-up is shown in Fig.III-4.

CHAPTER IV

BEAM TEST

A. Beam Line

Tests of calorimeters and study of cascade shower were carried out at the Fermilab M4 beam line (Fig.IV-1). We have used electron and negative charged hadron beams.

A pure electron beam with energy up to 150 GeV was produced by converting photons in a lead plate. Without any further electron selection, the hadron contamination was estimated to be less than 1 %, based on the distribution of the total collected charge for 25, 50, 75, 100, 125 and 150 GeV electrons (Fig.IV-2).

The hadron beam was composed of mostly pions and kaons. About 90 % of pions and less than 10 % of kaons were estimated to exist in the hadron beam [GR 81]. The electron contamination in the hadron beam of energies above 35 GeV was 2∿3 %. For the sake of hadron rejection study, the contamination was reduced further by inserting a 5.1 cm thick lead brick upstream. Since pions are the dominant component of the hadron beam, hereafter we call it as pion beam.

Particle momenta were measured event-by-event with a series of magnets and the multi-wire proportional chamber system with 1 mm wire spacing, located upstream and downstream of the magnets.

The momentum resolution was typically 0.46 % at 150 GeV. The beam size was defined as 3 cm x 3 cm by three trigger counters (S1, S2 and S3) and a large veto counter with a hole at the center (VETO). Flux of the beam defined by these counters was typically about 500 per pulse for electrons with a spill time of 1 sec and a repetition rate of 12 seconds.

B. Signal Read Out of Calorimeters

The calorimeter modules were both mounted on a table, which could be rotated horizontally around a pivot point that simulated the center of the interaction region in the CDF experiment. The electromagnetic calorimeter module could be rotated vertically around the axis that simulated the colliding beam axis. Thus the beam could be injected straight into any selected pad tower reproducing the polar angle for hadron calorimeter and both the polar and the azimuthal angle for electromagnetic calorimeter (see Fig.III-4).

Signals from anode wires, cathode pads and strips of both calorimeters were all fed directly into LeCroy 2285A 15-bit ADC modules through individual 280-nsec long RG58C/U coaxial cables. Since the signals from the pads and strips were positive, they were inverted by small ferrite core transformers.

The calorimeter modules were operated with a gas mixture of argon 49.3 %, ethane 49.3 %, and ethylalcohol 1.4 % at the

atmospheric pressure.

C. Fast Electronics System

Block diagram of the fast electronics is shown in Fig.IV-3. Standard NIM modules were used for the most part of the fast electronics. The electron and hadron beams were defined by the following trigger configuration called A trigger:

$$A = S1 \cdot S2 \cdot S3 \cdot \overline{(V1 + V2)} \cdot \overline{RMV} \ .$$

where $\overline{RMV}$ is called "Before-pile-up" which kills $S1 \cdot S2 \cdot S3 \ \overline{(V1 + V2)}$ trigger for 50 μs after any of S3, V1, or V2 signals arrived to it. In order to measure the pedestal of ADC 2285A during two beam spills, a trigger (B trigger)

$$B = PULSER \cdot BG5$$

was used, where the BG5 is the gate which opens at 5 sec later for 1 sec after the end of the beam spill. Adding these two trigger configurations, the special trigger called A' trigger was set up. The A' trigger was used in order to obtain more accurate pedestal value of ADC by measuring it during a beam spill.

D. Data Taking

One of the most important parts in the high energy experiment is a data acquisition system. A block diagram for the data acquisition system is shown in Fig.IV-4. The experiment was on-line to a PDP11/34 computer of the Digital Equipment Corporation (DEC). On the PDP11/34, we had 128 K words core

memories, a floating point hardware, a TU-10 magnetic tape drive, a Versatec line printer, two Tektronix storage scopes, a 10 M words RL02 floating head disk, an interrupt processing module "Bison Box", and a branch driver interface. We have used a standard CAMAC system in data taking. As an interface between the PDP11/34 and the CAMAC, Jorway 411 branch driver was used. The branch driver interface was a funnel of the data into the computer. Through the branch highway cable, the branch driver drove two A1 type standard crate controllers which control slave modules in each crate. We have used a module called "Bison Box" in data taking. The Bison Box had some important capabilities. One of them was to accept the interrupt signal and demand CPU to handle the interrupt. Another capability was to transmit the trigger-kill-signal to the fast electronics so that no more interrupt was accepted before the data processing was completed. The on-line program was written with data acquisition as its primary task. The computer handled the interrupt and transferred data from the LeCroy 2280 System Processor to data buffers by a direct memory access (DMA) transfer. The 64 data buffers (1 buffer was assigned to 1000 16-bit words) were prepared for the data acquisition. After the data buffers were filled up, the data were backed up into 800 bpi magnetic tape for the off-line analysis. The on-line program also provided analysis capabilities and various monitoring. The program monitored the efficiencies of MWPC's and pedestals of ADC's. The user could interact with the computer to have various services performed.

We could define histograms and display them on storage scopes during data taking. The MT format in data taking is shown in Table IV-1. The data length of the ADC was fixed, but that of MWPC's was variable depending on the hit multiplicity of chambers. The average data length was about 350 words per event for A trigger. On the data taking speed, it took a few msec to obtain data for one event, so that the computer could handle around maximum 150 event triggers per burst.

CHAPTER V

SHOWER DETECTOR PERFORMANCE

The off-line data analysis was performed using CYBER 175 computers of the Control Data Corporation (CDC) at Fermilab. In this Chapter, the performance of the prototype end plug electromagnetic (EM) gas calorimeter is studied. For the π/e separation capability, the information of the prototype end plug hadron gas calorimeter is added in the analysis.

A. General Response

In the early stage of the beam test, the general characteristics of the calorimeter were studied. The signal shapes from pad towers and anode wires were observed across 50 Ω termination. The rise time of the signals was about 60 nsec as shown in Fig.V-1(a),(b). Assuming the drift velocity of 50 mm/μsec with the present cell size, this rise time is consistent with the average transit time of the secondary electrons which are created uniformly in each tube cell by the electromagnetic shower and drift to the anode wire. The fall time of pad signals was typically about 400 nsec. The ADC gate width was set to 4 μsec so that the signal tail is well contained in the gate.

The londitudinal shower profiles for 25, 50, 75, 100 and 150 GeV electrons at $\eta = 1.474$ ($\theta = 25.8°$) are shown in Fig.V-2. These profiles were obtained after adjusting a gain of each chamber in the off-line analysis, assuming that the average longitudinal profile of a fixed energy shower is a smooth function of depth in the unit of radiation length. The gain adjustment for an individual chamber was found to be within $\pm$ 10 %.

In order to determine the optimum high voltage, the charge from anodes, pads, and strips was measured while varying the high voltage from 1.7 kV to 2.1 kV. Logarithmic plots of the total charge against the high voltage for 100 GeV electrons at $\eta = 1.474$ are shown in Fig.V-3. The logarithm of the total charge increase linearly with the high voltage and shows a break at 1.95 kV. The total charge from anode increases with the high voltage by a factor 2.4 per 100 V, and is 4.8 pc/GeV at 1.85 kV.

B. Linearity and Energy Resolution

The plots of the total charge versus electron energy at the high voltages of 1.80, 1.85, 1.90, and 1.95 kV are shown in Fig.V-4(a),(b). We observe the gradual deviation from linear dependence of the total charge beyond a certain value. The total charge where the saturation starts is almost the same at all high voltages. At high voltage of 1.80 kV and 1.85 kV, the total charge increases linearly with the electron energy up to 125 GeV

and shows saturation of 2 % at 150 GeV. Such a saturation was also found to depend upon a depth of the calorimeter. The charge from each layer for 100 GeV electrons at a certain high voltage is plotted against that at another high voltage, together with the layer numbers, in Fig.V-5(a),(b). The charge at 1.85 kV increases linearly with that at 1.75 kV (Fig.V-5(a)). On the other hand, the charge at 2.10 kV does not increase linearly with that at 1.85 kV, but shows a gain saturation (Fig.V-5(b)). The saturation is clearer in the front layers than in the back layers. It is because the lateral shower is narrower and so the charge density is higher in the front layers than in the back layers.

Energy resolution is plotted against the high voltage for 50 GeV and 100 GeV electrons in Fig.V-6. It shows that the resolution is minimum around the high voltage of 1.95 kV which coincides the break point seen in the logarithmic plot of the total charge against the high voltage (Fig.V-3). This is consistent with the idea that at the end of the proportional mode region the Landau tail is suppressed without saturating the main peak of energy loss (ΔE) of shower electrons [AT 83].

Taking the above condition into account, the optimum high voltage was determined to be 1.85 kV where the clear saturation was not seen up to 150 GeV. The energy resolution at 1.85 kV was 24 % / $\sqrt{E(GeV)}$, as shown in Fig.V-7. The energy resolutions were found to be the same for the pad signal and the anode signal.

Since the unit sampling thickness t is 0.627 radiation length at η = 1.474, the energy resolution we obtained is equivalent to 30 % $\sqrt{t(r.l.)/E(GeV)}$.

C. Lateral Shower Profile and Position Resolution

Using the pad and strip signals, the lateral shower profile was observed. Typical shower profiles for 100 GeV electrons and 100 GeV pions are shown in Fig.V-8(a),(b), respectively. The shower centroid $\bar{X}$ was calculated event-by-event as follows:

$$\bar{X} = \sum_i X_i A_i / \sum_i A_i , \qquad (5\text{-}1)$$

where A_i is the charge from a pad or a strip whose center is located at X_i. It was compared with the hit point measured by the beam multi-wire proportional chambers. The r.m.s. deviation (position resolution) thus calculated is plotted against the electron energy in Fig.V-9 for each pad and strip segment. In the figure, the X axis is a horizontal axis which is along the radius at a fixed azimuthal angle. The second pad segment gives the best resolution, 1.5 mm or better for electrons of energy equal to or greater than 50 GeV. This good spatial resolution will be quite useful in rejecting neutral background in the real experimental situation.

The second moment σ_x, which was also calculated event-by-event, is defined as follows:

$$\sigma_X = \{\sum_i (X_i - \bar{X})^2 A_i / \sum_i A_i\}^{1/2} \qquad (5\text{-}2)$$

The dependence of the second moment on the energy of electron is shown in Fig.V-10. This information can be used for π/e discrimination.

D. Uniformity

One of the main objectives of the calorimeter performance study was to confirm uniformness of the pad response independent of the pad size and the inherent capacitance. Fig.V-11 shows the ratio of the total charge from pads to that from anode wires over various positions along the radius at a fixed azimuthal angle as obtained with 50 GeV electron beam. Disregarding the fall off at both ends, the ratio is uniform within a maximum deviation of ± 3 %. The fall off in the large η region arose because signals from pads covering the η range between 2.2 and 2.3 were not read out, while the fall off in the small η region arose because the edge part of the effective region of the anode wire was not covered by the pad. The dependence of the total anode charge on the impact position of the incident particle is also shown in Fig.V-12. It was found to be uniform with the maximum deviation of ± 2 %, desregarding the fall off at both ends where the shower leaked out.

The energy resolution was also uniform over the same range as shown in Fig.V-13. The average value was 24 % / $\sqrt{E(GeV)}$ for both anode and pad for the pseudo-rapidity range of $1.31 < \eta <$

2.12.

E. π/e Separation

One of the important roles of calorimetry is the particle identification. Pion rejection against electron signal was studied using a negatively charged hadron beam (mostly pions) [HA 84]. The algorithm for obtaining the pion rejection factor is to count the fraction of pion events which fall inside the region of electrons in the distributions of the following measured quantities:

1) The total energy deposit in EM calorimeter (E_{EM}).

2) The ratio of the energy deposit in the first pad segment to the total energy deposit in EM calorimeter (R_1).

3) The ratio of the energy deposit in the third pad segment to the total energy deposit in EM calorimeter (R_3).

4) The lateral shower spread at the second pad segment (σ_2), where σ_2 is the standard deviation obtained by the Gaussian fit to lateral distribution of the shower on the pads.

5) The ratio of the total energy deposit in the EM calorimeter to the sum of energy deposit in EM and hadron calorimeters (R_{EM}). R_{EM} was defined by

$$R_{EM} = \frac{C\, E_{EM}}{C\, E_{EM} + E_H}, \qquad (5\text{-}3)$$

where E_H is the total energy deposit in hadron calorimeter and C is a constant.

A cut was applied to accept the particles inside a certain boundary dependent upon electron energy (E_e) in each distribution of above variables. For example, the R_{EM} cut was adjusted to retain 96 % electrons. The formulation about π/e separation is described in Appendix A.

Analysis of π/e separation was made by using various combinations of these five cuts. Figs.V-14(a),(b) show the E_{EM}&R_3 cuts. The ratio of the energy deposit in the third pad segment to total energy deposit in the EM calorimeter (R_3) is plotted against the total energy deposit (E_{EM}) in Figs.V-14(a),(b), for 25, 50, and 100 Gev electrons and 100 GeV pions, respectively. In the figures the boundaries for containing 95 % electrons are shown by broken lines. By this cut, the pion rejection factor is 1 x 10^{-2} or less for any electron energy. Because the exact amount of electron contamination is unknown, we consider the obtained rejection factors as the upper limits of the real pion rejection factors.

In order to study a situation in which momentum measurement in front of the calorimeters is poor, as in the case of the lower angular region of the CDF end plug, we compared the characteristics of electron signals at various energies, with those of the hadrons of the same or higher energies. We obtained the rejection factor of pions with the energy (E_π) equal to or greater than the electron energy (E_e),varying the electron energy. The study was made for electrons with energies (E_e) of

25, 50, 75, 100, 125, and 150 Gev and pions with energies (E_π) of 75, 100, 125, and 150 GeV. We incorporated the observed E_{EM} in the analysis because the probability for pions to deposit a part of their energy into the EM calorimeter with an amount right around the observed value of E_{EM} is fairly small.

Figs.V-15(a)-(c) show typical trends of pion rejection against the electron retention efficiency (electron acceptance). In these figures, the E_{EM} cut has accepted the particles whose E_{EM} were within $\pm 2\sigma_{Ee}$ around E_e except for the case only E_{EM} cut was used. Here σ_{Ee} is the standard deviation of the total energy deposit distribution in the EM calorimeter for electrons with the energy of E_e. The rejection factor obtained here has to be considered as the probability that pions fake electron signals by depositing their energies, in the EM calorimeter, in the particular energy region ($E_e \pm 2\sigma_{Ee}$) which is taken somewhat arbitrarily. When the pion energy (E_π) is equal to the electron energy (E_e), the pion rejection factor does not depend much on the type of the cut and is $1 \sim 2 \times 10^{-3}$ for 150 GeV electrons and pions at the electron retention efficiency of 85 %. For different energy combination of electrons and pions, the pion rejection factor becomes progressively better as we increase the number of cuts as shown in Fig.V-15(c). There is a possibility that the dependence of the pion rejection factor on the energy combination of electrons and pions is due to the electron contamination in the pion beam.

Figs.V-16(a),(b) show the pion rejection vs. the ratio of electron energy to pion energy (E_e/E_π). The cut on E_{EM} was made to accept the particles whose E_{EM} were within $\pm 2.5\ \sigma_{Ee}$ around E_e. As shown in Fig.V-16(a), the pion rejection factor of 5×10^{-3} or better for the electron retention efficiency of 85 % was obtained by the cut $E_{EM}\&R_1\&R_3\&\sigma_2$. This was the best result of the pion rejection with only EM calorimeter information. If, in addition, the hadron calorimeter information (R_{EM}) was used, the pion rejection factor was greatly improved as shown in Fig.V-16(b). It was less than 2×10^{-4} except for the case of $E_e = E_\pi$. We have used about 5×10^3 pion events in this analysis, and not a single event was left after the cut. The pion rejection factor for $E_e = E_\pi$ is better than 2×10^{-3} at the same electron retention efficiency. As mentioned before, the reason for no improvement of pion rejection for the case of $E_e = E_\pi$ might be due to the electron contamination in the pion beam.

CHAPTER VI

HIGH ENERGY ELECTROMAGNETIC CASCADE SHOWER

The average and fluctuation properties of the high energy electromagnetic cascade shower were studied for electron incidence by the use of the prototype end plug EM gas calorimeter. The result of the shower fluctuation study was applied to the π/e separation.

A. Average Shower Curve

We compare the observed average shower curve with the theoretical transition curve which was calculated by Rossi under Approximation A [RO 41]. In this approximation, the number of shower electrons $\Pi_A(E_\circ, E^*, t)$ is obtained for electron incidence as a function of incident energy $E_\circ$, radiator thickness t in radiation length, and the cut-off energy E^* (kinetic energy) as follows:

$$\Pi_A(E_\circ, E^*, t) = \frac{\ddot{n}(s)}{\sqrt{2\pi}\{\lambda_1''(s)t + (1/s^2)\}^{1/2}} \frac{1}{s} \left(\frac{E_\circ}{E^*}\right)^s e^{\lambda_1(s)t}, \tag{6-1}$$

where s is called the "age parameter" and is related to thickness t as

$$t = -\frac{1}{\lambda_1'(s)}\left\{\ell n\frac{E_\circ}{E^*} - \frac{1}{s}\right\}. \tag{6-2}$$

The detailed description about these equations is made in

Appendix B.

The number of shower electrons was measured for electron incidence in the present experiment with proportional chambers in the electromagnetic calorimeter at various depths. The gain of chambers was calibrated by the energy loss of a non-interacting (no hadronic interaction) pion in the calorimeter. Because the total nuclear absorption length of the calorimeter is approximately unity, about 35 % of hadron events has no nuclear interaction in the calorimeter. From the Gaussian fit of the pulse height distribution for these events, we could make gain calibration of each chamber with the accuracy of σ_G/G = 12 % in average. The detailed procedure of the gain calibration is described in Appendix C. The number of electrons of the electromagnetic cascade shower in each chamber was obtained from its pulse height. The pulse height was normalized by the average pulse height of non-interacting pions of 75 GeV.

The observed average shower curve and calculated shower curve under Approximation A with various cut-off energies for incidence of 75 GeV electrons are shown in Figs.VI-1(a)-(c). Since the chambers of plane No. 1, 26, 27, and 29 were not working, we renumbered plane numbers from No. 2 ∿ 38 to No. 1 ∿ 37. The horizontal axes of Figs.VI-1(a)-(c) are drawn with these new plane numbers. The correspondence between the plane number and the depth in radiation length is tabulated in Table VI-1. Following points were taken into account for the evaluation of

radiation length at chamber positions:

1) Vessel wall (1.27 cm thick Fe plate) and holder plate (2.54 cm thick Al plate) of the calorimeter were included in the calculation as front material.

2) Chamber materials between two lead sheets were included.

3) The data of electromagnetic shower were taken with incident angle θ of 73.7° to the calorimeter surface. The thickness of the calorimeter was multiplied by a factor of $1/\sin\theta$ = 1.042.

As shown in Figs.VI-1(a)-(c), discrepancies between the measured shower curve and the calculated one depend on the cut-off energy E^* assumed in the calculation.

As Muller did [MU 72], we define the correction function $\rho(E_\circ, E^*, s)$ for our shower curve obtained by a gas calorimeter as

$$\rho(E_\circ, E^*, s) \equiv \frac{P_m(E_\circ, t)}{\Pi_A(E_\circ, E^*, t)} , \qquad (6\text{-}3)$$

where P_m and Π_A are the measured and calculated shower curves, respectively. The $\rho(E_\circ, E^*, s)$ is a function of the incident energy $E_\circ$, the cut-off energy E^* used in the shower curve calculation under Approximation A, and the age parameter s. Figs.VI-2(a)-(c) show s-dependence of $\rho(E_\circ, E^*, s)$ at a incident energy $E_\circ$ = 75 GeV for cut-off energies E^* = 3, 7.4, and 20 MeV. The result of Muller for 15 GeV incident electrons is also plotted in these figures. As he mentioned in his paper, his result showed no energy dependence of $\rho(E_\circ, E^*, s)$ in the energy region from 2 GeV to 15 GeV. Our result roughly agrees with that

of Muller for $s \lesssim 1$.

The $\rho(E_o, E^*, s)$ function is plotted with respect to s for incident energies from 25 GeV to 100 GeV at a cut-off energy $E^* = 3$ MeV in Fig.VI-3. Muller's result for $E_o = 15$ GeV and the line obtained by the fit of our result are also shown in the figure. Our result was parametrized by the use of least squares fit method as

$$\rho(E_o, E^*, s) = 1.58 - 1.92s + 0.73s^2 . \qquad (6\text{-}4)$$

The reduced X^2 for this fit was 0.7. Since our result as well as Muller's shows no significant energy dependence within the uncertainty of chamber gain, all points were used for the fit.

B. Longitudinal Shower Fluctuation

B-1. General Property of EM Shower Fluctuation Observed by a Gas Calorimeter

The property of the EM shower fluctuation can be observed through following quantities.

(1) Event-by-event Shower Curve

Event-by-event shower curves and the average shower curve are plotted in Figs.VI-4(a)-(d) for electrons of energies from 25 GeV to 100 GeV. From these figures we make following observations:

1) The ratio of the pulse height fluctuation to the average pulse height becomes small as the incident energy of electron increases. This is because the increase of number of shower electrons with incident energy makes statistical fluctuation small. This is the reason why the energy resolution becomes better as the incident energy increases.

2) If a shower develops more (less) rapidly than the average at the early stage, the shower decreases more (less) rapidly than the average at the later stage.

(2) Pulse Height Distribution in Each Chamber

Figs.VI-5(a) to VI-8(f) show pulse height distributions of individual chambers (plane No. 1, 5, 11, 21, 29, and 37) for electrons of energies from 25 GeV to 100 GeV. The distribution is fitted with a (symmetric) Gaussian curve. We observe following points from these figures:

1) Pulse height (PH) distribution at the early part of the shower (plane No. 1) shows asymmetry and has high energy tail.

2) PH distribution near the shower maximum (plane No. 11) is symmetric and can be fitted well with a Gaussian curve.

3) PH distribution at the later part of the shower (plane No. 29, 37) shows asymmetry and has high energy tail.

The symmetry or asymmetry is a combined effect of the shower development itself and the others (e.g. the Landau fluctuation in ionization process in the detector). This will be discussed

again in section B-4.

(3) Standard Deviation of Chamber Pulse Height

The mean pulse height of a chamber ($\langle p_i \rangle$), the standard deviation of the pulse height of a chamber (σ_i), and the ratio of the standard deviation to the mean pulse height ($\sigma_i/\langle p_i \rangle$) are shown for electrons of energies from 25 GeV to 100 GeV in Figs.VI-9 to VI-11. These figures show that $\sigma_i/\langle p_i \rangle$ takes the minimum value not at, but just behind the shower maximum. This phenomenon is somewhat strange. One may expect the minimum at the shower maximum, since the statistical error of number of shower electrons becomes minimum at the shower maximum. There is rather strange behavior of σ_i in its i dependence. The σ_i seems to have two peaks instead of one around the shower maximum at high energies above 100 GeV. We will discuss these properties later.

B-2. Classification of Fluctuations in the EM Gas Calorimeter

Following fluctuations are known for gas calorimeter signal.

(1) Sampling Fluctuation

The cascade shower terminates with finite number of generated electrons. The main reason of the termination is the energy loss of shower electron by ionizing material in

calorimeter. The statistical (fractional) fluctuation in the total number of generated shower electrons can be called as "intrinsic shower fluctuation". When we use sampling calorimeter like our gas calorimeter, we count the number of shower electrons through finite sampling. Since we observe a part of the total number of generated shower electrons, the (fractional) fluctuation in the number of shower electrons observed with a sampling calorimeter is larger than the intrinsic shower fluctuation and is called as "sampling fluctuation". The sampling fluctuation is caused by the stochastic nature of the shower development.

(2) Track Length Fluctuation

The wide spread angles of the secondary electrons correspond to large fluctuations in track length of shower electrons. Fischer [FI 78] obtained by his Monte Carlo calculation the angular distribution of shower electrons as shown in Figs.VI-12(a),(b) for the "standard calorimeter". According to Fischer's definition, the "standard calorimeter" is the detector made of lead-proportional chamber sandwich with 48 samples in a total depth of 16 radiation lengths, i.e. a sampling thickness is 1/3 radiation lengths. Fig.VI-12(a) shows a strong forward peak along the shower axis (angle $\theta = 0°$). However, there is a considerable spread in the angle; and about 12 % of all electrons are back scattered into the sampling gap. For low

energy electrons, E < 3 MeV, the peak at $\theta = 0°$ vanishes and a $\cos^2\theta$ -distribution is approached (Fig.VI-12(b)). This was expected [LE 63] from multiple scattering arguments.

(3) Landau Fluctuation

This is the fluctuation in the ionization energy loss of a charged particle in thin absorber. Landau treated this problem and found the solution called Landau distribution [LA 44].

(4) Noise in Read Out Electronics

The noise in various parts of the read out electronics can affect the calorimeter signal.

The energy resolution of the "standard calorimeter" as a function of the incident energy is shown in Fig.VI-13. The fluctuation due to the noise in read out electronics is neglected in the figure. The figure shows the energy resolution as given by the different effects mentioned above. The lowest curve corresponds to the fluctuation in the number of shower electrons (sampling fluctuation) only. The two curves labeled "Track Length" and "Landau" build up the effective resolution from this optimum. The total resolution follows an approximate $1/\sqrt{E}$ dependence. The predicted resolution for the corresponding liquid argon calorimeter is also indicated. The resolution as a

function of sampling thickness t (always for a constant total depth of 16 radiation lengths) is given in Fig.VI-14 for 1 GeV incident energy.

B-3. Correlation Matrix; Definition and Properties

(1) Definition of Correlation Matrix

We will use the correlation matrix as a tool to investigate the fluctuation of the shower. At first, we define the pulse height deviation δ_{ik} from the mean value of the i-th chamber for the k-th event as follows:

$$\delta_{ik} = p_{ik} - \frac{1}{N}\sum_k p_{ik} = p_{ik} - \langle p_i \rangle , \qquad (6\text{-}5)$$

where

p_{ik} = pulse height of the i-th chamber for the k-th event,

N = total number of events,

$\langle\ \rangle$ means an average over total number of events.

Then, the correlation matrix C is defined as

$$C_{ij} \equiv \frac{1}{N}\sum_k \delta_{ik}\delta_{jk} = \langle \delta_i \delta_j \rangle , \qquad (6\text{-}6)$$

where C_{ij} = the i-th row j-th column element of the correlation matrix.

By definition, the diagonal and off-diagonal elements of correlation matrix are the variance and covariance of the pulse

height fluctuation of chambers, respectively.

(2) Unnormalized Correlation Matrix

Tables.VI-2(a)-(d) show correlation matrix elements for electrons of energies from 25 GeV to 100 GeV. Figs.VI-15(a)-(d) show j-dependence of correlation matrix element C_{ij} for electrons of energies from 25 GeV to 100 GeV. The diagonal elements C_{ii} are shown in Fig.VI-16 for various energies of electrons. Figs.VI-17(a)-(d) show correlation matrix elements as three-dimensional plots. The following properties of the fluctuation or correlation matrix for the gas calorimeter are pointed out by investigation of these figures:

1) A plane has positive correlation to the planes near by and has negative correlation to the planes far off.

2) The number of nodes of the curve C_{ij} vs. j is one or two. If plane number i which is fixed for C_{ij} is around shower maximum, the number of nodes is two. Other cases have only one node.

3) The C_{ii} gives a discontinuous point in the C_{ij} vs. j curve.

4) The sum of C_{ij} over j is nearly equal to zero.

(3) Normalized Correlation Matrix

The normalization of the correlation matrix C is made as follows:

$$(C_N)_{ij} \equiv \frac{C_{ij}}{\sqrt{C_{ii}C_{jj}}} , \qquad (6\text{-}7)$$

where $(C_N)_{ij}$ is the i-th row j-th column element of the normalized correlation matrix.

By definition, the diagonal element of normalized correlation matrix $(C_N)_{ij}$ is unity. As we know from Eqs.(6-5)-(6-7), the normalized correlation matrix element is independent of the uncertainty of the chamber gain. Figs. VI-18(a)-(d) show normalized correlation matrix elements $(C_N)_{ij}$'s with respect to the plane number j for electrons of energies from 25 GeV to 100 GeV.

The discreteness of the diagonal elements in the normalized correlation matrix elements is clear again. Note that there is no strong energy dependence of the normalized correlation matrix.

B-4. Formulation of Fluctuations in the EM Gas Calorimeter

In order to understand the general property of fluctuations including special feature of shower fluctuation in the gas calorimeter, a formulation about fluctuations will be made in this section. The fluctuation for each event is given by a vector $\mathcal{S}$ each component δ_i of which represents the pulse height deviation from the average of the corresponding chamber. Then, we define the distribution function $F(\mathcal{S})$ of the pulse height deviation $\mathcal{S}$ for global fluctuation [Formulation (1)]. In the definition of $F(\mathcal{S})$, we assume a quadratic form on the power of

exponential, using a symmetric matrix A. By diagonalization of matrix A, we obtain a distribution function $\tilde{F}(\tilde{\delta})$ of an independent (uncorrelated) pulse height deviation $\tilde{\delta}$ [Formulation (3)]. The matrix A is related to correlation matrix C as $A = 1/2C^{-1}$ [Formulation (4)]. Therefore, we can obtain matrix A from C. The global fluctuation of pulse height is separated into the fluctuation of cascade shower process and the fluctuation originated from characteristics of the detector [Formulation (6)]. Then, we make two assumptions about the property of these two kinds of fluctuation. Under these assumptions, we define new correlation matrices C^S and C^D corresponding to the shower and detector induced fluctuations, respectively. The special relation between total pulse height variance σ_E^2 and matrices C, C^S, and C^D is found [Formulation (7)]. Finally, we make generalization of correlation matrix C^S to correlation function $C^S(E_\circ, E_d^*, t, t')$, where $E_\circ$, E_d^* are the incident energy of electron and the cut-off energy of detector, respectively; and t, t' are two different depths of absorber [Formulation (8)]. The generalization is important, since the correlation matrix C^S of the shower induced fluctuation is a fundamental quantity of the cascade shower process.

(1) Definition of a Distribution Function $F(\delta)$ of the Global PH Deviation δ

The number of shower electrons is fairly large for high energy cascade shower (typically, $\sim$ 700 electrons at shower maximum for a 100 GeV incident electron). Therefore, the pulse height distribution for a chamber in the gas calorimeter is symmetric for high energy incident electrons, except for those of chambers positioned at very early or late stage of the shower. This is illustrated in Figs.VI-5(a) to VI-8(f). Thus we approximate the pulse height distribution for a chamber with a Gaussian function.

Under this approximation, we can define a distribution function $F(\delta)$ of PH deviation as

$$F(\delta) = K e^{-\delta^T A \delta} , \tag{6-8}$$

where

$$\delta_i = p_i - \langle P_i \rangle , \tag{6-9}$$

$$\delta = \begin{pmatrix} \delta_1 \\ \zeta \\ \delta_n \end{pmatrix} , \tag{6-10}$$

K = a normalization constant ,

A = n x n symmetric matrix ($A_{ij} = A_{ji}$).

The number of chamber planes (n) is 37 for our gas calorimeter. A symmetric matrix A is introduced to take into account the correlation among pulse heights of chambers. If the matrix A is diagonal, the pulse height of each chamber is independent from others, while the non-vanishing non-diagonal elements of A give

the correlation between pulse heights of chambers.

(2) Estimation of (a) Pulse Height(s) of (a) Chamber(s) from Pulse Heights of Other Chambers

As an application of the distribution function $F(\delta)$ defined by Eq.(6-8), we will derive a formula to estimate the pulse height(s) of (an) unmeasured chamber(s) from those of measured chambers. This would be practically useful if it is necessary to estimate the most probable pulse heights of dead chambers.

1) A case in which there is only one chamber whose pulse height needs to be estimated from those of all other chambers.

Assume we know, for a given event, pulse height deviations ($\delta_j = \delta_j^c$) from the mean values for all chambers except for the i-th chamber. The distribution function of the PH deviation $f_i(\delta_i)$ for the i-th chamber is obtained as follows:

$$f_i(\delta_i) \equiv [F(\delta)]_{\substack{\delta_j = \delta_j^c \\ j \neq i}} \tag{6-11}$$

$$= [K e^{-\delta^T A \delta}]_{\substack{\delta_j = \delta_j^c \\ j \neq i}}$$

$$= [K e^{-A_{ii}\delta_i^2 - 2\delta_i \sum_{j\neq i} \delta_j A_{ji} - \sum_{j,k\neq i} A_{jk}\delta_j\delta_k}]_{\substack{\delta_j = \delta_j^c \\ j\neq i}}$$

$$= K e^{-A_{ii}\delta_i^2 - 2\delta_i \sum_{j\neq i} \delta_j^c A_{ji} - \sum_{j,k\neq i} A_{jk}\delta_j^c\delta_k^c}$$

$$= K e^{-a_i\delta_i^2 - b_i\delta_i - c_i}$$

$$= K e^{\frac{b_i^2}{4a_i} - c_i} \times e^{-a_i(\delta_i + \frac{b_i}{2a_i})^2},$$

where

$$a_i \equiv A_{ii},$$

$$b_i \equiv 2 \sum_{j\neq i} \delta_j^c A_{ji},$$

$$c_i \equiv \sum_{j,k\neq i} A_{jk}\delta_j^c\delta_k^c.$$

If we define

$$d_i \equiv K e^{\frac{b_i^2}{4a_i} - c_i},$$

$$\sigma_i^2 \equiv \frac{1}{2a_i},$$

$f_i(\delta_i)$ is finally expressed as

$$f_i(\delta_i) = d_i e^{-\frac{(\delta_i + \frac{b_i}{2a_i})^2}{2\sigma_i^2}} \tag{6-12}$$

Thus the distribution function for the i-th chamber $f_i(\delta_i)$ is

Gaussian. The mean $\langle\delta_i\rangle$ and standard deviation σ_i of the PH deviation δ_i are

$$\langle\delta_i\rangle = -\frac{b_i}{2a_i} = -\frac{\sum_{j\neq i} A_{ij}\delta_j^C}{A_{ii}} , \tag{6-13}$$

$$\sigma_i = \frac{1}{\sqrt{2a_i}} = \frac{1}{\sqrt{2A_{ii}}} . \tag{6-14}$$

The most probable PH deviation of the i-th camber δ_i^{mp} is obtained as a function of PH deviations of other chambers δ_j's ($j\neq i$) as

$$\delta_i^{mp} \equiv \langle\delta_i\rangle = -\frac{\sum_{j\neq i} A_{ij}\delta_j}{A_{ii}} . \tag{6-15}$$

ii) A case in which there are some chambers whose pulse heights need to be estimated from those of all other chambers.

Assume we do not know, for a given event, pulse height deviations δ_{k_i}'s from the mean values of the k_i($i=1\sim m$)-th chambers. The most probable values of pulse height deviations of the k_i-th chambers $\delta_{k_i}^{mp}$'s are calculated by making derivatives of $F(\delta)$ for δ_{k_i}'s as follows:

$$\frac{\partial F(\delta)}{\partial\delta_{k_i}} = -K\, e^{-\delta^T A\delta}\frac{\partial}{\partial\delta_{k_i}}(\delta^T A\delta)$$

$$= -K\, e^{-\delta^T A\delta}\frac{\partial}{\partial\delta_{k_i}}\left[a_{k_ik_i}\delta_{k_i}^2 + 2\delta_{k_i}\sum_{j\neq k_i} a_{k_ij}\delta_j + \sum_{i,j\neq k_i} a_{ij}\delta_i\delta_j\right]$$

$$= -2K\, e^{-\delta^T A\delta}\left(a_{k_ik_i}\delta_{k_i} + \sum_{j\neq k_i} a_{k_ij}\delta_j\right) . \tag{6-16}$$

We require $\frac{\partial F(\delta)}{\partial\delta_{k_i}} = 0$.

Then

$$\delta_{k_i} = \frac{-1}{a_{k_ik_i}}\sum_{j\neq k_i} a_{k_ij}\delta_j$$

$$= \frac{-1}{a_{k_ik_i}}\left[\sum^{u}_{j\neq k_i} a_{k_ij}\delta_j + \sum^{k} a_{k_ij}\delta_j\right] , \tag{6-17}$$

where Σ^u means sum over chambers with unknown pulse heights,

Σ^k means sum over chambers with known pulse heights.

If we define $b_{k_i} \equiv \sum^{k}_{j} a_{k_ij}\delta_j$,

$$a_{k_ik_i}\delta_{k_i} + \sum^{u}_{j\neq k_i} a_{k_ij}\delta_j = -b_{k_i} ,$$

$$\sum^{u}_{j} a_{k_ij}\delta_j = -b_{k_i} . \tag{6-18}$$

In Eq.(6-18), i runs from 1 to m. Then we obtain linear equations of m unknown quantities. The most probable values of the pulse height deviations $\delta_{k_i}^{mp}$'s are thus obtained as the solutions for the linear equations:

$$a_{k_i k_1}\delta^{mp}_{k_1} + a_{k_i k_2}\delta^{mp}_{k_2} + \cdots + a_{k_i k_i}\delta^{mp}_{k_i} + \cdots + a_{k_i k_m}\delta^{mp}_{k_m} = - b_{k_i} ,$$

where $i = 1 \sim m$. (6-19)

If we define matrix A_u and vectors δ^{mp}_u, b_u as

$$A_u \equiv \begin{bmatrix} a_{k_1 k_1} & \cdots & a_{k_1 k_m} \\ \vdots & & \vdots \\ a_{k_m k_1} & \cdots & a_{k_m k_m} \end{bmatrix}, \quad \delta^{mp}_u \equiv \begin{bmatrix} \delta^{mp}_{k_1} \\ \vdots \\ \delta^{mp}_{k_m} \end{bmatrix}, \quad b_u \equiv \begin{bmatrix} b_{k_1} \\ \vdots \\ b_{k_m} \end{bmatrix},$$

the solutions are given by

$$\delta^{mp}_u = - A_u^{-1} b_u . \tag{6-20}$$

(3) Diagonalization of the Matrix A and a Distribution Function $\tilde{F}(\tilde{\delta})$ of an Independent PH Deviation $\tilde{\delta}$

As we saw in section B-3, the pulse height fluctuation of a chamber is correlated to those of the other chambers. From the correlated fluctuations, we can derive uncorrelated independent fluctuations by diagonalizing the symmetric matrix A:

$$\begin{aligned} \delta^T A \delta &= \delta^T T^T (TAT^T) T\delta \\ &= \tilde{\delta}^T D \tilde{\delta} \\ &= \sum_i d_i \tilde{\delta}_i^2 , \end{aligned} \tag{6-21}$$

where T = an orthogonal transformation matrix ,

$$\tilde{\delta} \equiv T\delta , \tag{6-22}$$

$$D \equiv TAT^T = \begin{bmatrix} d_1 & & 0 \\ & \ddots & \\ 0 & & d_n \end{bmatrix} . \tag{6-23}$$

Namely, the independent PH deviation $\tilde{\delta}$ was obtained by the use of the orthogonal matrix T. The deviation $\tilde{\delta}$ is actually derived from our experimental result in section B-5-(1).

The diagonalization of matrix A gives us a distribution function $\tilde{F}(\tilde{\delta})$ of the independent PH deviation $\tilde{\delta}$ from the distribution function $F(\delta)$ as follows:

$$\begin{aligned} F(\delta) &= K e^{-\sum_i d_i \tilde{\delta}_i^2} \\ &= \frac{1}{(2\pi)^{n/2} \prod_{i=1}^{n} \tilde{\sigma}_i} e^{-\sum_i \frac{\tilde{\delta}_i^2}{2\tilde{\sigma}_i^2}} \\ &= \prod_i \left(\frac{1}{\sqrt{2\pi}\tilde{\sigma}_i} e^{-\frac{\tilde{\delta}_i^2}{2\tilde{\sigma}_i^2}} \right) \\ &= \prod_i \tilde{f}_i(\tilde{\delta}_i) \end{aligned} \tag{6-24}$$

$$\equiv \tilde{F}(\tilde{\delta}) \quad , \tag{6-25}$$

where $$K \equiv \frac{1}{(2\pi)^{n/2} \prod_{i=1}^{n} \tilde{\sigma}_i} \quad , \tag{6-26}$$

$$d_i \equiv \frac{1}{2\tilde{\sigma}_i^2} \quad , \tag{6-27}$$

$$\tilde{f}_i(\tilde{\delta}_i) \equiv \frac{1}{\sqrt{2\pi}\tilde{\sigma}_i} e^{-\frac{\tilde{\delta}_i^2}{2\tilde{\sigma}_i^2}} \quad . \tag{6-28}$$

We could rewrite the n-dimensional distribution function $F(\delta)$ of the dependent PH deviation δ as a product of one-dimensional distribution functions $\tilde{f}_i(\tilde{\delta}_i)$'s of the independent PH deviations $\tilde{\delta}_i$'s.

(4) Relation between the Matrix A and Correlation Matrix C

In order to use the distribution functions $F(\delta)$ and $\tilde{F}(\tilde{\delta})$, we need to know the matrix A. The matrix A is used to represent the correlation between pulse height fluctuations of two chambers. Here we introduce the correlation matrix C. The element C_{ij} of the correlation matrix is defined by using $F(\delta)$ as

$$C_{ij} \equiv \int\cdots\int_{-\infty}^{\infty} F(\delta)\delta_i\delta_j d\delta \Big/ \int\cdots\int_{-\infty}^{\infty} F(\delta) d\delta \quad , \tag{6-29}$$

where $d\delta = \prod_{i=1}^{n} d\delta_i$.

The relation between the matrix A and the correlation matrix C is obtained from the formula (6-29). In order to calculate the formula (6-29), we make transformation of cordinate from δ to $\tilde{\delta}$ as follows:

$$d\delta = \left\| \begin{matrix} \frac{\partial \delta_1}{\partial \tilde{\delta}_1} & \cdots & \frac{\partial \delta_1}{\partial \tilde{\delta}_n} \\ \\ \frac{\partial \delta_n}{\partial \tilde{\delta}_1} & \cdots & \frac{\partial \delta_n}{\partial \tilde{\delta}_n} \end{matrix} \right\| d\tilde{\delta}$$

$$= |\det T^T| d\tilde{\delta}$$

$$= |\det T| d\tilde{\delta} \quad , \tag{6-30}$$

where $\delta = T^T\tilde{\delta}$,

$$d\tilde{\delta} = \prod_{i=1}^{n} d\tilde{\delta}_i \quad .$$

Then

$$\int\cdots\int_{-\infty}^{\infty} F(\delta) d\delta = \int\cdots\int_{-\infty}^{\infty} K e^{-\sum_{\ell} d_\ell \tilde{\delta}_\ell^2} |\det T| d\tilde{\delta}$$

$$= \int\cdots\int_{-\infty}^{\infty} K \left(\prod_{\ell=1}^{n} e^{-d_\ell \tilde{\delta}_\ell^2} \right) |\det T| \prod_{i=1}^{n} d\tilde{\delta}_i$$

$$= K\,|\det T| \prod_{\ell=1}^{n} \left[\int_{-\infty}^{\infty} e^{-d_\ell \tilde{\delta}_\ell^2} d\tilde{\delta}_\ell\right]$$

$$= K\,|\det T| \prod_{\ell=1}^{n} \sqrt{\frac{\pi}{d_\ell}} \quad , \tag{6-31}$$

$$\int\cdots\int_{-\infty}^{\infty} F(\delta)\delta_i\delta_j d\delta = \int\cdots\int_{-\infty}^{\infty} K\Big(\prod_{\ell=1}^{n} e^{-d_\ell \tilde{\delta}_\ell^2}\Big)\Big[\sum_{m=1}^{n} t_{mi}\tilde{\delta}_m\Big]\Big[\sum_{k=1}^{n} t_{kj}\tilde{\delta}_k\Big]$$

$$\times\,|\det T| \prod_{\ell=1}^{n} d\tilde{\delta}_\ell$$

$$= K\,|\det T| \sum_{m,k} t_{mi}t_{kj} \prod_{\ell=1}^{n} \left[\int_{-\infty}^{\infty} e^{-d_\ell \tilde{\delta}_\ell^2} \tilde{\delta}_m\tilde{\delta}_k d\tilde{\delta}_\ell\right]$$

$$= K\,|\det T| \sum_{m} t_{mi}t_{mj} \Big[\prod_{\ell\neq m} \int_{-\infty}^{\infty} e^{-d_\ell \tilde{\delta}_\ell^2} d\tilde{\delta}_\ell\Big]$$

$$\times \int_{-\infty}^{\infty} e^{-d_m \tilde{\delta}_m^2} \tilde{\delta}_m^2 d\tilde{\delta}_m$$

$$= K\,|\det T| \sum_{m} t_{mi}t_{mj} \Big(\prod_{\ell\neq m} \sqrt{\frac{\pi}{d_\ell}}\Big)\frac{1}{2}\sqrt{\frac{\pi}{d_m^3}}$$

$$= K\,|\det T| \Big(\prod_{\ell=1}^{n} \sqrt{\frac{\pi}{d_\ell}}\Big) \sum_{m=1}^{n} \frac{t_{mi}t_{mj}}{2d_m} \quad . \tag{6-32}$$

Therefore ,

$$C_{ij} = \sum_{m=1}^{n} \frac{t_{mi}t_{mi}}{2d_m}$$

$$= \frac{1}{2} \sum_{m} t_{im}^{T} \left(\frac{1}{d_m}\right) t_{mj}$$

$$= -\frac{1}{2} \left(T^T D^{-1} T\right)_{ij} \quad .$$

From Eq.(6-23),

$$C = \frac{1}{2} T^T D^{-1} T$$

$$= \frac{1}{2} T^T (TAT^T)^{-1} T$$

$$= \frac{1}{2} A^{-1} \quad . \tag{6-33}$$

The matrix A is written by the correlation matrix C as

$$A = \frac{1}{2} C^{-1} \quad . \tag{6-34}$$

(5) Diagonalization of Correlation Matrix C

From the relation between the matrix A and the correlation matrix C, we can derive relations between the eigenvalues and eigenvectors of the matrix A and those of the correlation matrix C as follows:

From formulae (6-23) and (6-34),

$$D = \frac{1}{2} TC^{-1}T^T$$

$$= \frac{1}{2} (TCT^T)^{-1} \quad , \tag{6-35}$$

where T is the orthogonal matrix which makes A diagonal.

Then

$$TCT^T = \frac{1}{2} D^{-1} = \begin{bmatrix} \frac{1}{2d_1} & & 0 \\ & \ddots & \\ 0 & & \frac{1}{2d_n} \end{bmatrix} \quad . \tag{6-36}$$

We define a diagonal matrix Λ as

$$\Lambda = \begin{bmatrix} \lambda_1 & & 0 \\ & \ddots & \\ 0 & & \lambda_n \end{bmatrix} \equiv \frac{1}{2} D^{-1} \qquad (6\text{-}37)$$

Therefore,

$$TCT^T = \Lambda . \qquad (6\text{-}38)$$

This means the orthogonal matrix T which makes the matrix A diagonal also makes the correlation matrix C diagonal. The correlation matrix C has the same eigenvectors as those of the matrix A. The eigenvalues of the matrix C are related to those of the matrix A as

$$\lambda_i = \frac{1}{2d_i} , \qquad (6\text{-}39)$$

where λ_i's and d_i's are eigenvalues of the matrix C and A, respectively.

Properties of eigenvalues and eigenvectors of correlation matrix and independent fluctuations are shown in section B-5-(1).

(6) Separation of Global Fluctuation into Shower Fluctuation and Detector Fluctuation

As we discussed in section B-2, the pulse height fluctuation of a chamber in the EM gas calorimeter is mainly composed of sampling fluctuation, track length fluctuation, Landau fluctuation and the fluctuation caused by the noise of read out electronics. Since the sampling fluctuation is caused by the stochastic nature of cascade shower development, hereafter we

call this fluctuation as the "shower fluctuation". Other three kinds of fluctuation are all caused by the characteristics of the detector. If we use plastic scintillator or liquid argon instead of gas for the detection of cascade shower electrons, the track length fluctuation and the Landau fluctuation are substantially reduced [FI 78]. We will define the "detector fluctuation" as the sum of the track length fluctuation, the Landau fluctuation, and the fluctuation caused by the electronic noise. Hence, the global fluctuation of the pulse height of a chamber in the EM gas calorimeter is composed of the shower fluctuation and the detector fluctuation.

The global PH deviation δ_i of the i-th chamber is written as

$$\delta_i = \delta_i^S + \delta_i^D , \qquad (6\text{-}40)$$

where δ_i^S and δ_i^D stand for the shower and the detector fluctuations, respectively.

The i,j-th element of correlation matrix C which is defined for the global fluctuation is now expressed as

$$\begin{aligned} C_{ij} &= \langle (\delta_i^S + \delta_i^D)(\delta_j^S + \delta_j^D) \rangle \\ &= \langle \delta_i^S \delta_j^S \rangle + \langle \delta_i^D \delta_j^S \rangle + \langle \delta_i^S \delta_j^D \rangle + \langle \delta_i^D \delta_j^D \rangle . \end{aligned} \qquad (6\text{-}41)$$

Here we make two assumptions:

Assumption 1. The detector fluctuation is independent of the shower fluctuation.

Assumption 2. The detector fluctuation of each chamber is

independent of those of other chambers.

From the Assumption 1, the cross terms between the detector fluctuation and the shower fluctuation are zeros:

$$\langle \delta_i^D \delta_j^S \rangle = 0 \quad , \quad \langle \delta_i^S \delta_j^D \rangle = 0 \quad . \tag{6-42}$$

From the Assumption 2, the fourth term of Eq.(6-41) becomes

$$\langle \delta_i^D \delta_j^D \rangle \rightarrow \langle \delta_i^D \delta_j^D \rangle \hat{\delta}_{ij} \, , \tag{6-43}$$

where $\hat{\delta}_{ij}$ is the Kronecker δ.

Then

$$C_{ij} = \langle \delta_i^S \delta_j^S \rangle + \langle \delta_i^D \delta_j^D \rangle \hat{\delta}_{ij} \, . \tag{6-44}$$

We introduce two new correlation matrices here. One is the correlation matrix of shower fluctuation C^S and the other is the correlation matrix of detector fluctuation C^D. They are defined as follows:

$$C_{ij}^S \equiv \langle \delta_i^S \delta_j^S \rangle \, , \tag{6-45}$$

$$C_{ij}^D \equiv \langle \delta_i^D \delta_j^D \rangle \hat{\delta}_{ij} \, . \tag{6-46}$$

The correlation matrix of global fluctuation C is written as the sum of the correlation matrix of shower fluctuation C^S and the correlation matrix of detector fluctuation C^D.

$$C_{ij} = C_{ij}^S + C_{ij}^D \, . \tag{6-47}$$

It is to be noted that the correlation matrix C^D is a diagonal matrix, while the matrix C^S is not diagonal. The above formulation is visualized in Fig.VI-19. The figure shows a diagonal element C_{ii} is discrete from off-diagonal elements, reflecting the vanishing off-diagonal elements of C^D. As

mentioned in section B-3 in this Chapter, the discreteness of a diagonal element was actually observed for our correlation matrices C (see Fig.VI-15(a)-(d)). Thus the above formulation is consistent with our experimental result. Properties of C^S and C^D are studied in section B-5-(2) in this Chapter.

The normalization of the correlation matrix C^S is made as follows:

$$(C_N^S)_{ij} \equiv \frac{C_{ij}^S}{\sqrt{C_{ii}^S \, C_{jj}^S}} \, , \tag{6-48}$$

where $(C_N^S)_{ij}$ is the i-th row j-th column element of the normalized correlation matrix of shower fluctuation.

Since C^S as well as C is a symmetric matrix, it is diagonalized by an orthogonal matrix T^S which is different from T.

$$T^S C^S (T^S)^T = \Lambda^S = \begin{bmatrix} \lambda_1^S & & 0 \\ & \ddots & \\ 0 & & \lambda_n^S \end{bmatrix} \, , \tag{6-49}$$

where λ_i^S's are eigenvalues of the matrix C^S.

The orthogonal matrix T^S transforms a dependent PH deviation δ^S caused by the shower fluctuation to an independent PH deviation $\tilde{\delta}^S$:

$$\tilde{\delta}^S = T^S \delta^S \, . \tag{6-50}$$

The eigenvalues and eigenvectors of C^S are obtained in section

B-5-(3) in this Chapter.

(7) Relation between the Total PH Fluctuation and Shower and Detector Fluctuations

In qualifying the calorimeter performance, one of the most important quantities is the energy resolution $\sigma_E/\langle E\rangle$, where $\langle E\rangle$ and σ_E are the mean and the standard deviation of the total pulse height E of the calorimeter, respectively. We now discuss the relation between the total PH fluctuation and shower and detector fluctuations. First, we obtain the relation between σ_E and correlation matrix of global fluctuation C as follows:

$$\sigma_E^2 \equiv \int\cdots\int_{-\infty}^{\infty} F(\delta)\ (E - \langle E\rangle)^2 d\delta \Big/ \int\cdots\int_{-\infty}^{\infty} F(\delta) d\delta \qquad (6\text{-}51)$$

$$= \int\cdots\int_{-\infty}^{\infty} F(\delta) \Big(\sum_i \delta_i\Big)^2 d\delta \Big/ \int\cdots\int_{-\infty}^{\infty} F(\delta) d\delta$$

$$= \int\cdots\int_{-\infty}^{\infty} F(\delta) \sum_{ij} \delta_i \delta_j d\delta \Big/ \int\cdots\int_{-\infty}^{\infty} F(\delta) d\delta$$

$$= \sum_{ij} \int\cdots\int_{-\infty}^{\infty} F(\delta)\, \delta_i \delta_j d\delta \Big/ \int\cdots\int_{-\infty}^{\infty} F(\delta) d\delta$$

$$= \sum_{ij} C_{ij} \ . \qquad (6\text{-}52)$$

Thus the total PH variance σ_E^2 is written as the sum of elements of the correlation matrix C. It is also described with quantities of the shower and detector fluctuations:

From Eqs.(6-46) and (6-47),

$$\sigma_E^2 = \sum_{ij} C_{ij}^S + \sum_i C_{ii}^D \qquad (6\text{-}53)$$

$$= \sum_{ij} \int\cdots\int_{-\infty}^{\infty} F^S(\delta^S)\, \delta_i^S \delta_j^S d\delta^S \Big/ \int\cdots\int_{-\infty}^{\infty} F^S(\delta^S) d\delta^S$$

$$+ \sum_i \int\cdots\int_{-\infty}^{\infty} F^D(\delta^D)\, \delta_i^{D2} d\delta^D \Big/ \int\cdots\int_{-\infty}^{\infty} F^D(\delta^D) d\delta^D$$

$$= \int\cdots\int_{-\infty}^{\infty} F^S(\delta^S)\, (\delta_E^S)^2 d\delta^S \Big/ \int\cdots\int_{-\infty}^{\infty} F^S(\delta^S) d\delta^S$$

$$+ \sum_i (\sigma_i^D)^2$$

$$= (\sigma_E^S)^2 + (\sigma_E^D)^2 \ , \qquad (6\text{-}54)$$

where $F^S(\delta^S)$ and $F^D(\delta^D)$ are the distribution functions of PH deviations caused by the shower (δ^S) and detector (δ^D) fluctuations, respectively; σ_E^S and σ_E^D are standard deviations of the total PH fluctuations caused by the shower and detector fluctuations, respectively; the fluctuations are represented by vectors

$$\delta^S = \begin{bmatrix} \delta_1^S \\ \vdots \\ \delta_n^S \end{bmatrix} , \qquad \delta^D = \begin{bmatrix} \delta_1^D \\ \vdots \\ \delta_n^D \end{bmatrix} ;$$

and other variables are as

$$d\delta^S = \prod_{i=1}^{n} d\delta_i^S \ , \qquad d\delta^D = \prod_{i=1}^{n} d\delta_i^D \ ,$$

$$\delta_E^S \equiv \sum_i \delta_i^S \ ,$$

$$(\sigma_E^S)^2 = \sum_{ij} C_{ij}^S \ , \tag{6-55}$$

$$(\sigma_E^D)^2 = \sum_i (\sigma_i^D)^2 = \sum_i C_{ii}^D \ . \tag{6-56}$$

Eq.(6-54) means that the total PH variance σ_E^2 of global fluctuation is written as the sum of the total PH variances, $(\sigma_E^S)^2$ and $(\sigma_E^D)^2$, of the shower and detector fluctuations, respectively.

The formula (6-55) is modified to another form by the use of independent PH deviation $\tilde{\delta}^S$ as follows:

From Eq.(6-50),

$$(\sigma_E^S)^2 = \sum_{ij} \int\cdots\int_{-\infty}^{\infty} F^S(\delta^S)\delta_i^S\delta_j^S d\delta^S \Big/ \int\cdots\int_{-\infty}^{\infty} F^S(\delta^S) d\delta^S \tag{6-57}$$

$$= \sum_{ij} \int\cdots\int_{-\infty}^{\infty} \bar{F}^S(\tilde{\delta}^S) \Big(\sum_\ell t_{\ell i}^S \tilde{\delta}_\ell^S\Big)\Big(\sum_m t_{mj}^S \tilde{\delta}_m^S\Big) |\det T^S| d\tilde{\delta}^S$$

$$\Big/ \int\cdots\int_{-\infty}^{\infty} \bar{F}^S(\tilde{\delta}^S) |\det T^S| d\tilde{\delta}^S$$

$$= \sum_{ij\ell m} t_{\ell i}^S t_{mj}^S \int\cdots\int_{-\infty}^{\infty} \tilde{F}^S(\tilde{\delta}^S)\tilde{\delta}_\ell^S\tilde{\delta}_m^S d\tilde{\delta}^S \Big/ \int\cdots\int_{-\infty}^{\infty} \tilde{F}^S(\tilde{\delta}^S) d\tilde{\delta}^S$$

$$= \sum_{ij\ell} t_{\ell i}^S t_{\ell j}^S \int\cdots\int_{-\infty}^{\infty} \tilde{F}^S(\tilde{\delta}^S)(\tilde{\delta}_\ell^S)^2 d\tilde{\delta}^S \Big/ \int\cdots\int_{-\infty}^{\infty} \tilde{F}^S(\tilde{\delta}^S) d\tilde{\delta}^S$$

$$= \sum_{ij\ell} t_{\ell i}^S t_{\ell j}^S (\tilde{\sigma}_\ell^S)^2 \ , \tag{6-58}$$

where $d\tilde{\delta}^S = \prod_{i=1}^{n} d\tilde{\delta}_i^S$,

$$\bar{F}^S(\tilde{\delta}^S) \equiv F^S((T^S)^T\tilde{\delta}^S) = F^S(\delta^S) \ ,$$

$$\int\cdots\int \tilde{F}^S(\tilde{\delta}^S)\tilde{\delta}_\ell^S\tilde{\delta}_m^S d\tilde{\delta}^S \Big/ \int\cdots\int \tilde{F}^S(\tilde{\delta}^S) d\tilde{\delta}^S = \langle\tilde{\delta}_\ell^S\tilde{\delta}_m^S\rangle$$

$$= \Lambda_{\ell m}^S = \begin{cases} 0 \text{ for } \ell \neq m \\ \lambda_\ell^S = (\tilde{\sigma}_\ell^S)^2 \text{ for } \ell = m \ , \end{cases} \tag{6-59}$$

$\tilde{\sigma}_\ell^S$ = standard deviation of the ℓ-th independent PH deviation of shower fluctuation $\tilde{\delta}_\ell^S$.

If we define

$$S_\ell \equiv \sum_i t_{\ell i}^S \ , \tag{6-60}$$

we finally obtain a formula for σ_E^S:

$$(\sigma_E^S)^2 = \sum_\ell (S_\ell\tilde{\sigma}_\ell^S)^2 = \sum_\ell S_\ell^2\lambda_\ell^S \ . \tag{6-61}$$

By definition, S_ℓ is the sum of components of the eigenvector which corresponds to the eigenvalue λ_ℓ^S. Eq.(6-61) means that the total PH variance $(\sigma_E^S)^2$ of the shower fluctuation is written as a quadratic sum of the product of S_ℓ and the standard deviation $\tilde{\sigma}_\ell^S$ of the ℓ-th independent PH deviation $\tilde{\delta}_\ell^S$.

From Eqs.(6-54), (6-56), and (6-61), the total PH variance σ_E^2 is written as

$$\sigma_E^2 = \sum_{\ell}(S_\ell\ \bar{\sigma}_\ell^S)^2 + \sum_i(\sigma_i^D)^2 \qquad (6\text{-}62)$$

$$= \sum_{\ell} S_\ell^2 \lambda_\ell^S + \sum_i (\sigma_i^D)^2 \ . \qquad (6\text{-}63)$$

(8) Generalization of Correlation Matrix of Shower Fluctuation C^S to Correlation Function $C^S(E_\circ, E^*, t, t')$

If Assumptions 1 and 2 made in Formulation (6) are correct, the correlation matrix of shower fluctuation C^S is a fundamental quantity which describes the fluctuation process of the EM cascade shower. It is not affected by the fluctuation due to the characteristics of the detector (detector fluctuation). Hence, it is valuable to generalize the correlation matrix C^S to the correlation "function" $C^S(t,t')$. The generalization of C^S is made as follows. Since the correlation matrix element C_{ij}^S for shower fluctuation is defined by

$$C_{ij}^S \equiv \int\cdots\int_{-\infty}^{\infty} F^S(\delta^S)\delta_i^S\delta_j^S d\delta^S \Big/ \int\cdots\int_{-\infty}^{\infty} F^S(\delta^S)\, d\delta^S \ , \qquad (6\text{-}64)$$

the correlation function $C^S(t,t')$ is obtained by the following substitutions:

$$\delta_i^S \longrightarrow \delta^S(t)$$

$$\delta_j^S \longrightarrow \delta^S(t')$$

$$d\delta^S = \prod_i d\delta_i^S \longrightarrow \prod_{t''} d\delta^S(t'')$$

$$F^S(\delta^S) \longrightarrow F^S(\delta^S) \ .$$

Then the correlation function $C^S(t,t')$ is written as

$$C^S(t,t') \equiv \int\cdots\int_{-\infty}^{\infty} F^S(\delta^S)\delta^S(t)\delta^S(t')\prod_{t''} d\delta^S(t'')$$

$$\Big/ \int\cdots\int_{-\infty}^{\infty} F^S(\delta^S)\prod_{t''} d\delta^S(t'') \ . \qquad (6\text{-}65)$$

If the dependences on the incident energy $E_\circ$ and the cut-off energy of detector E_d^* are included to $C^S(t,t')$, the formula (6-65) is modified to

$$C^S(E_\circ, E_d^*, t, t') \equiv \int\cdots\int_{-\infty}^{\infty} F^S(E_\circ, E_d^*, \delta^S)\delta^S(E_\circ, E_d^*, t)\delta^S(E_\circ, E_d^*, t')$$

$$\times \prod_{t''} d\delta^S(E_\circ, E_d^*, t'') \Big/ \int\cdots\int_{-\infty}^{\infty} F^S(E_\circ, E_d^*, \delta^S)\prod_{t''} d\delta^S(E_\circ, E_d^*, t'') \ .$$

(6-66)

The parametrization of the correlation function of shower fluctuation $C^S(E_\circ, E_d^*, t, t')$ is made in section B-5-(5) in this Chapter.

The correlation matrices C, C_N, and C_N^S are also generalized to the correlation functions $C(E_\circ, E_d^*, t, t')$, $C_N(E_\circ, E_d^*, t, t')$, and $C_N^S(E_\circ, E_d^*, t, t')$, respectively:

$$C(E_\circ, E_d^*, t, t') \equiv \int\cdots\int_{-\infty}^{\infty} F(E_\circ, E_d^*, \delta)\delta(E_\circ, E_d^*, t)\delta(E_\circ, E_d^*, t')$$

$$\times \prod_{t''} d\delta(E_\circ, E_d^*, t'') \Big/ \int\cdots\int_{-\infty}^{\infty} F(E_\circ, E_d^*, \delta)\prod_{t''} d\delta(E_\circ, E_d^*, t'') \ ,$$

(6-67)

$$C_N(E_o,E_d^*,t,t') \equiv \frac{C(E_o,E_d^*,t,t')}{\sqrt{C(E_o,E_d^*,t,t)C(E_o,E_d^*,t',t')}} , \qquad (6\text{-}68)$$

$$C_N^S(E_o,E_d^*,t,t') \equiv \frac{C^S(E_o,E_d^*,t,t')}{\sqrt{C^S(E_o,E_d^*,t,t)C^S(E_o,E_d^*,t',t')}} . \qquad (6\text{-}69)$$

B-5. Experimental Results in terms of the Formulation

In terms of the formulation in section B-4, the following experimental results were obtained for high energy EM cascade shower observed by the EM gas calorimeter.

(1) Diagonalization of Correlation Matrix C and Independent Fluctuation

Eigenvalues and eigenvectors of the correlation matrix of global fluctuation C were obtained from the observed shower developments for incident electrons of energies from 25 GeV to 100 GeV. Tables VI-3(a)-(d) show numerical values of eigenvalues and corresponding eigenvectors of correlation matrix C. In these tables, the eigenvalues are numbered from the largest to the smallest. Therefore, the first eigenvalue is the largest. Fig.VI-20 shows eigenvalues λ_i's with respect to their number i for 75 GeV electrons. Since $\sqrt{\lambda_i} = \tilde{\sigma}_i$, the largest independent fluctuation is about 2 times larger than the second one, where $\tilde{\sigma}_i$ is a standard deviation of independent PH deviation $\tilde{\delta}_i$.

The components of eigenvectors x_i's are shown for 75 GeV electrons in Figs.VI-21(a)-(f). We observe the followings from these figures:

1) Components of the first eigenvector x_1 versus the chamber plane number j show the shape similar to a sinusoidal curve.

2) There is a trend that the number of nodes of the curve ($x_i(j)$ vs. j) increases as the corresponding eigenvalue becomes small.

The dependent fluctuation of chamber pulse height is demonstrated in Figs.VI-22(a)-(d). The figures show two-dimensional scatter plots of dependent PH deviations (δ_i vs. δ_j) for 75 GeV electrons. Points in the figures show ellipse-like distributions. The principal axes of the ellipse are not parallel to coordinate axes. This means there is a non-vanishing correlation between δ_i and δ_j. Two-dimensional scatter plots of independent PH deviations ($\tilde{\delta}_i$ vs. $\tilde{\delta}_j$) for 75 GeV electrons are shown in Figs.VI-23(a)-(d). The figures show no correlation between $\tilde{\delta}_i$ and $\tilde{\delta}_j$. These properties are the same for other energies (25, 50, and 100 GeV).

(2) Correlation Matrices of Shower Fluctuation (C^S) and Detector Fluctuation (C^D)

According to Assumptions 1 and 2 in Formulation (6) in section B-4, we have obtained C^S and C^D from our data. The diagonal element C^S_{ii} was obtained by the interpolation

($2 \leq i \leq 36$) and extrapolation ($i=1, 37$) of off-diagonal elements C^S_{ii}'s ($i \neq j$). The diagonal elements C^D_{ii}'s were obtained by Eq.(6-47).

Tables VI-4 and VI-5 show numerical values of C^S_{ii} and C^D_{ii} for energies from 25 GeV to 100 GeV, respectively. They are also shown in figures (C^S_{ii} in Fig.VI-24, C^D_{ii} in Fig.VI-25). From these figures, we observe the followings:

1) The curve C^S_{ii} vs. i has clear two peaks (Fig.VI-24). This is not the case for the curve C^D_{ii} vs. i (Fig.VI-25).

2) The curve C^D_{ii} vs. i has a shape similar to the shower curve.

Figs.VI-26(a)-(d) show normalized correlation matrix elements $(C^S_N)_{ij}$'s with respect to j for energies from 25 GeV to 100 GeV.

(3) Diagonalization of C^S

Eigenvalues and eigenvectors of the correlation matrix of shower fluctuation C^S were obtained for energies from 25 GeV to 100 GeV. Eigenvalues and corresponding eigenvectors are tabulated in Tables VI-6(a)-(d). Eigenvalues were numbered by the same manner as used in section B-5-(1). The same figures as obtained for C were also derived for C^S. Eigenvalue λ^S_i vs. i is shown for 75 GeV electrons in Fig.VI-27. Elements of eigenvector $\mathbf{x}^S_i(j)$ are plotted against the element number j in Figs.VI-28(a)-(f). The general properties of the eigenvalues and

eigenvectors of C^S are almost the same as those of C. To be mentioned here is a trend of the curves $\mathbf{x}^S_i(j)$ vs. j ($i=1\sim6$). For the correlation matrix of global fluctuation C, there is a trend that the number of nodes of the curve $\mathbf{x}_i(j)$ vs. j increases as corresponding eigenvalue becomes small. This trend is clearer for the correlation matrix of shower fluctuation C^S. The number of nodes for C^S increases more systematically than that for C.

(4) Standard Deviation σ_E of the Total PH Fluctuation and Its Relation to C^S and C^D

By using Eqs.(6-52), (6-55), and (6-56), we have obtained standard deviations σ_E, σ^S_E, and σ^D_E from our experimental result. Fig.VI-29 shows energy resolutions $\sigma_E/\langle E\rangle$, $\sigma^S_E/\langle E\rangle$, and $\sigma^D_E/\langle E\rangle$ with respect to $1/\sqrt{E_\circ}$, where $E_\circ$ is an incident energy. With the expected relation $\sigma_E/\langle E\rangle = K/\sqrt{E_\circ}$ ($K = 24.7\pm0.5$ %(GeV)$^{\frac{1}{2}}$) for the energy resolution of calorimeter, we found that the relations $\sigma^S_E/\langle E\rangle = K^S/\sqrt{E_\circ}$ and $\sigma^D_E/\langle E\rangle = K^D/\sqrt{E_\circ}$ were approximately satisfied, where $K^S = 10.1\pm1.1$ %(GeV)$^{\frac{1}{2}}$ and $K^D = 22.8\pm0.1$ %(GeV)$^{\frac{1}{2}}$. Fig.VI-30 shows energy dependence of $\sigma_E/\ \sigma^S_E$.

The standard deviation σ^S_E of shower fluctuation is obtained not only from Eq.(6-55) but also from Eq.(6-61). By diagonalization of C^S and the use of Eq.(6-60), we obtained S_ℓ and λ^S_ℓ. The S_ℓ vs. ℓ is shown in Fig.VI-31 for 75 GeV electrons. Figs.VI-32(a)-(d) show $S^2_\ell\lambda^S_\ell$ vs. ℓ for electrons of energies from 25 GeV to 100 GeV.

(5) Parametrization of Correlation Function $C^S(E_o, E_d^*, t, t')$

In section B-4, we have generalized the correlation matrix of shower fluctuation C^S to a continuous function $C^S(E_o, E_d^*, t, t')$ which was called as the correlation function. The parametrization of the correlation function will be made in this section. In order to observe the global structure of C^S, we present the three-dimensional plots of C^S (Figs.VI-33(a)-(d)). These figures suggest us to use the two-dimensional Fourier series to parametrize $C^S(E_o, E_d^*, t, t')$. Since it is not favorable to use too many parameters, we limit the Fourier series to the second order. Hence the $C^S(E_o, E_d^*, t, t')$ is expanded as

$$
\begin{aligned}
C^S(E_o, E_d^*, t, t') = {} & \frac{1}{4} a_{00}(E_o, E_d^*) \\
& + \frac{1}{2} \sum_{n=1}^{2} [a_{n0}(E_o, E_d^*) \cos\{n\pi(2t-\ell-L)/(L-\ell)\} \\
& \quad + b_{n0}(E_o, E_d^*) \sin\{n\pi(2t-\ell-L)/(L-\ell)\} \\
& \quad + a_{0n}(E_o, E_d^*) \cos\{n\pi(2t'-\ell-L)/(L-\ell)\} \\
& \quad + c_{0n}(E_o, E_d^*) \sin\{n\pi(2t'-\ell-L)/(L-\ell)\}] \\
& + \sum_{m,n=1}^{2} [a_{mn}(E_o, E_d^*) \cos\{m\pi(2t-\ell-L)/(L-\ell)\} \cos\{n\pi(2t'-\ell-L)/(L-\ell)\} \\
& \quad + b_{mn}(E_o, E_d^*) \sin\{m\pi(2t-\ell-L)/(L-\ell)\} \cos\{n\pi(2t'-\ell-L)/(L-\ell)\} \\
& \quad + c_{mn}(E_o, E_d^*) \cos\{m\pi(2t-\ell-L)/(L-\ell)\} \sin\{n\pi(2t'-\ell-L)/(L-\ell)\} \\
& \quad + d_{mn}(E_o, E_d^*) \sin\{m\pi(2t-\ell-L)/(L-\ell)\} \sin\{n\pi(2t'-\ell-L)/(L-\ell)\}] ,
\end{aligned}
\qquad (6\text{-}70)
$$

where

$$\ell = t_f - \Delta t/2 = 1.92 \text{ r.}\ell. ,$$

$$L = t_\ell + \Delta t/2 = 23.69 \text{ r.}\ell. ,$$

Δt = sampling thickness of an unit layer in radiation length,

t_f, t_ℓ are thicknesses at the first and the last chambers in radiation length, respectively.

The Fourier series is orthonormal in the interval $[\ell, L]$. The formula (6-70) has 25 coefficients. Since the correlation function $C^S(E_o, E_d^*, t, t')$ is symmetric for the exchange of t and t' as

$$C^S(E_o, E_d^*, t, t') = C^S(E_o, E_d^*, t', t) , \qquad (6\text{-}71)$$

there are relations between coefficients:

$$
\begin{aligned}
a_{mn} &= a_{nm} , \\
b_{mn} &= c_{nm} , \\
d_{mn} &= d_{nm} .
\end{aligned}
\qquad (6\text{-}72)
$$

Thus the real number of coefficients reduces to 15. By considering these 15 coefficients as parameters, we made a least squares fit of the correlation matrix elements C^S_{ij} to the two-dimensional second order Fourier series.

The reproduced correlation matrices with optimized values of parameters are shown in Figs.VI-34(a)-(d) as three-dimensional plots for energies from 25 GeV to 100 GeV. We see the global structure of the correlation function was reproduced by the

formula (6-70). The reduced X^2 of fitting is typically 0.98 for 25 GeV. The cross sections of these three-dimensional plots are shown for 75 GeV electrons with original matrix elements in Figs.VI-35(a)-(h) for off-diagonal elements (C^s_{ij} vs. j) and Fig.VI-36 for diagonal elements (C^s_{ii} vs. i). The optimized values of parameters are tabulated in Table VI-7 for various energies. The parameters show almost the linear dependence of energy (Figs.VI-37(a)-(d)).

C. Application of Study of Longitudinal Shower Fluctuation to π/e Separation

C-1. Method of π/e Separation

As an application of study of the longitudinal shower fluctuation, we propose a new method of π/e separation (see Chapter I-B-2). We assume a case in which we have only an electromagnetic calorimeter. The conventional method as shown in Chapter V-E uses the following variables for π/e separation:

1) The total energy deposit in the calorimeter (E).

2) The ratio of the energy deposit in the front segment or rear segment of the calorimeter to the total energy deposit in the calorimeter. In Chapter V-E, we used ratios R_1 (for front segment) and R_3 (for rear segment).

3) The lateral shower spread. The variable σ_2 was used in Chapter V-E.

Instead of using the variables R_1 and R_3, here we use the information of longitudinal shower development more effectively. In the present method, we use the variable X^2 defined event-by-event as

$$X^2 \equiv \delta^T A \delta = (\delta^T T^T)(TAT^T)(T\delta) = \tilde{\delta}^T D \tilde{\delta} = \sum_i d_i \tilde{\delta}_i^2 , \qquad (6\text{-}73)$$

where

$$A = \frac{1}{2} C^{-1} ,$$

$$D = TAT^T = \begin{bmatrix} d_1 & & 0 \\ & \ddots & \\ 0 & & d_n \end{bmatrix} ,$$

$$\tilde{\delta} = T\delta ,$$

$$\delta_i = p_i - \langle p_i^e \rangle ,$$

p_i = pulse hight of the i-th chamber for electrons or pions,

$\langle p_i^e \rangle$ = average pulse height of electrons at the i-th chamber.

The matrix A is calculated from correlation matrix C which is obtained for electron events.

Namely, the method is as follows. First, we assume the average PH of electrons $\langle p_i^e \rangle$ for a single event. Then we obtain dependent PH deviation δ_i by subtracting $\langle p_i^e \rangle$ from the pulse height p_i of a chamber. We transform δ_i by transformation matrix T in order to obtain independent PH deviation $\tilde{\delta}_i$. The $\tilde{\delta}_i$ is a

variable independent of the correlated fluctuation of chamber PH. Therefore, if we make cut on $\tilde{\delta}_i$ instead of δ_i, we can include more electrons in the cut region. But the same is not true for pions, since we use $\langle p_i^e \rangle$ and C which are obtained for electrons. The $\tilde{\delta}_i$ obtained from a pion event is not independent; and $|\tilde{\delta}_i|$ is far bigger than that for electron. Therefore, we can make more rejection of pion by using cut of $\tilde{\delta}_i$ instead of δ_i. The X^2 cut makes $\tilde{\delta}_i$ cut for all i values in one time.

This is not the case for R_1 and R_3. The R_1 and R_3 are based on the dependent pulse height deviations δ_i, therefore they are the dependent variables on the correlated fluctuation of the electron shower in chamber PH. Hence, the R_1, R_3 cuts are affected by the correlated fluctuation of chamber PH.

For the actual π/e separation analysis, the information of the total pulse height E was added to the X^2. In order to include it, we have defined a new X-square X_G^2 as follows:

$$X_G^2 \equiv X^2 + X_E^2 , \tag{6-74}$$

$$\text{where} \quad X_E^2 \equiv \frac{(E-\langle E^e \rangle)^2}{2(\sigma_E^e)^2} , \tag{6-75}$$

$\langle E^e \rangle$ = mean of the total pulse height for electrons,

σ_E^e = standard deviation of the total pulse height for electrons,

E = the total pulse height for electrons or pions.

C-2. π/e Separation with a New Method

Figs.VI-38(a),(b) show the first independent PH deviation $\tilde{\delta}_1$ which corresponds to the largest eigenvalue obtained from the formulae shown in section C-1 in this Chapter for 50 GeV electrons and 100 GeV pions, respectively. As described in section C-1, the $\tilde{\delta}_1$ for pion is calculated by the use of the mean pulse heights of chambers for 50 GeV electrons instead of using those for 100 GeV pions. In these figures, we observe the $\tilde{\delta}_1$ distribution of pions is wider than that of electrons. If we make a cut as shown in the figures, the pion rejection is 11.5 % with electron retention efficiency of 91.6 %. We repeat this kind of rejection for various independent PH deviations when we use X^2 or X_G^2. The same distributions are shown for 2nd independent fluctuation in Figs.VI-39(a),(b). Figs.VI-40(a),(b) show X_G^2 distribution for electrons of 50 GeV and pions of 100 GeV, respectively. These figures show good separation of electrons from pions. With the cut shown in the figures, we obtain pion rejection of less than 2×10^{-4} with electron retention efficiency of 99.2 %. Same distributions are shown for 100 GeV electrons and pions in Figs.VI-41(a),(b), respectively.

Pion rejection factor vs. the electron retention efficiency for X_G^2 cut are shown in Figs.VI-42(a)-(c) for various energy combinations of electrons and pions. The X_G^2 cut is very effective for the case E_e = 50 GeV and E_π = 100 GeV. No improvement of the pion rejection, compared with conventional

cuts (see Chapter V-E), was obtained for the case $E_e = E_\pi$. This is shown more clearly in Fig.VI-43(a),(b) which show the pion rejection factor as a function of the ratio of electron energy to pion energy (E_e/E_π) with the electron retention efficiencies of 85 % and 98 %, respectively. The X_G^2 cut is very effective except for the case $E_e = E_\pi$. By using the X_G^2 cut, we have obtained more than factor 10 better pion rejection ($<2\times10^{-4}$) than the conventional cut ($E\&R_1\&R_3$ cut) shown in Fig.VI-43(c). As we mentioned in Chapter V-E, the reason of no improvement of pion rejection for the case $E_e = E_\pi$ might be due to the electron contamination in pion beam.

CHAPTER VII

DISCUSSION OF RESULTS

A. Calorimeter Performance

A prototype module of the end plug EM gas calorimeter for CDF has been constructed and its performances have been measured. Energy resolution, pulse height linearity, position resolution, response uniformity, and π/e separation capability are all found to be quite satisfactory.

The energy resolution of $30\sqrt{t(r.\ell.)/E(GeV)}$ % is equivalent to the world average for gas calorimeters as shown in Table I-1. This energy resolution corresponds to 1.7 % for 200 GeV electrons. Since the end plug is in a small angular region, the decay electron from W or Z bosons often has such energy at $\theta=15^\circ$. The energy resolution of 1.7 % is fairly close to the level of systematic error. Since the end plug EM gas calorimeter is a large system, it is not easy to keep the systematic error below 1.7 %. We need various monitoring systems, e.g. gas pressure, gas composition, temperature, and high voltage monitors. The gain calibration using Cd^{109} sources and non-interacting (no hadronic interaction) hadrons and muons will be made. By the use of all these monitoring and calibration systems, we expect we can keep the systematic error below 1 % level. In this sense, the intrinsic energy resolution of 24 $\%/\sqrt{E}$ (1.7 % for E = 200 GeV) is

fairly good for high energy electrons. The detailed discussion about the energy resolution of EM gas calorimeter according to the newly obtained formulae in chapter VI-B will be made in section C of this Chapter.

The position resolution is important to know the impact point of a photon or an electron on the calorimeter. The overlap of an energetic π° and a charged hadron constitutes a background for an electron, e.g. the decay electron from W or Z bosons. Therefore the measurement of the impact point of a photon is important to reject such background. Since tracking chamber has poor momentum resolution in the end plug region, the E/p cut which require $E/p \simeq 1$ is not effective, where E is the energy observed by the calorimeter, and P is the momentum measured by the tracking chamber. For our calorimeter, we have obtained the position resolution of 1.5 mm for 50 GeV electrons. For the background of π° and a charged hadron, we observe the energy deposit of two photons and one hadron. We expect about the same position resolution for two photons from π° as that for an electron, since the signal of two photons should be very similar to that of an electron. But we need to take into account the effect of an interacting hadron. About 65 % of hadrons has hadronic interaction in the calorimeter. The position resolution should be obtained with the effect of an interacting hadron for the study of this background problem.

The discussion about π/e separation performance will be made in section C in this Chapter.

About the end plug EM gas calorimeter, one thing we have not studied is the effect of the magnetic field. Since the end plug EM gas calorimeter is in the 15 KG solenoidal field, there will be a possible problem for proportional chamber caused by the magnetic field. One problem is the curving of the electron or ion tracks in the chamber due to V x B Lorentz force. It potentially causes inefficiency and lengthening of dirft time. But according to the Monte Carlo study of AMY [AM 83], the magnetic field reduces the fluctuations caused by wide angle electrons. They have obtained energy resolution of

$$\sigma/E \sim 15\ \%/\sqrt{E}\ ,$$

for the magnetic field of 30 KG with 4 mm Pb sampling. In their case, proportional tubes are parallel to the magnetic field, while in our case tubes are perpendicular to the field. We need more study about the effect of the magnetic field on gain of a chamber in the future.

B. Average Shower Curve

As shown in Fig.VI-3, the correction function $\rho(E_o,E^*,s)$ obtained by our calorimeter with cut-off energy $E^* = 3$ MeV shows a rough agreement with low energy data obtained by Muller for $s \lesssim 1$. For $s > 1$, however, our $\rho(E_o,E^*,s)$ is systematically lower than Muller's. He obtained the data by using plastic

scintillators instead of chambers. Mitsui [MI 81] derived the $\rho(E_o,E^*,s)$ from the shower curve obtained by many authors with various shower detectors, including the result of Muller and his own, as shown in Fig.VII-1. The figure shows that Mitsui's $\rho(E_o,E^*,s)$ is the same as ours for $s \lesssim 1$. The property of $\rho(E_o,E^*,s)$ is similar for various detectors in this s region. But for $s > 1$, there are discrepancies among results. Since the shower curve observed by various detectors is dependent on the detector, the $\rho(E_o,E^*,s)$ function depends on the detector. One reason for this is the difference of the cut-off energy of detectors E_d^*. But it seems to be impossible to explain consistently the $\rho(E_o,E^*,s)$ of various detectors for $s > 1$, including our data, by the difference of the cut-off energy E_d^* alone.

The $\rho(E_o,E^*,s)$ derived from our gas calorimeter is well fitted to formula (6-4) for energies from 25 GeV to 100 GeV. It has no dependence on incident energy E_o in this region. Therefore, we expect the actual shower curve at energy higher than 100 GeV can also be represented by the shower curve $\Pi_A(E_o,E^*,t)$ obtained by Rossi and the correction function $\rho(E_o,E^*,s)$ derived here.

C. Longitudinal Shower Fluctuation

C-1. Validity of the Assumptions 1 and 2

As we discussed in Chapter VI-B-4, the global fluctuation can be separated into two fluctuations; one is the shower fluctuation and the other is the detector fluctuation. The shower fluctuation is defined as the fluctuation of the cascade shower development and makes sampling fluctuation in a sampling calorimeter. On the other hand, the detector fluctuation is defined as the sum of the track length fluctuation, the Landau fluctuation, and the fluctuation due to the noise of the read out electronics. In our case, the noise of the read out electronics was negligibly small compared with other fluctuations, judging from the pedestal distributions of ADC's.

We made following two assumptions in Chapter VI-B-4:

Assumption 1. The detector fluctuation is independent of the shower fluctuation.

$$\langle \delta_i^S \delta_j^D \rangle = 0 \text{ for any } i, j \ . \tag{7-1}$$

Assumption 2. The detector fluctuation of each chamber is independent of those of other chambers.

$$\langle \delta_i^D \delta_j^D \rangle \rightarrow \langle \delta_i^D \delta_j^D \rangle \hat{\delta}_{ij} \ . \tag{7-2}$$

In order to check the validity of the above assumptions, we made following studies:

1) Comparison between C_N, C_N^S of our gas calorimeter and C_N of a liquid argon calorimeter by Cerri et al. [CE 77].

2) Comparison of σ_E, σ_E^S, and σ_E^D with the result of Fischer's Monte Carlo [FI 78].

(1) Comparison with the Result of a Liquid Argon Calorimeter

For the liquid argon calorimeter of Cerri et al., the fluctuation due to the noise of the read out electronics is very small compared with the global fluctuation [CE 77]. Therefore we neglect the fluctuation caused by the noise in the detector fluctuation for their result as well as ours. And it is pointed out by many authors [FI 78,IW 80] that the liquid argon calorimeter has very small track length and Landau fluctuations (detector fluctuation) compared with the gas calorimeter (see Figs.VI-13 and VI-14).

Figs.VII-2(a)-(h) show the elements of the normalized correlation matrix of global fluctuation C_N obtained by a liquid argon calorimeter by Cerri et al., together with those obtained by our gas calorimeter for 25 GeV electrons. The elements of the normalized correlation matrix of shower fluctuation C_N^S obtained by our gas calorimeter for the same energy electrons are also shown in these figures. We observe the discreteness of the diagonal elements of the matrix C_N for our gas calorimeter, but not for the liquid argon calorimeter. This means that (1) the discreteness of the diagonal elements of the correlation matrix C is due to the detector fluctuation (track length and Landau fluctuations). These figures also show that the normalized correlation matrix C_N of the liquid argon calorimeter agrees well with the normalized correlation matrix of shower fluctuation C_N^S of our gas calorimeter. This means that (2) the detector

fluctuation has no correlation between chambers, and also (3) the detector fluctuation has no correlation to the shower fluctuation. The statements (1), (2), and (3) are equivalent to the Assumptions 1 and 2. Thus, the correctness of the Assumptions 1 and 2 was proved.

(2) σ_E , σ_E^S, and σ_E^D Compared with the Result of Fischer's Monte Carlo

Fischer has studied by a Monte Carlo method on the pulse height fluctuation of the gas calorimeter, and estimated the sampling, track length, and Landau fluctuations [FI 78]. According to his Monte Carlo [FI 78], the energy resolution ($\sigma_E/\langle E\rangle$) of the gas calorimeter is determined by about 40 % of shower fluctuation and 60 % of detector fluctuation for incident energy of 1 GeV and sampling thickness of 0.58 radiation length which is the same thickness as that of our calorimeter. In other words, the global fluctuation is about 2.5 times larger than the shower fluctuation ($\sigma_E / \sigma_E^S \approx 2.5$). This is shown in his figure (Fig.VI-14). By this fact we can check our Assumptions 1 and 2. The Assumptions 1 and 2 lead to the Eq.(6-54):

$$\sigma_E^2 = (\sigma_E^S)^2 + (\sigma_E^D)^2 \tag{6-54}$$

As shown in Fig.VI-29, σ_E, σ_E^S, and σ_E^D satisfy the relations:

$$\sigma_E/\langle E\rangle = K/\sqrt{E_\circ} \ , \tag{7-3}$$

$$\sigma_E^S/\langle E\rangle = K^S/\sqrt{E_\circ} \ , \tag{7-4}$$

$$\sigma_E^D/\langle E\rangle = K^D/\sqrt{E_\circ} \ . \tag{7-5}$$

We expect, as a good assumption, these formulae are satisfied for the energy region not only from 25 GeV to 100 GeV but also down to 1 GeV. Then, we compare our result on (σ_E/σ_E^s) shown in Fig.VI-30 with the result of Fischer $(\sigma_E/\sigma_E^s \simeq 2.5)$. Fig.VI-30 shows that our result is in good agreement with that of Fischer. Again the goodness of the Assumptions 1 and 2 was demonstrated.

C-2. Property of Shower Fluctuation

(1) Function $C^s(E_o, E_d^*, t, t')$

As shown in Figs.VI-33(a) to VI-36, the correlation matrix of shower fluctuation C^s is successfully fitted to two-dimensional 2nd order Fourier series. The curve C_{ii}^s vs. i shows two peaks, where a hollow place between them is immediately behind the shower maximum (see Fig.VI-9, Fig.VI-24, and Fig.VI-36). This is the reason why the curve σ_i vs. i seems to have two peaks at higher energies (> 100 GeV) and the curve $\sigma_i/\langle p_i \rangle$ vs. i takes minimum immediately behind the shower maximum as mentioned in Chapter VI-B-1 (see Fig.VI-10, Fig.VI-11). The two peaks of σ_i vs. i and the minimum of $\sigma_i/\langle p_i \rangle$ vs. i just behind the shower maximum are caused by the property of shower fluctuation. Why does the shower fluctuation take the minimum value (the hollow place of C_{ii}^s vs. i) immediately behind the shower maximum rather than exactly at the shower maximum? For the present, we do not know the reason. But we know the fact

that the "center of gravity" of the average shower curve is slightly behind the shower maximum, since the average shower curve is steeper in front part than in back part (see Fig.VI-9). The minimum of the shower fluctuation corresponds to the center of gravity of the average shower curve. We need more study on this problem.

(2) Energy Resolution $\sigma_E^s/\langle E \rangle$ in Terms of Independent Shower Fluctuation

From Eq.(6-50), the dependent PH deviation δ^s of shower fluctuation is written as follows:

$$\delta^s = (T^s)^T \tilde{\delta}^s$$

$$= ((x_1^s)^T, \cdots, (x_n^s)^T) \begin{bmatrix} \tilde{\delta}_1^s \\ \vdots \\ \tilde{\delta}_n^s \end{bmatrix}$$

$$= \begin{bmatrix} t_{11}^s \\ \vdots \\ t_{1n}^s \end{bmatrix} \tilde{\delta}_1^s + \cdots + \begin{bmatrix} t_{n1}^s \\ \vdots \\ t_{nn}^s \end{bmatrix} \tilde{\delta}_n^s = \sum_\ell (x_\ell^s)^T \tilde{\delta}_\ell^s , \qquad (7\text{-}6)$$

where

$$T^s = \begin{bmatrix} x_1^s \\ \vdots \\ x_n^s \end{bmatrix} , \qquad (7\text{-}7)$$

x_ℓ^s = the ℓ-th eigenvector corresponds to eigenvalue λ_ℓ^s.

The dependent PH deviation δ^s is written by the linear

combination of eigenvectors $(x_\ell^s)^T$. The $\tilde{\delta}_\ell^s$ is the ℓ-th coefficient of the linear combination. As we mentioned in Chapter VI-B-4, the eigenvalue λ_ℓ^s is the variance of the independent PH deviation $\tilde{\delta}_\ell^s$. Therefore, the λ_ℓ^s defines the average weight of the eigenvector x_ℓ^s in the linear combination which makes the dependent PH deviation δ^s. Fig.VI-27 shows that, in the average, the first mode fluctuation (the first eigenvector x_1^s, Fig.VI-28(a)) is about 2 times larger than the second mode fluctuation (the 2nd eigenvector x_2^s, Fig.VI-28(b)) in the dependent PH deviation δ^s.

In Chapter VI-B-4, we obtained the following relation for shower fluctuation:

$$(\sigma_E^s)^2 = \sum_\ell S_\ell^2 (\tilde{\sigma}_\ell^s)^2 = \sum_\ell S_\ell^2 \lambda_\ell^s . \qquad (6\text{-}61)$$

The variance $(\sigma_E^s)^2$ of the total PH fluctuation caused by shower fluctuation is the sum of $S_\ell^2\lambda_\ell^s$ over ℓ=1 to 37. The $S_\ell^2\lambda_\ell^s$ is plotted against ℓ in Figs.VI-32(a)-(d). These figures show which independent fluctuations mainly determine the energy resolution $\sigma_E^s/\langle E\rangle$. There seems to be no systematic behavior in these figures. The systematics might be swept by the uncertainty of the chamber gain.

C-3. Distribution Function of PH Deviation

The distribution function $F(\delta)$ of the PH deviation δ for global fluctuation is an important function for the gas calorimeter, because it describes fluctuations in the gas calorimeter. As shown in Figs.VI-5(a) to VI-8(f), for high energy cascade shower, the pulse height distribution of each chamber is approximately Gaussian due to enough electron statistics, except for the chambers at very early part and very late part of the shower.

Therefore, formula (6-8)

$$F(\delta) = K e^{-\delta^T A \delta} \qquad (6\text{-}8)$$

is a good approximation for the fluctuation of high energy cascade shower observed by the gas calorimeter. In Eq.(6-8), A is the symmetric matrix derived from correlation matrix C by

$$A = \frac{1}{2} C^{-1} . \qquad (6\text{-}34)$$

Since $F(\delta)$ includes detector fluctuation, it is a function dependent on the detector.

The distribution function $F^S(\delta^S)$ of the PH deviation δ^S for shower fluctuation is a fundamental function for high energy cascade shower. By the same reason as for the case of $F(\delta)$, the $F^S(\delta^S)$ is approximately described as

$$F^S(\delta^S) = K' e^{-(\delta^S)^T A^S \delta^S} , \qquad (7\text{-}8)$$

$$\text{where} \quad A^S = \frac{1}{2} (C^S)^{-1} , \qquad (7\text{-}9)$$

$$K' = \text{a constant.}$$

The n-dimensional function $F^S(\delta^S)$ is generalized to the

"infinite" dimensional function (functional) $F^S(E_\circ, E_d^*, \delta^S)$ defined for the incident energy $E_\circ$, the cut-off energy of detector E_d^*, and the PH deviation $\delta^S(E_\circ, E_d^*, t)$ which is a function of $E_\circ$, E_d^*, and the arbitrary thickness t in radiation length. For high energy cascade shower, the $F^S(E_\circ, E_d^*, \delta^S)$ is approximately described by the formula:

$$F^S(E_\circ, E_d^*, \delta^S) = K'' \exp\{-\int\int_0^\infty A^S(E_\circ, E_d^*, t', t'')\delta^S(E_\circ, E_d^*, t') \times \delta^S(E_\circ, E_d^*, t'')dt'dt''\} , \quad (7\text{-}10)$$

where K" = a constant.

The function $A^S(E_\circ, E_d^*, t', t'')$ is derived from the correlation function of shower fluctuation $C^S(E_\circ, E_d^*, t', t'')$ as

$$A^S(E_\circ, E_d^*, t', t'') = \frac{1}{2} C^{S\,-1}(E_\circ, E_d^*, t', t''), \quad (7\text{-}11)$$

where

$$\int_0^\infty C^{S\,-1}(E_\circ, E_d^*, t', t'')C^S(E_\circ, E_d^*, t'', t)dt'' = \delta(t'-t) , \quad (7\text{-}12)$$

$\delta(t'-t)$ is the δ function.

Since the functional $F^S(E_\circ, E_d^*, \delta^S)$ is defined for the shower fluctuation instead of the global fluctuation, it is expected to be fairly independent of the detector. The normalized correlation matrix $\hat{C}_N$ obtained by a liquid argon calorimeter agrees well with the normalized correlation matrix of shower fluctuation C_N^S obtained by our gas calorimeter. This fact shows the detector independence of the correlation function $C^S(E_\circ, E_d^*, t', t'')$ and the distribution functional $F^S(E_\circ, E_d^*, \delta^S)$.

In Chapter VI-B-5, we obtained the function $C^S(E_\circ, E_d^*, t', t'')$ as the two-dimensional 2nd order Fourier series. The $C^S(E_\circ, E_d^*, t', t'')$ is a very important function in order to derive the distribution functional $F^S(E_\circ, E_d^*, \delta^S)$.

C-4. New Method of π/e Separation

As described in Chapter VI-C, the π/e separation was remarkably improved for the case of $E_e < E_\pi$ in comparison with the conventional method by the use of the variable X_G^2 defined by Eqs.(6-73), (6-74), and (6-75):

$$X^2 \equiv \delta^T A \delta = (\delta^T T^T)(TAT^T)(T\delta) = \tilde{\delta}^T D \tilde{\delta} = \sum_i d_i \tilde{\delta}_i^2 , \quad (6\text{-}73)$$

$$X_E^2 = (E - \langle E^e \rangle)^2 / 2(\sigma_E^e)^2 , \quad (6\text{-}75)$$

$$X_G^2 = X^2 + X_E^2 . \quad (6\text{-}74)$$

The method using X_G^2 is to request, for the electron identification, the fluctuations being such as expected to the electron "eigen-fluctuations" when transformed by the diagonalization matrix T. If the particle is a pion, the fluctuations thus transformed are way off from the eigenvalues for the electrons (see Chapter VI-C), hence the particle can be rejected. This method can be used by any other sampling calorimeters by making PH deviations δ_i's of the i-th chamber and correlation matrix C as follows:

$$\delta_i = p_i - \langle p_i^e \rangle ,$$

$$C_{ij} = \langle \delta_i \delta_j \rangle .$$

There are two possible reasons against improvement of the π/e separation for $E_e = E_\pi$ by any methods (see Chapters V-E, VI-C):

(1) Intrinsic limit of π/e separation performance of the calorimeter

Since incident hadron beams are mostly negative charged pions, the charge exchange interaction at very early part of the calorimeter can be one reason of this limit. The probability of the charge exchange interaction of negative charged pion with front part of our calorimeter is calculated in Appendix D and is about order 2 smaller ($\sim 10^{-5}$) compared with π/e separation factor ($\sim 10^{-3}$). Therefore, the charge exchange interaction is not the reason of limiting the π/e separation performance of our calorimeter.

(2) Electron contamination in hadron beam

The electron contamination is a more plausible reason. But unfortunately it is very difficult, in the present experiment, to estimate electron contamination quantitatively in the hadron beam of Fermilab M4 beam line.

CHAPTER VIII

CONCLUSIONS

A gas sampling electromagnetic cascade shower detector (calorimeter) was constructed using the chambers with newly developed conductive plastic tubes as sampling media. Its performance as the calorimeter was measured. The behavior of the electromagnetic cascade shower was studied by this detector. The experimental results are summarized as follows.

A. Detector Performance

A prototype of the 30° sector of the full-size end plug electromagnetic gas calorimeter for CDF has been built and its characteristics have been studied at energies from 25 GeV to 150 GeV. We obtained the following results as the performance of this calorimeter:

(1) The energy resolution at the optimized high voltage of 1.85 kV was 30 $\sqrt{t(r.l.)/E(GeV)}$ %.

(2) The spatial resolution calculated from the second pad segment was found to be 1.5 mm or better for electrons with energy equal to or greater than 50 GeV.

(3) The total charge from both pad and anode was uniform within the maximum deviation of ± 3 %.

(4) By the use of the conventional method, the pion rejection

factor at any pion energies from 75 GeV to 150 GeV was 5×10^{-3} or less with the electron retention efficiency of 85 % in the electron energy range from 25 GeV to 150 GeV. This was improved by using the information from hadron calorimeter or by applying the special method discussed in Chapter VI-C.

These characteristics meet the design specifications for CDF. Technically, it was demonstrated that the proportional chamber with conductive plastic tubes operates stably as the sampling medium for a high energy electromagnetic calorimeter.

B. High Energy Cascade Shower

The high energy electromagnetic cascade shower was observed by the use of a gas calorimeter. Its average and fluctuation properties have been studied for electron incidence at energies from 25 GeV to 100 GeV. The results were as follows:

(1) The average transition curve (shower curve) of the electromagnetic cascade shower was measured with a system of proportional chambers as sensitive media and lead plates as radiators. The correction function $\rho(E_o,E^*,s)$ for the shower curve $\Pi_A(E_o,E^*,t)$ calculated by Rossi under Approximation A was obtained for electron of energies from 25 GeV to 100 GeV. The function $\rho(E_o,E^*,s)$ is independent of incident energy in this region within the uncertainty of chamber gain. It was parametrized as

$$\rho(E_o,E^*,s) = 1.58 - 1.92s + 0.73s^2$$

with a cut-off energy $E^* = 3$ MeV.

(2) The formulation of the electromagnetic cascade shower fluctuation observed by a sampling calorimeter has been made in terms of the correlation matrix. In this formulation, the global fluctuation was separated into the shower fluctuation (sampling fluctuation) and the detector fluctuation (track length fluctuation, Landau fluctuation, and the fluctuation caused by the noise of read out electronics). For the case that the noise is negligibly small, the following assumptions about the properties of the shower and detector fluctuations are correct within the experimental error:

i) The detector fluctuation is independent of the shower fluctuation.

ii) The detector fluctuation of each chamber is independent of those of other chambers.

This is mathematically expressed as follows:

$$C_{ij} = C^S_{ij} + C^D_{ij} ,$$

$$\text{where} \quad \delta_i = \delta^S_i + \delta^D_i ,$$

$$C_{ij} = \langle \delta_i \delta_j \rangle ,$$

$$C^S_{ij} = \langle \delta^S_i \delta^S_j \rangle ,$$

$$C^D_{ij} = \langle \delta^D_i \delta^D_j \rangle \hat{\delta}_{ij} ;$$

δ_i, δ^S_i, and δ^D_i are the pulse height deviations of the i-th

chamber due to global, shower, and detector fluctuations, respectively; $\hat{\delta}_{ij}$ is the Kronecker δ.

(3) The correlation function $C^S(E_o,E_d^*,t,t')$ defined as the generalization of the correlation matrix of shower fluctuation C^S is a basic quantity of the cascade shower. Its independence from detector was shown by the comparison of our results with those of a liquid argon calorimeter. The distribution functional of pulse height deviation $F^S(E_o,E_d^*,\delta^S)$ which gives the probability of the fluctuation of shower development is approximately derived from the correlation function $C^S(E_o,E_d^*,t,t')$ for high energy cascade shower. The experimental formula of the correlation function $C^S(E_o,E_d^*,t,t')$ was represented by a two-dimensional 2nd order Fourier series (formula (6-70)) for the electromagnetic cascade shower at energies from 25 GeV to 100 GeV.

(4) The correlation matrix C is important for application. By a special method utilizing the correlation matrix C, we obtained more than factor 10 better π/e separation ($<2\times10^{-4}$) than that by the conventional method, when the electron energy E_e is less than the pion energy E_π. For the case of $E_e=E_\pi$, the possibility of the electron contamination in the hadron beam prohibited a crucial test.

APPENDIX A

FORMULATION ABOUT THE π/e SEPARATION

A-1. Event Distribution in the Five-Dimensional Space

As shown in Fig.A-1, the π/e separation analysis using conventional method (see Chapter V-E) is based on the five variables E_1, E_2, E_3, σ_2, and E_H whose meanings are as follows:

E_i = observed energy deposit of the i-th segment of EM calorimeter,

σ_2 = observed lateral spread of cascade shower at the second pad segment,

E_H = observed energy deposit in hadron calorimeter.

Each event has certain values of these five variables. Therefore, an event is a point in the five-dimensional space S defined by variables E_1, E_2, E_3, σ_2, and E_H. We define event distribution functions $n_e(E_1,E_2,E_3,\sigma_2,E_H;E_e)$ and $n_\pi(E_1,E_2,E_3,\sigma_2,E_H;E_\pi)$ in space S for electrons and pions, respectively (see Fig.A-2). The E_e and E_π are the incident energy of electrons and pions, respectively. For the actual π/e separation analysis, we have used variables E_{EM}, R_1, R_3, σ_2, and R_{EM} defined as follows:

$$E_{EM} = E_1 + E_2 + E_3 , \tag{A-1}$$

$$R_1 = E_1/E_{EM} , \tag{A-2}$$

$$R_3 = E_3/E_{EM} , \tag{A-3}$$

$$R_{EM} = \frac{C\,E_{EM}}{C\,E_{EM} + E_H} \quad , \tag{A-4}$$

where C is a constant.

The five-dimensional space S' is defined by variables E_{EM}, R_1, R_3, σ_2, and R_{EM}. We define event distribution functions $n_e'(E_{EM},R_1,R_3,\sigma_2,R_{EM};E_e)$ and $n_\pi'(E_{EM},R_1,R_3,\sigma_2,R_{EM};E_\pi)$ in space S' for electrons and pions, respectively (see Fig.A-3). The total number of events in space S' is calculated for electrons,

$$N_e^{tot}(E_e) = \int_0^\infty\int_0^1\int_0^1\int_0^\infty\int_0^1 n_e'(E_{EM},\ R_1,\ R_3,\ \sigma_2,\ R_{EM};\ E_e) \times dE_{EM}dR_1dR_3d\sigma_2dR_{EM} \quad , \tag{A-5}$$

and for pions,

$$N_\pi^{tot}(E_\pi) = \int_0^\infty\int_0^1\int_0^1\int_0^\infty\int_0^1 n_\pi'(E_{EM},\ R_1,\ R_3,\ \sigma_2,\ R_{EM};\ E_\pi) \times dE_{EM}dR_1dR_3d\sigma_2dR_{EM} \quad . \tag{A-6}$$

A-2. Definition of Electron Retention Efficiency and π/e Separation Factor

We assume volume D in space S' as shown in Fig.A-3. The number of elctrons in volume D for energy E_e is calculated as

$$N_e(E_e,\ D) = \iiiiint_D n_e'(E_{EM},\ R_1,\ R_3,\ \sigma_2,\ R_{EM};\ E_e) \times dE_{EM}dR_1dR_3d\sigma_2dR_{EM} \quad . \tag{A-7}$$

The electron retention efficiency $E_{eff}(E_e,\ D)$ is defined as the probability for electron of energy E_e to be inside of the volume D:

$$E_{eff}(E_e,\ D) \equiv \frac{N_e(E_e,D)}{N_e^{tot}(E_e)} \quad . \tag{A-8}$$

The number of pions in volume D for energy E_π is calculated as

$$N_\pi(E_\pi,\ D) = \iiiiint_D n_\pi'(E_{EM},\ R_1,\ R_3,\ \sigma_2,\ R_{EM};\ E_\pi) \times dE_{EM}dR_1dR_3d\sigma_2dR_{EM} \quad . \tag{A-9}$$

The π/e separation factor (pion rejection factor) $P_{sep}(E_\pi,\ D)$ is defined as the probability for pion of energy E_π to be inside of the volume D:

$$P_{sep}(E_\pi,\ D) \equiv \frac{N_\pi(E\ ,D)}{N_\pi^{tot}(E_\pi)} \quad . \tag{A-10}$$

Since the electron retention efficiency E_{eff} is a function of E_e and D, the volume D is a function of E_e and E_{eff}. Then,

$$P_{sep}(E_\pi,\ D) = P_{sep}(E_\pi,\ E_e,\ E_{eff}) \quad . \tag{A-11}$$

Therefore, the $P_{sep}(E_\pi,\ E_e,\ E_{eff})$ is the probability that the pion of energy E_π falls into the volume D for which the electron of energy E_e has the retention efficiency of E_{eff}. For π/e separation analysis of Chapter V-E, the volume D was defined as follows:

$$\begin{aligned}
E_{EM}^{min}(E_e) &\leq E_{EM} \leq E_{EM}^{max}(E_e) \\
R_1^{min}(E_e) &\leq R_1 \leq R_1^{max}(E_e) \\
R_3^{min}(E_e) &\leq R_3 \leq R_3^{max}(E_e) \\
\sigma_2^{min}(E_e) &\leq \sigma_2 \leq \sigma_2^{max}(E_e) \\
R_{EM}^{min}(E_e) &\leq R_{EM} \leq R_{EM}^{max}(E_e) \quad .
\end{aligned} \tag{A-12}$$

APPENDIX B

ANALYTIC EXPRESSION OF THE AVERAGE TRANSITION CURVE OF ELECTROMAGNETIC CASCADE SHOWER

The following approximations are used in Rossi's Approximation A [RO 41,NI 67]:

1) The energy dependence of interaction cross sections of shower electron and photon is neglected by the use of the asymptotic forms.

2) Collision processes of electron are neglected.

3) Compton scattering is neglected.

4) The finite production angle is neglected.

In this approximation the following parametric equation is obtained for the number of shower electrons $\Pi_A(E_\circ, E^*, t)$ of energies larger than the cut-off energy E^* (kinetic energy) at a depth t in radiation length, for a primary energy $E_\circ$:

$$\Pi_A(E_\circ, E^*, t) = \left\{ \frac{H(s)}{\sqrt{2\pi}[\lambda_1''(s)t + (1/s^2)]^{1/2}} \right\} \frac{1}{s} \left(\frac{E_\circ}{E^*}\right)^s e^{\lambda_1(s)t} . \tag{B-1}$$

Here the "age parameter" s is a quantity which increases with increasing absorber thickness t and which is unity at the shower maximum. It is related to $E_\circ$, E^*, and t as follows:

$$t = -\frac{1}{\lambda_1'(s)}\left[\ell n \frac{E_\circ}{E^*} - \frac{1}{s}\right] . \tag{B-2}$$

The functions H(s) and $\lambda_1(s)$ and its derivatives $\lambda_1'(s)$, $\lambda_1''(s)$ are calculated from the following equations:

$$H(s) = \frac{\mu_\circ + \lambda_1(s)}{\lambda_1(s) - \lambda_2(s)} , \tag{B-3}$$

$$\lambda_1(s) = -\frac{[A(s) + \mu_\circ]}{2} + \frac{1}{2}\{[A(s) - \mu_\circ]^2 + 4B(s)C(s)\}^{1/2} , \tag{B-4}$$

$$\lambda_2(s) = -\frac{[A(s) + \mu_\circ]}{2} - \frac{1}{2}\{[A(s) - \mu_\circ]^2 + 4B(s)C(s)\}^{1/2} , \tag{B-5}$$

$$A(s) = 1.36\frac{d}{ds}\ell n(s+1)! - \frac{1}{(s+1)(s+2)} - 0.075 , \tag{B-6}$$

$$B(s) = 2\left[\frac{1}{s+1} - \frac{1.36}{(s+2)(s+3)}\right] , \tag{B-7}$$

$$C(s) = \frac{1}{s+2} + \frac{1.36}{s(s+1)} , \tag{B-8}$$

$$\mu_\circ = 0.773 . \tag{B-9}$$

APPENDIX C

GAIN CALIBRATION OF CHAMBERS USING GAUSSIAN FIT

For the study of detector performance as shown in Chapter V, it is not necessary to know the number of shower electrons. The charge was used as the unit of the calorimeter output. After the calibration factor of ADC was multiplied to chamber output, the relative gain of each chamber was adjusted by assuming that, in average, the longitudinal shower profile is a smooth function of depth in the unit of radiation length. After these adjustment the shower curve became as shown in Fig.V-2.

For the study of cascade shower behavior, we need to know the absolute number of shower electrons in each chamber. Since electromagnetic calorimeter has the total length of about one absorption length, the 35 % of pion events has no hadronic interaction in the calorimeter. The gain calibration of chambers was made by the measurement of energy losses of these pions. The average pulse height of 75 GeV non-interacting (no hadronic interaction) pions is measured and considered as it is equivalent to that of a single shower electron. The procedure of gain calibration of chambers is as follows.

As the initial gain of the chamber, we have used the same gain as that used for the analysis of detector performance. The

non-interacting pion events were selected by the use of a cut on the total pulse height distribution of pions (A trigger events). The pedestal measurement was made by using A' trigger events (see Chapter IV-C). The A' trigger gave us more accurate pedestal than the B trigger, since it measured pedestal during a beam spill instead of measuring pedestal during two beam spills (B trigger). Because of the scheme of A' trigger, it included the events which had a part of the pion signal. Therefore we made a cut on the total pulse height distribution not only for A trigger events but also for A' trigger events. The total pulse height distribution with a cut line is shown in Figs.C-1(a),(b) for A' and A triggers, respectively.

Since the noise of each chamber was fairly large compared with a non-interacting pion signal, the pulse height distribution was Gaussian instead of Landau distribution. Therefore we made Gaussian fit not only for the pedestal (A' trigger) distribution but also for the pulse height (A trigger) distribution of non-interacting pions. Figs.C-2(a)-(d) show pedestal distributions with fitted Gaussian distribution for chamber plane No. 1, 12, 24, and 37. Since the chambers of plane No. 1, 26, 27, and 29 were not working, we renumbered plane numbers from No. 2 $\sim$ 38 to No. 1 $\sim$ 37. The same distributions of non-interacting pion pulse height are shown in Figs.C-3(a)-(d) for same chambers. The fit region in the distribution was from -3.0σ to $+3.0\sigma$ for each chamber, where the σ is the standard deviation of the fitted

Gaussian distribution.

The real mean pulse height of non-interacting pions was obtained by the subtraction of the mean of fitted Gaussian distribution for pedestal from that for the pulse height of non-interacting pions. The result is tabulated in Table C-1. The average uncertainty of the real mean pulse height of non-interacting pions over all working chambers was 12 %. For the absolute gain, the pulse height linearity and energy resolution of the calorimeter are almost the same as those for the gain used for the analysis of detector performance. Energy resolutions derived with the absolute gain and the gain used for the analysis of detector performance were 25.2 $\%/\sqrt{E}$ and 24.6 $\%/\sqrt{E}$, respectively.

APPENDIX D

CALCULATION OF THE PROBABILITY OF CHARGE EXCHANGE INTERACTION

The probability of charge exchange interaction of negative charged pion with front part of our calorimeter is calculated as follows. The total cross section of the interaction

$$\pi^- + p \rightarrow \pi^\circ + n$$

is estimated from lower energy data (momentum of incident pion = 5 GeV/c $\sim$ 20 GeV/c) to be about 4 μb for 75 GeV/c pion incidence [BR 72]. Interaction probability P is calculated by

$$P = \sigma_A \times \ell \times \rho \times N_A/A \ , \qquad (D\text{-}1)$$

where σ_A = cross section for the target material having atomic weight A,

ℓ = length of target material,

ρ = density of target material,

N_A = Avogadro number,

A = atomic weight of target material.

We assume followings as the front part material of our calorimeter (see Table III-1):

Vessel wall	Fe	1.27 cm
Holder plate	Al	2.54 cm
The 1st and 2nd lead plates	Pb	0.6 cm

By taking into account the nuclear dependence of cross section,

the probability P is calculated as follows:

$$P = 4 \times 10^{-30} \times 6.02 \times 10^{23} \times \{(26)^{2/3} / 55.8 \times 1.27 \times 7.87 + (13)^{2/3} / 27.0 \times 2.54 \times 2.70 + (82)^{2/3} / 207.2 \times 0.6 \times 11.35\} = 0.9 \times 10^{-5}.$$

REFERENCES

[AM 83] AMY, A Letter of Intent for A High Resolution Lepton Detector for TRISTAN, (1983).

[AN 78] R.L. Anderson et al., IEEE Trans. Nucl. Sci. NS-25 (1978) 340.

[AT 75] M. Atac, editor of the Proceedings of the Calorimeter Workshop, FNAL, 1975.

[AT 81a] M. Atac, IEEE Trans. Nucl. Sci. NS-28 (1981) 492.

[AT 81b] M. Atac et al., IEEE Trans. Nucl. Sci. NS-28 (1981) 500.

[AT 83] M. Atac et al., Nucl. Instr. and Meth. 205 (1983) 113.

[BA 78] G. Battistoni et al., Nucl. Instr. and Meth. 152 (1978) 423.

[BA 79] A. Babaev et al., Nucl. Instr. and Meth. 160 (1979) 427.

[BA 82] C. Baltay and H. Gordon, in the Proceedings of the 1982 DPF Summer Study on Elementary Particle Physics and Future Facilities, Snowmass, 1982, edited by R. Donaldson et al., p.500; S.H. Aronson et al., in the same proceedings, p.505.

[BE 64] E.E. Becklin and J.A. Earl, Phys. Rev. 136B (1964) 237.

[BL 50] W. Blocker, R. Kenney, and W. Panofsky, Phys. Rev. 79 (1950) 419.

[BR 72] E. Bracci et al., CERN/HERA 72-1 (1972) 98.

[BU 73] Yu.B. Bushnin et al., Nucl. Instr. and Meth. 106 (1973) 493.

[BU 74] Yu.B. Bushnin et al., Nucl. Instr. and Meth. 120 (1974) 391.

[BU 78] C. Buchanan et al., UCLA Preprint (1978).

[CE 77] C. Cerri and F. Sergiampietri, Nucl. Instr. and Meth. 141 (1977) 207.

[CO] Conductive plastic tubes described in this paper are now commercially available at Tokyo Printing Ink Mfg. Co. Ltd., No. 7-15, Tabatashinanomachi, 2-chome, Kita-ku, Tokyo, Japan.

[CR 67] C.J. Crannell, Phys. Rev. 161 (1967) 310.

[DE 81] Design Report for the Fermilab Collider Detector Facility (CDF), August, 1981.

[EN 83] R. Engelmann et al., Nucl. Instr. and Meth. 216 (1983) 45.

[FA 78] C.W. Fabjan et al., Nucl. Instr. and Meth. 158 (1978) 93.

[FI 78] H.G. Fischer, Nucl. Instr. and Meth. 156 (1978) 81.

[FO 78] R.L. Ford and W.R. Nelson, SLAC-Report 210 (1978).

[GE 78] E. Gebathuler et al., Nucl. Instr. and Meth. 157 (1978) 47.

[GR 81] D. Green, Fermilab Internal Report (1981).

[HA 83a] Y. Hayashide et al., Nucl. Instr. and Meth. 216 (1983) 127.

[HA 83b] Y. Hayashide et al., Nucl. Instr. and Meth. 216 (1983) 135.

[HA 84] Y. Hayashide et al., IEEE Trans. Nucl. Sci. NS-31 (1984) 74.

[HAD] The hadron calorimeter module was constructed by W. Carithers, W. Chinowsky, R. Ely, M. Gold, P. Rowson, and K. Shinsky of Lawrence Berkeley Laboratory, University of California. We thank them for making their data available to us.

[HI 76] D. Hitlin et al., Nucl. Instr. and Meth. 137 (1976) 225.

[HU 72] E.B. Hughes et al., Stanford University report, No. 627 (1972).

[IW 80] S. Iwata DPNU-13-80.

[JA 70] R. Jakeway and I.R. Calder, Nucl. Instr. and Meth. 84 (1970) 79.

[KN 75] J.P. Knauer and D.E. Yount, Nucl. Instr. and Meth. 129 (1975) 91.

[KO 82] K. Kondo, in the Proceedings of the Gas Calorimeter Workshop, Fermilab, 1982, edited by M. Atac, p63.

[LA 44] L. Landau, J. Exp. Phys. (USSR) 8 (1944) 201.

[LE 63] H. Lengeler, W. Tejessy, and M. Deutschmann, Z. Phys. 175 (1963) 283; Nuovo Cimento 28 (1963) 1501.

[LO 79] E. Locci and M. Spiro, Nucl. Instr. and Meth. 164 (1979) 37.

[ME 70] H. Messel and D.F. Crawford, Electron - Photon Shower Distribution Function (Pergamon, New York, 1970).

[ME 75] C.A. Meegan and J.A. Earl, Astrophys. J. 197 (1975) 219.

[MI 81] K. Mitsui, Nucl. Instr. and Meth. 185 (1981) 433.

[MU 67] V.S. Murzin, Progr. Element. Part. Cosmic Ray Physics (1967) 247.

[MU 72] D. Muller, Phys. Rev. 5 (1972) 2677.

[MU 81] J.J. Mueller et al., IEEE Trans. Nucl. Sci. NS-28 (1981) 496.

[NE 66] W.R. Nelson et al., Phys. Rev. 149 (1966) 201.

[NI 67] J. Nishimura, in Encyclopedia of Physics, edited by S. Flugge (Springer, Berlin, 1967), Vol. XLVI/2, p.1.

[RO 41] B. Rossi and K. Greisen, Rev. Mod. Phys. 13 (1941) 249; B. Rossi, High-Energy Particles (Prentice-Hall, Englewood Cliffs, N.J., 1961)

[SO 73] D.I. Sober et al., Nucl. Instr. and Meth. 109 (1973) 29.

[ST 78] S.L. Stone et al., Nucl. Instr. and Meth. 151 (1978) 387.

[TH 64] H. Thom, Phys. Rev. 136B (1964) 447.

[WI 74] W.J. Willis and V. Radeka, Nucl. Instr. and Meth. 120 (1974) 221.

[YU 70] T. Yuda et al., Nuovo Cimento 65A (1970) 205; Nucl. Instr. Meth. 73 (1969) 301.

TABLE CAPTIONS

Table I-1 Resolution of sampling calorimeters.

Table III-1 Configuration of chambers in the electromagnetic gas calorimeter. All 38 chambers have pad patterns on one side. Chambers No. 6 through No. 25 have strips on the other side, θ - strips on even-numbered chambers and ϕ - strips on odd-numbered chambers.

Table IV-1 Data tape format.

Table VI-1 Correspondence between chamber plane number and the depth in radiation length.

Table VI-2 Correlation matrix elements C_{ij}'s of the electromagnetic cascade shower for energies of a) 25 GeV, b) 50 GeV, c) 75 GeV, and d) 100 GeV.

Table VI-3 Eigenvalues and corresponding eigenvectors of the correlation matrix C for energies of a) 25 GeV, b) 50 GeV, c) 75 GeV, and d) 100 GeV.

Table VI-4 Diagonal elements of the correlation matix of shower fluctuation C^S for energies from 25 GeV to 100 GeV.

Table VI-5 Diagonal elements of the correlation matix of detector fluctuation C^D for energies from 25 GeV to 100 GeV.

Table VI-6 Eigenvalues and corresponding eigenvectors of the correlation matrix of shower fluctuation C^S for energies of a) 25 GeV, b) 50 GeV, c) 75 GeV, and d) 100 GeV.

Table VI-7 Optimized coefficient values [in unit of (No. of electrons)^2] of the fit of correlation matrix C^S to the two dimensional 2nd order Fourier series.

Table C-1 Non-interacting (no hadronic interaction) pion pulse height obtained by the Gaussian fit for each chamber.

FIGURE CAPTIONS

Fig. I-1 Elevation view of the CDF central detector.

Fig. I-2 Layout of the prototype module for the CDF end plug electromagnetic gas calorimeter.

Fig. II-1 Structure and dimensions of the extruded conductive plastic tube.

Fig. II-2 Cutting of wall sheets of the conductive plastic tube for resistivity measurements.

Fig. II-3 Connection of a lead wire to the conductive plastic tube. A conductive glue "GRAFIT 33" gives a good contact between the copper tape and the conductive plastic.

Fig. II-4 (a) Structure and elements of a proportional counter made of conductive plastic cathode. Wire setting in the tube is determined by V-shaped holes in the end caps. (b) Cathode and anode connections used for the present measurements. The cathode strips are 1 cm wide and the anode wire is 30 μm or 50 μm in diameter.

Fig. II-5 Typical (a) anode and (b) cathode signals observed with a transient digitizer (10 nsec step) connected to the output of the amplifier. The original signals are inverted by the amplifier. The wire diameter is 30 μm, and the applied high voltage is 2.2 kV. The gas is 80 % Ar and 20 % isobutane mixture with a flow rate of 100 cc/minute. The amplifier gain is about 10. The anode and each strip of cathode are connected with 1 kΩ resistor to the ground.

Fig. II-6 Typical pulse height distribution of a single event on cathode strips read out with a voltage sensitive ADC, LeCroy 2259A. The Gaussian fit for the distribution gives a FWHM of 3.6 cm and a precision of the centroid of 150 μm.

Fig. II-7 Spread of cathode induced signal along the anode wire vs. resistivity of the tube. The spread σ is defined by the standard deviation in the Gaussian fitting, and the error indicates the fluctuation in σ for about ten events.

Fig. II-8 Gain uniformity of anode signal along the tube.

Fig. II-9 Pulse height change of anode signal caused by the bend of the tube.

Fig. II-10 Pulse height of anode signal with respect to the distance from the tube end (edge effect on the pulse height).

Fig. II-11 (a) Setting of cathode strips for the measurement of two-dimensional distribution of the cathode signal. The distributions of the cathode signal parallel and perpendicular to the anode are observed at $\theta = 0°$ and $\theta = 90°$, respectively. (b) Angular dependence of the half maximum point of the cathode signal picked up with parallel strips.

Fig. III-1 Structure of a proportional chamber. The conductive plastic tubes array was sandwiched with copper-clad G-10 panels.

Fig. III-2 Structure of the proportional tubes which were used in the electromagnetic gas calorimeter.

Fig. III-3 Patterns and dimensions of pick-up electrodes; (a) pad, (b) θ-strip, and (c) ϕ-strip.

Fig. III-4 Photograph of combined set up of the electromagnetic and hadron gas calorimeters.

Fig. IV-1 Layout of Fermilab M4 beam line. Scintillation counters S1, S2, S3 and VETO defined a passage of a particle. Multiwire proportional chambers, H1-H5 and V1-V3, together with string of magnets were used for the measurement of beam particle momenta.

Fig. IV-2 The total charge distribution for 25, 50, 75, 100, 125 and 150 GeV electrons. A peak around 0 pC shows hadron contamination.

Fig. IV-3 Block diagram of the fast electronics.

Fig. IV-4 Block diagram of the data acquisition system.

Fig. V-1 Signals from a pad tower in the second segment and an anode of the 12-th chamber in the following time scales; (a) 50 nsec/div. and (b) 200 nsec/div.

Fig. V-2 Longitudinal shower profiles of 25, 50, 75, 100 and 150 GeV electrons at $\eta = 1.474$.

Fig. V-3 Logarithmic plots of the total charge versus the high voltage for 100 GeV electrons at $\eta = 1.474$.

Fig. V-4 Plots of the total charge as a function of electron energy at the high voltages of 1.80, 1.85, 1.90, and 1.95 kV; (a) for pad and (b) for anode.

Fig. V-5 (a) Plots of the charge from each chamber plane at 1.85 kV versus that at 1.75 kV for 100 GeV electrons. (b) Plots of the charge at 2.10 kV versus that at 1.85 kV for 100 GeV electrons. The numbers by the data points show individual chamber plane numbers.

Fig. V-6 Energy resolution dependence upon the high voltage for 50 GeV and 100 GeV electrons.

Fig. V-7 Energy resolution as a function of electron energy at the high voltage of 1.85 kV. The energy resolution for anode and pad are 23.5 % / $\sqrt{E(\text{GeV})}$ and 24.2 % / $\sqrt{E(\text{GeV})}$, respectively.

Fig. V-8 Typical lateral shower profiles in the first, second, and third pad segments; (a) for 100 GeV electrons and (b) for 100 GeV pions.

Fig. V-9 Position resolution as a function of electron energy for pad segments and strip segments.

Fig. V-10 The second moment as a function of electron energy for pad segments. The error bar shows not the error of the mean but the standard deviation of the distribution of the second moment.

Fig. V-11 Ratio of the total charge from pads to that from anodes as a function of pseudo-rapidity η for 50 GeV electrons.

Fig. V-12 The total charge from anodes as a function of η for 50 GeV electrons.

Fig. V-13 Energy resolution as a function of η for 50 GeV electrons.

Fig. V-14 The ratio of energy deposit in the third pad segment to the total energy deposit (R_3) with respect to the total energy deposit (E_{EM}). The boundaries for containing 95 % electrons were shown in broken lines; (a) for 25, 50, and 100 GeV electrons and (b) for 100 GeV pions.

Fig. V-15 Pion rejection factor versus the electron retention

efficiency for various kinds of cuts; (a) for E_π = 75 GeV and E_e = 75 GeV, (b) for E_π = 150 GeV and E_e = 150 GeV, and (c) for E_π = 150 GeV and E_e =75 GeV.

Fig. V-16 Pion rejection factor versus the ratio of electron energy to pion energy (E_e/E_π) with the electron retention efficiency of 85 %; (a) for the cut (E_{EM} &R_1&R_3&σ_2) using only EM calorimeter and (b) for the cut (E_{EM}&R_1&R_3&σ_2&R_{EM}) using both EM and hadron calorimeters.

Fig. VI-1 Observed average shower curve $P_m(E_o,t)$ and the calculated shower curve $\pi_A(E_o,E^*,t)$ under Approximation A with cut-off energies E* of (a) 3 MeV, (b) 7.4 MeV, and (c) 20 MeV for incident energy E_o = 75 GeV.

Fig. VI-2 Shower curve correction function $\rho(E_o,E^*,s)$ dependence upon the shower age s for incident energy E_o = 75 GeV with cut-off energies E* of (a) 3 MeV, (b) 7.4 MeV, and (c) 20 MeV.

Fig. VI-3 Shower curve correction function $\rho(E_o,E^*,s)$ with respect to the shower age s for incident energies E_o of 25, 50, 75, and 100 GeV [present], and 15 GeV [MU 72], with cut-off energy E^* = 3 MeV.

Fig. VI-4 Event-by-event shower curves and the average shower curve for electrons of energies of (a) 25 GeV, (b) 50 GeV, (c) 75 GeV, and (d) 100 GeV.

Fig. VI-5 Pulse height distribution of individual chambers (plane No. 1, 5, 11, 21, 29, and 37) for 25 GeV electrons.

Fig. VI-6 Pulse height distribution of indivdual chambers (plane No. 1, 5, 11, 21, 29, and 37) for 50 GeV electrons.

Fig. VI-7 Pulse height distribution of individual chambers (plane No. 1, 5, 11, 21, 29, and 37) for 75 GeV electrons.

Fig. VI-8 Pulse height distribution of individual chambers (plane No. 1, 5, 11, 21, 29, and 37) for 100 GeV electrons.

Fig. VI-9 Average shower curves of 25, 50, 75, and 100 GeV electrons.

Fig. VI-10 Standard deviations of chamber pulse height for 25, 50, 75, and 100 GeV electrons.

Fig. VI-11 Ratios of the standard deviation to the average of pulse height of chambers for 25, 50, 75, and 100 GeV electrons.

Fig. VI-12 (a) Angular distribution of shower electrons. (b) Same for electron energies below 3 MeV.

Fig. VI-13 Energy resolution of the "standard calorimeter" as a function of incident energy. The contributions from sampling, track length, and Landau fluctuations are indicated.

Fig. VI-14 Energy resolution as a function of plate thickness for 1 GeV incident energy.

Fig. VI-15 Correlation matrix element C_{ij} with respect to j for electrons of energies (a) 25 GeV, (b) 50 GeV, (c) 75 GeV, and (d) 100 GeV.

Fig. VI-16 Diagonal element C_{ii} of correlation matrix with respect to i for 25, 50, 75, and 100 GeV electrons.

Fig. VI-17 Three-dimensional plot of correlation matrix elements C_{ij}'s for electrons of energies (a) 25 GeV, (b) 50 GeV, (c) 75 GeV, and (d) 100 GeV.

Fig. VI-18 Normalized correlation matrix element $(C_N)_{ij}$ with respect to j for electrons of energies (a) 25 GeV, (b) 50 GeV, (c) 75 GeV, and (d) 100 GeV.

Fig. VI-19 Relation between definitions of matrices C, C^S, and C^D.

Fig. VI-20 Eigenvalues λ_i's of correlation matix C.

Fig. VI-21 Elements of eigenvectors x_i (i=1∿6) of correlation matrix C.

Fig. VI-22 Two-dimensional distribution of dependent PH deviations (δ_i, δ_j) for 75 GeV electrons.

Fig. VI-23 Two-dimensional distribution of independent PH deviations ($\tilde{\delta}_i$, $\tilde{\delta}_j$) for 75 GeV electrons.

Fig. VI-24 Diagonal element C^S_{ii} of the correlation matrix of shower fluctuation with respect to i for 25, 50, 75, and 100 GeV electrons.

Fig. VI-25 Diagonal element C^D_{ii} of the correlation matrix of detector fluctuation with respect to i for 25, 50, 75, and 100 GeV electrons.

Fig. VI-26 Normalized correlation matrix element of shower fluctuation $(C^S_N)_{ij}$ with respect to j for electrons of energies (a) 25 GeV, (b) 50 GeV, (c) 75 GeV, and (d) 100 GeV.

Fig. VI-27 Eigenvalues λ^S_i's of the correlation matrix of shower fluctuation C^S.

Fig. VI-28 Elements of eigenvectors $\mathbf{x}^S_i$ (i=1∿6) of the correlation matrix of shower fluctuation C^S.

Fig. VI-29 Energy resolution dependence upon the $1/\sqrt{E_o}$ for global $(\sigma_E/\langle E\rangle)$, shower $(\sigma^S_E/\langle E\rangle)$, and detector $(\sigma^D_E/\langle E\rangle)$ fluctuations, where E_o is the incident energy.

Fig. VI-30 σ_E/σ^S_E plotted as a function of incident energy E_o.

Fig. VI-31 S_ℓ with respect to ℓ for 75 GeV electrons.

Fig. VI-32 $S^2_\ell\lambda^S_\ell$ with respect to ℓ for (a) 25 GeV, (b) 50 GeV, (c) 75 GeV, and (d) 100 GeV electrons.

Fig. VI-33 Three-dimensional plot of the correlation matrix elements C^S_{ij}'s of shower fluctuation for (a) 25 GeV, (b) 50 GeV, (c) 75 GeV, and (d) 100 GeV electrons.

Fig. VI-34 Three-dimensional plot of the reproduced correlation matrix elements C^S_{ij}'s of shower fluctuation for (a) 25 GeV, (b) 50 GeV, (c) 75 GeV, and (d) 100 GeV electrons.

Fig. VI-35 Comparison of the correlation matrix element of shower fluctuation C^S_{ij} (error bars) with the fitted function of Fourier series (solid line) for 75 GeV electrons.

Fig. VI-36 Comparison of the diagonal element C^S_{ii} (error bars) of the correlation matrix of shower fluctuation with the fitted function of Fourier series (solid line) for 75 GeV electrons.

Fig. VI-37 Optimized coefficient value of the two-dimensional 2nd order Fourier series as a function of incident energy.

Fig. VI-38 Distribution of the first independent PH deviation δ_1; (a) for 50 GeV electrons and (b) for 100 GeV pions.

Fig. VI-39 Distribution of the 2nd independent PH deviation δ_2; (a) for 50 GeV electrons and (b) for 100 GeV pions.

Fig. VI-40 X^2_G distribution; (a) for 50 GeV electrons and (b) for 100 GeV pions, where the X^2_G was calculated by the use of the average shower curve of 50 GeV electrons.

Fig. VI-41 X^2_G distribution; (a) for 100 GeV electrons and (b) for 100 GeV pions, where the X^2_G was calculated by the use of the average shower curve of 100 GeV electrons.

Fig. VI-42 Pion rejection factor versus the electron retention efficiency for X^2_G cut; (a) for E_π = 75 GeV and E_e = 75 GeV, (b) for E_π = 100 GeV and E_e = 100 GeV, and (c) for E_π = 100 GeV and E_e = 50 GeV.

Fig. VI-43 Pion rejection factor versus the ratio of electron energy to pion energy (E_e/E_π); (a) for X^2_G cut with the electron retention efficiency of 85 %, (b) for X^2_G cut with the electron retention efficiency of 98 %, and (c) for $E\&R_1\&R_3$ cut with the electron retention efficiency of 85 %.

Fig. VII-1 Shower curve correction factors $\rho(s)$ estimated by Mitsui from the results obtained by many authors including him for lead radiator [MI 81]. Data points are as follows:
(1) cloud chamber [TH 64,BE 64] ϕ : 1 GeV, ⋈ : 0.5 GeV, ⋐ : 0.99 GeV, ⋈ : 0.53 GeV; (2) bubble chamber [LE 63] ⧫ : 0.37 GeV, ◆ : 0.19 GeV; (3) scintillation counter [JA 70,MU 72,ME 75] ⊗ : 15 GeV, ↑ : 10 GeV, ⧖ : 2 GeV, ⧗ : 6 GeV, ● : 4 GeV, x : 3 GeV, △ : 2 GeV, □ : 1.5 GeV, ◹ : 1 GeV, ◪ : 0.5 GeV, ▲ : 7.65 GeV, ○: 5 GeV, ⊖ : 3 GeV, ⊕ : 1.75 GeV, ▽ : 1 GeV; (4) proportional chamber [MI 81] ◓ : 9 GeV, ⊙ : 0.6 GeV.

Fig. VII-2 Normalized correlation function $C_N(t,t')$ plotted as a function of t' for the results obtained by a liquid argon calorimeter [CE 77] and a gas calorimeter [present]. The normalized correlation function of shower fluctuation $C^S_N(t,t')$ was also plotted for the result obtained by a gas calorimeter [present].

Fig. A-1 Output variables of the electromagnetic and hadron

calorimeters. They were used for the π/e separation.

Fig. A-2 Electron and pion distributions in the five-dimensional space S defined by the variables E_1, E_2, E_3, σ_2, and E_H.

Fig. A-3 Electron and pion distributions in the five-dimensional space S' defined by the variables E_{EM}, R_1, R_3, σ_2, and R_{EM}.

Fig. C-1 The total pulse height distribution of the EM gas calorimeter for 75 GeV pions; (a) for A' trigger and (b) for A trigger.

Fig. C-2 Pedestal distribution (pulse height distributions for A' trigger events) of chamber with fitted Ganssian distribution for plane No. 1, 12, 24, and 37.

Fig. C-3 Pulse height distribution of chamber for non-interacting (no hadronic interaction) pions with fitted Gaussian distribution for plane No. 1, 12, 24, and 37.

Table I-1 Resolution of Sampling Calorimeters.

Detector type	Resolution $\frac{\sigma}{\langle E\rangle} \times \sqrt{E}$ [% $GeV^{1/2}$]	Resolution $\frac{\sigma}{\langle E\rangle} \times \sqrt{\frac{E}{t}}$ [% $(GeV/r.\ell.)^{1/2}$]	Energy Range [GeV]	Absorber Thickness [r.ℓ.]	Ref
Liquid Argon	8	27	2.5 ~ 11	Fe 0.085	[WI 74]
	8	15	0.75 ~ 4	Pb 0.27	[FA 78]
	9.5	15	0.125 ~ 4	Pb 0.39	[HI 76]
	7	29	20 ~ 40	Fe 0.057	[CE 77]
	9.5	33	3 ~ 13	Fe 0.085	[BA 79]
Plastic Scintillator	11	13	0.1 ~ 2.4	Pb 0.75	[ST 78]
	18.3	14	3 ~ 50	Pb 1.68	[KN 75]
	25	16	0.2 ~ 15	Pb 2.5	[MU 72]
	25	33	15 ~ 40	Fe 0.57	[BU 74]
	13	22	5 ~ 10	Pb 0.36	[LO 79]
Gas Chamber	17	24	0.5 ~ 15	Pb 0.50	[AN 78]
	40	32	0.5 ~ 15	Fe 1.53	[AN 78]
	17	35	0.5 ~ 3.2	Pb 0.23	[MU 81]
	24	29	10 ~ 46	Pb 0.68	[AT 81b]
	17	30	0.5 ~ 12	Pb 0.32	[BU 78]

Table III-1

Configuration of Chambers in the Electromagnetic Gas Calorimeter.

Vessel Wall Fe 1/2 in. 0.722 rad l.
Holder plate Al 1 in. 0.286 rad l.

Chamber No.				
1	Pad Segment-I 2.82 rad l.			
2				
3				
4				
5				
6	Pad Segment-II 11.29 rad l.	θ-strip No. 1	θ-strip Segment-I	φ-strip No. 1
7				φ-strip No. 2
8		θ-strip No. 2		
9				φ-strip No. 3
10		θ-strip No. 3		φ-strip No. 4
11				φ-strip No. 5
12		θ-strip No. 4		φ-strip No. 6
13				φ-strip No. 7
14		θ-strip No. 5		φ-strip No. 8
15				φ-strip No. 9
16		θ-strip No. 6	θ-strip Segment-II	φ-strip No.10
17				
18		θ-strip No. 7		
19				
20		θ-strip No. 8		
21				
22		θ-strip No. 9		
23				
24		θ-strip No.10		
25				
26	Pad Segment-III 7.34 rad l.			
27				
28				
29				
30				
31				
32				
33				
34				
35				
36				
37				
38				

Table IV-1 Data Tape Format.

1st Word	No. of bytes of this event
2nd "	Trigger type
3rd "	Run No.
4th "	Event No.
5th "	No use
6th "	16 ch coincidence resister
7th ~ 22nd "	No use
23rd "	Word count for ADC 2285A/15 data
24th "	Controll word for ADC 2285A/15 data
25th ~ 336th "	ADC 2285A/15 data (312 words)
337th "	Word count for PWC data
338th "	Controll word for PWC data
339th ~ 346th "	Variable length PWC data (typically 8 words)
347th "	Controll word for PWC data

Table VI-1

Correspondence between Chamber Plane Number and the Depth in Radiation Length.

Chamber Plane No.	Depth (r.ℓ.)	Chamber Plane No.	Depth (r.ℓ.)
1	2.21	21	13.98
2	2.80	22	14.57
3	3.39	23	15.16
4	3.98	24	15.75
5	4.56	25	16.33
6	5.15	26	16.92
7	5.74	27	17.51
8	6.33	28	18.10
9	6.92	29	18.69
10	7.51	30	19.28
11	8.10	31	19.87
12	8.68	32	20.45
13	9.27	33	21.04
14	9.86	34	21.63
15	10.45	35	22.22
16	11.04	36	22.81
17	11.63	37	23.40
18	12.22		
19	12.80		
20	13.39		

Table VI-2(a) Correlation Matrix elements C_{ij} for 25 GeV.

1	614.	466.	368.	439.	513.	413.	277.	184.	78.	-16.
	-154.	-159.	-257.	-260.	-264.	-268.	-278.	-194.	-190.	-190.
	-135.	-137.	-110.	-106.	-93.	-80.	-67.	-60.	-53.	-40.
	-32.	-31.	-22.	-16.	-20.	-13.	-14.			
2	466.	1077.	630.	773.	885.	740.	576.	374.	80.	-23.
	-231.	-282.	-426.	-425.	-434.	-443.	-449.	-349.	-317.	-338.
	-235.	-244.	-174.	-196.	-167.	-138.	-108.	-98.	-68.	-89.
	-54.	-44.	-28.	-21.	-24.	-20.	-16.			
3	368.	630.	774.	750.	904.	775.	590.	408.	138.	20.
	-192.	-249.	-363.	-418.	-427.	-436.	-456.	-349.	-298.	-317.
	-234.	-250.	-168.	-191.	-164.	-137.	-110.	-95.	-81.	-68.
	-49.	-44.	-29.	-22.	-26.	-17.	-18.			
4	439.	773.	750.	1705.	1330.	1265.	963.	752.	329.	142.
	-175.	-336.	-519.	-620.	-631.	-642.	-673.	-573.	-467.	-458.
	-358.	-387.	-250.	-283.	-248.	-212.	-177.	-146.	-115.	-102.
	-72.	-63.	-50.	-30.	-40.	-22.	-26.			
5	513.	885.	904.	1330.	2411.	1673.	1445.	1079.	454.	252.
	-202.	-394.	-663.	-769.	-811.	-853.	-881.	-698.	-592.	-609.
	-482.	-497.	-345.	-379.	-328.	-277.	-226.	-196.	-166.	-137.
	-102.	-83.	-58.	-34.	-47.	-26.	-33.			
6	413.	740.	775.	1265.	1673.	2635.	1603.	1257.	668.	401.
	-31.	-322.	-584.	-744.	-834.	-924.	-954.	-759.	-646.	-663.
	-515.	-553.	-373.	-397.	-351.	-306.	-260.	-219.	-178.	-132.
	-111.	-91.	-71.	-44.	-54.	-23.	-34.			
7	277.	578.	590.	963.	1445.	1603.	2440.	1256.	736.	577.
	76.	-250.	-464.	-614.	-698.	-782.	-832.	-700.	-609.	-649.
	-500.	-508.	-356.	-415.	-366.	-316.	-266.	-219.	-171.	-128.
	-114.	-79.	-64.	-37.	-46.	-26.	-28.			
8	184.	374.	408.	752.	1079.	1257.	1256.	2173.	818.	665.
	248.	-52.	-256.	-447.	-567.	-646.	-679.	-620.	-491.	-574.
	-441.	-462.	-335.	-361.	-316.	-270.	-225.	-183.	-141.	-126.
	-97.	-66.	-58.	-32.	-44.	-20.	-24.			
9	78.	80.	138.	329.	454.	668.	736.	818.	1493.	657.
	351.	99.	-61.	-105.	-231.	-357.	-437.	-389.	-299.	-349.
	-288.	-299.	-246.	-273.	-238.	-204.	-170.	-135.	-100.	-78.
	-64.	-32.	-34.	-22.	-23.	-7.	-12.			
10	-16.	-23.	20.	142.	252.	401.	577.	665.	657.	1555.
	513.	275.	101.	-11.	-124.	-236.	-318.	-280.	-260.	-286.
	-251.	-261.	-205.	-213.	-163.	-173.	-134.	-122.	-90.	-72.
	-68.	-31.	-42.	-24.	-28.	-13.	-13.			
11	-154.	-251.	-192.	-175.	-202.	-31.	76.	248.	351.	513.
	1504.	371.	297.	238.	118.	-1.	-80.	-47.	-69.	-71.
	-81.	-76.	-84.	-109.	-99.	-88.	-78.	-61.	-44.	-36.
	-45.	-25.	-33.	-17.	-11.	-8.	-7.			
12	-159.	-282.	-249.	-336.	-396.	-322.	-250.	-52.	99.	275.
	371.	1232.	432.	334.	263.	192.	129.	75.	59.	15.
	4.	5.	1.	-36.	-30.	-24.	-18.	-5.	8.	0.
	-22.	-6.	-4.	-4.	-2.	-7.	-1.			
13	-257.	-426.	-363.	-519.	-663.	-584.	-464.	-256.	-61.	101.
	297.	432.	1111.	467.	412.	356.	295.	221.	193.	159.
	117.	119.	64.	78.	63.	47.	32.	34.	35.	25.
	13.	13.	2.	2.	12.	3.	8.			
14	-260.	-425.	-418.	-620.	-769.	-744.	-614.	-447.	-105.	-11.
	238.	334.	467.	1174.	467.	457.	419.	298.	233.	239.
	186.	173.	115.	118.	99.	80.	61.	49.	37.	44.
	21.	22.	14.	5.	19.	4.	5.			
15	-264.	-434.	-427.	-631.	-811.	-834.	-698.	-547.	-231.	-124.
	118.	263.	412.	467.	1117.	506.	502.	368.	286.	289.
	222.	214.	147.	171.	145.	118.	92.	74.	56.	47.
	31.	29.	20.	10.	18.	7.	9.			
16	-268.	-443.	-436.	-642.	-853.	-924.	-782.	-646.	-357.	-236.
	-1.	192.	156.	407.	506.	1059.	584.	438.	338.	339.
	258.	295.	178.	224.	170.	156.	122.	98.	75.	50.
	42.	35.	26.	16.	17.	9.	14.			
17	-278.	-449.	-456.	-673.	-881.	-954.	-832.	-679.	-437.	-318.
	-80.	129.	295.	419.	502.	584.	1105.	495.	391.	388.
	302.	331.	227.	268.	226.	185.	144.	116.	88.	69.
	54.	44.	31.	15.	26.	15.	15.			
18	-194.	-349.	-349.	-573.	-698.	-759.	-700.	-620.	-389.	-280.
	-47.	75.	221.	298.	368.	638.	495.	725.	345.	354.
	273.	292.	189.	209.	183.	156.	130.	104.	78.	61.
	49.	35.	30.	16.	21.	10.	11.			
19	-190.	-317.	-298.	-467.	-592.	-646.	-609.	-491.	-299.	-260.
	-69.	59.	193.	233.	286.	338.	391.	345.	534.	305.
	249.	237.	169.	180.	158.	137.	115.	93.	72.	56.
	50.	34.	30.	20.	23.	13.	12.			

25 GeV

20	-190.	-338.	-317.	-458.	-609.	-663.	-649.	-574.	-349.	-286.
	-71.	15.	159.	239.	289.	339.	388.	354.	305.	602.
	271.	272.	206.	225.	193.	161.	129.	109.	89.	63.
	51.	32.	30.	18.	20.	15.	13.			
21	-135.	-235.	-234.	-358.	-482.	-515.	-500.	-441.	-288.	-251.
	-81.	4.	117.	186.	222.	258.	302.	273.	249.	271.
	397.	228.	163.	166.	147.	128.	109.	86.	63.	56.
	45.	31.	24.	16.	17.	10.	10.			
22	-137.	-244.	-250.	-367.	-497.	-553.	-508.	-462.	-299.	-281.
	-76.	5.	119.	173.	214.	255.	331.	292.	237.	272.
	228.	439.	185.	142.	167.	142.	117.	97.	77.	56.
	44.	34.	28.	18.	20.	10.	12.			
23	-110.	-174.	-168.	-250.	-345.	-373.	-356.	-335.	-246.	-205.
	-84.	1.	64.	115.	147.	178.	227.	189.	169.	206.
	163.	185.	253.	144.	126.	107.	89.	75.	60.	47.
	39.	26.	22.	15.	14.	8.	6.			
24	-106.	-196.	-191.	-283.	-379.	-397.	-415.	-361.	-273.	-213.
	-109.	-26.	78.	118.	171.	224.	268.	209.	180.	225.
	166.	192.	144.	374.	128.	118.	109.	84.	60.	52.
	43.	27.	25.	14.	14.	10.	8.			
25	-93.	-167.	-164.	-248.	-328.	-351.	-366.	-316.	-238.	-193.
	-98.	-30.	63.	99.	145.	190.	226.	183.	158.	193.
	147.	167.	126.	126.	303.	107.	98.	78.	58.	49.
	42.	27.	24.	16.	15.	11.	9.			
26	-80.	-138.	-137.	-212.	-277.	-306.	-316.	-270.	-204.	-173.
	-88.	-24.	47.	80.	118.	156.	185.	156.	137.	161.
	128.	142.	107.	118.	107.	232.	87.	71.	56.	46.
	40.	26.	23.	17.	17.	11.	11.			
27	-67.	-108.	-110.	-177.	-226.	-260.	-266.	-225.	-170.	-154.
	-78.	-18.	32.	61.	92.	122.	144.	130.	115.	129.
	109.	117.	89.	109.	98.	87.	161.	65.	54.	43.
	38.	26.	23.	19.	18.	12.	12.			
28	-60.	-98.	-95.	-146.	-196.	-219.	-219.	-183.	-135.	-122.
	-61.	-5.	34.	49.	74.	98.	116.	104.	93.	109.
	86.	97.	75.	84.	78.	71.	65.	129.	46.	36.
	33.	23.	20.	17.	17.	10.	11.			
29	-53.	-88.	-81.	-115.	-166.	-178.	-171.	-141.	-100.	-90.
	-44.	8.	35.	37.	58.	75.	88.	78.	72.	89.
	63.	77.	60.	60.	58.	56.	54.	46.	96.	29.
	28.	19.	17.	15.	16.	9.	10.			
30	-40.	-69.	-68.	-102.	-137.	-132.	-128.	-126.	-78.	-72.
	-36.	0.	25.	44.	47.	50.	69.	61.	56.	83.
	56.	56.	47.	52.	49.	46.	43.	36.	29.	84.
	26.	21.	16.	10.	12.	10.	7.			
31	-32.	-54.	-49.	-72.	-102.	-111.	-114.	-97.	-64.	-68.
	-45.	-22.	13.	21.	31.	42.	54.	49.	50.	51.
	45.	44.	30.	43.	42.	40.	38.	33.	28.	28.
	53.	19.	15.	10.	10.	10.	7.			
32	-31.	-44.	-44.	-63.	-83.	-91.	-79.	-66.	-32.	-31.
	-25.	-6.	13.	22.	29.	35.	44.	35.	34.	32.
	31.	34.	26.	27.	27.	26.	26.	23.	19.	21.
	19.	38.	12.	8.	9.	8.	6.			
33	-22.	-28.	-29.	-50.	-58.	-71.	-64.	-58.	-34.	-42.
	-33.	-4.	2.	15.	20.	26.	31.	30.	30.	30.
	24.	28.	22.	25.	24.	23.	23.	20.	17.	16.
	15.	12.	28.	9.	9.	7.	6.			
34	-16.	-21.	-22.	-30.	-34.	-44.	-37.	-32.	-22.	-24.
	-19.	-4.	2.	5.	10.	16.	15.	16.	20.	18.
	16.	18.	15.	14.	16.	17.	19.	17.	15.	10.
	10.	8.	9.	18.	8.	5.	6.			
35	-20.	-24.	-26.	-40.	-47.	-54.	-46.	-44.	-23.	-28.
	-11.	-2.	12.	19.	18.	17.	26.	21.	23.	20.
	17.	20.	14.	14.	15.	17.	18.	17.	16.	12.
	10.	9.	9.	6.	18.	5.	6.			
36	-13.	-20.	-17.	-22.	-29.	-23.	-26.	-20.	-7.	-13.
	-8.	-7.	3.	4.	7.	9.	15.	10.	13.	15.
	10.	10.	8.	10.	11.	11.	12.	10.	9.	10.
	10.	8.	7.	5.	5.	12.	5.			
37	-14.	-16.	-18.	-26.	-33.	-34.	-28.	-24.	-12.	-13.
	-7.	-1.	8.	5.	9.	14.	15.	11.	12.	13.
	10.	12.	6.	8.	9.	11.	12.	11.	10.	7.
	7.	6.	6.	6.	6.	5.	11.			

Table VI-2(b) Correlation Matrix elements C_{ij} for 50 GeV.

1	730.	812.	698.	932.	1083.	1050.	921.	720.	422.	230.
	-1.	-211.	-338.	-471.	-524.	-577.	-630.	-505.	-493.	-508.
	-396.	-419.	-310.	-319.	-272.	-225.	-177.	-163.	-148.	-108.
	-85.	-94.	-53.	-50.	-40.	-28.	-19.			
2	812.	1884.	1252.	1650.	1986.	1929.	1724.	1308.	785.	387.
	-10.	-327.	-598.	-802.	-918.	-1034.	-1089.	-882.	-845.	-920.
	-710.	-744.	-557.	-534.	-465.	-397.	-329.	-293.	-258.	-185.
	-169.	-121.	-100.	-93.	-71.	-49.	-35.			
3	698.	1252.	1534.	1654.	2026.	2001.	1756.	1418.	840.	477.
	67.	-339.	-596.	-799.	-919.	-1039.	-1105.	-906.	-865.	-889.
	-723.	-759.	-580.	-547.	-475.	-404.	-332.	-296.	-260.	-192.
	-163.	-127.	-105.	-96.	-73.	-52.	-32.			
4	932.	1650.	1654.	3063.	3091.	3145.	2899.	2331.	1522.	935.
	293.	-314.	-810.	-1109.	-1328.	-1548.	-1724.	-1419.	-1367.	-1430.
	-1148.	-1218.	-925.	-908.	-786.	-663.	-540.	-484.	-429.	-325.
	-275.	-209.	-175.	-147.	-121.	-87.	-60.			
5	1083.	1986.	2026.	3091.	5160.	4281.	3977.	3378.	2217.	1410.
	612.	-231.	-956.	-1445.	-1742.	-2038.	-2321.	-1879.	-1853.	-1934.
	-1947.	-1625.	-1232.	-1218.	-1060.	-902.	-745.	-661.	-577.	-442.
	-377.	-280.	-229.	-207.	-161.	-112.	-80.			
6	1050.	1929.	2001.	3145.	4281.	6132.	4692.	4067.	2762.	1900.
	919.	-37.	-893.	-1486.	-1869.	-2252.	-2586.	-2168.	-2116.	-2211.
	-1815.	-1949.	-1457.	-1395.	-1225.	-1055.	-884.	-789.	-693.	-542.
	-432.	-326.	-287.	-248.	-191.	-137.	-102.			
7	921.	1724.	1756.	2899.	3977.	4692.	6147.	4141.	2999.	2100.
	1213.	178.	-684.	-1361.	-1786.	-2212.	-2553.	-2121.	-2081.	-2238.
	-1786.	-1965.	-1464.	-1415.	-1241.	-1066.	-892.	-802.	-713.	-539.
	-461.	-344.	-287.	-254.	-194.	-142.	-101.			
8	720.	1308.	1418.	2331.	3378.	4067.	4141.	5721.	3075.	2407.
	1537.	314.	-363.	-1086.	-1508.	-1930.	-2332.	-2012.	-1972.	-2078.
	-1667.	-1860.	-1400.	-1391.	-1226.	-1060.	-894.	-779.	-664.	-547.
	-438.	-342.	-277.	-248.	-168.	-146.	-93.			
9	422.	785.	840.	1522.	2217.	2762.	2999.	3075.	3783.	2231.
	1578.	767.	36.	-527.	-923.	-1319.	-1693.	-1458.	-1477.	-1583.
	-1339.	-1458.	-1115.	-1091.	-958.	-825.	-692.	-625.	-557.	-451.
	-360.	-279.	-228.	-194.	-148.	-121.	-74.			
10	230.	387.	477.	935.	1410.	1900.	2100.	2407.	2231.	3909.
	1869.	1048.	438.	-124.	-492.	-860.	-1258.	-1173.	-1199.	-1338.
	-1166.	-1268.	-964.	-998.	-876.	-753.	-630.	-573.	-516.	-420.
	-331.	-266.	-201.	-177.	-127.	-103.	-68.			
11	-1.	-10.	67.	293.	612.	919.	1213.	1537.	1578.	1869.
	3646.	1198.	710.	319.	-46.	-412.	-727.	-791.	-828.	-905.
	-807.	-857.	-705.	-757.	-664.	-571.	-478.	-416.	-355.	-279.
	-233.	-193.	-151.	-126.	-98.	-79.	-41.			
12	-211.	-327.	-339.	-314.	-231.	-57.	178.	514.	767.	1048.
	1198.	2493.	913.	717.	453.	189.	-46.	-157.	-181.	-342.
	-339.	-374.	-325.	-390.	-355.	-319.	-284.	-250.	-216.	-194.
	-136.	-124.	-93.	-87.	-69.	-52.	-32.			
13	-338.	-598.	-596.	-810.	-956.	-893.	-684.	-363.	36.	438.
	710.	913.	2455.	958.	785.	615.	488.	292.	198.	165.
	23.	29.	-15.	-71.	-72.	-72.	-73.	-75.	-76.	-62.
	-64.	-39.	-32.	-24.	-18.	-26.	-19.			
14	-471.	-802.	-799.	-1109.	-1445.	-1486.	-1361.	-1086.	-527.	-124.
	319.	717.	956.	2576.	998.	1019.	908.	657.	585.	523.
	320.	336.	186.	157.	126.	95.	64.	50.	35.	14.
	19.	0.	-6.	12.	1.	-6.	-11.			
15	-524.	-910.	-919.	-1323.	-1742.	-1869.	-1786.	-1508.	-923.	-492.
	66.	453.	765.	994.	2542.	1188.	1218.	929.	840.	798.
	568.	592.	394.	352.	297.	241.	185.	161.	137.	97.
	75.	47.	38.	46.	27.	11.	7.			
16	-277.	-1034.	-1039.	-1548.	-2038.	-2252.	-2212.	-1930.	-1319.	-860.
	-412.	189.	615.	1013.	1188.	2508.	1528.	1149.	1096.	1073.
	816.	849.	602.	548.	407.	387.	306.	272.	238.	181.
	131.	94.	83.	79.	53.	28.	25.			
17	-930.	-1089.	-1105.	-1724.	-2321.	-2586.	-2553.	-2332.	-1693.	-1258.
	-727.	-49.	488.	908.	1218.	1529.	2809.	1455.	1228.	1339.
	1073.	1107.	809.	734.	639.	543.	447.	395.	345.	259.
	204.	160.	125.	119.	72.	58.	46.			
18	-505.	-882.	-906.	-1419.	-1879.	-2168.	-2121.	-2012.	-1458.	-1173.
	-791.	-157.	292.	657.	928.	1199.	1455.	1907.	1168.	1210.
	964.	984.	724.	687.	592.	497.	402.	354.	307.	222.
	192.	141.	111.	99.	72.	50.	38.			
19	-493.	-845.	-865.	-1367.	-1853.	-2116.	-2081.	-1972.	-1477.	-1196.
	-828.	-181.	198.	585.	840.	1098.	1324.	1168.	1734.	1198.
	970.	984.	740.	736.	643.	550.	457.	394.	332.	263.
	203.	157.	131.	112.	78.	59.	41.			

50 GeV

20	-508.	-920.	-889.	-1430.	-1934.	-2211.	-2238.	-2078.	-1583.	-1338.
	-903.	-342.	165.	523.	798.	1073.	1339.	1210.	1198.	1867.
	1073.	1098.	826.	805.	700.	595.	490.	434.	377.	294.
	222.	172.	142.	125.	94.	74.	50.			
21	-396.	-710.	-723.	-1148.	-1547.	-1815.	-1786.	-1667.	-1339.	-1166.
	-807.	-339.	23.	320.	568.	816.	1070.	964.	970.	1073.
	1493.	947.	722.	717.	622.	530.	438.	388.	338.	257.
	203.	159.	129.	114.	84.	62.	41.			
22	-419.	-744.	-759.	-1218.	-1625.	-1949.	-1965.	-1860.	-1458.	-1268.
	-857.	-374.	29.	336.	592.	849.	1107.	984.	984.	1098.
	947.	1486.	812.	793.	688.	584.	479.	420.	361.	290.
	233.	189.	144.	130.	108.	75.	51.			
23	-310.	-557.	-580.	-925.	-1232.	-1457.	-1464.	-1400.	-1115.	-964.
	-705.	-325.	-15.	186.	394.	602.	809.	724.	740.	826.
	722.	812.	907.	632.	551.	470.	389.	343.	297.	234.
	184.	146.	120.	104.	80.	59.	40.			
24	-319.	-534.	-547.	-908.	-1218.	-1395.	-1415.	-1391.	-1091.	-998.
	-757.	-390.	-71.	157.	352.	548.	734.	687.	736.	805.
	714.	793.	632.	1000.	519.	463.	407.	358.	309.	243.
	207.	158.	122.	106.	91.	63.	38.			
25	-272.	-465.	-475.	-786.	-1060.	-1225.	-1241.	-1226.	-958.	-876.
	-664.	-355.	-72.	126.	297.	467.	639.	592.	643.	700.
	622.	688.	591.	519.	838.	419.	368.	323.	277.	221.
	187.	145.	113.	98.	83.	59.	37.			
26	-225.	-397.	-404.	-663.	-902.	-1055.	-1066.	-1060.	-825.	-753.
	-571.	-319.	-72.	95.	241.	387.	543.	497.	550.	595.
	530.	584.	470.	463.	419.	676.	330.	288.	246.	200.
	168.	133.	103.	90.	75.	54.	36.			
27	-177.	-329.	-332.	-540.	-745.	-884.	-892.	-894.	-692.	-630.
	-478.	-264.	-73.	64.	185.	306.	447.	402.	457.	490.
	438.	479.	389.	407.	368.	330.	515.	253.	215.	178.
	148.	120.	94.	81.	67.	50.	35.			
28	-163.	-293.	-296.	-484.	-661.	-789.	-802.	-779.	-625.	-573.
	-416.	-250.	-75.	50.	161.	272.	396.	354.	394.	434.
	388.	420.	343.	358.	323.	288.	253.	439.	194.	166.
	135.	111.	87.	74.	62.	47.	35.			
29	-148.	-258.	-260.	-429.	-577.	-693.	-713.	-664.	-557.	-516.
	-355.	-216.	-76.	35.	137.	238.	345.	307.	332.	377.
	338.	361.	297.	309.	277.	246.	215.	194.	363.	154.
	123.	102.	81.	66.	57.	44.	34.			
30	-108.	-185.	-192.	-325.	-442.	-542.	-539.	-547.	-451.	-420.
	-279.	-194.	-62.	14.	97.	181.	259.	222.	263.	294.
	257.	290.	234.	243.	221.	200.	178.	166.	154.	257.
	108.	86.	69.	58.	50.	41.	26.			
31	-85.	-169.	-163.	-275.	-377.	-432.	-461.	-438.	-360.	-331.
	-233.	-136.	-64.	19.	75.	131.	204.	192.	203.	222.
	203.	233.	184.	207.	187.	168.	148.	135.	123.	108.
	218.	71.	56.	47.	40.	33.	20.			
32	-64.	-121.	-127.	-209.	-280.	-326.	-344.	-342.	-279.	-266.
	-193.	-124.	-39.	0.	47.	94.	160.	141.	157.	172.
	159.	189.	146.	158.	145.	133.	120.	111.	102.	86.
	71.	137.	50.	43.	36.	31.	20.			
33	-53.	-100.	-105.	-175.	-229.	-287.	-287.	-277.	-228.	-201.
	-151.	-93.	-32.	-6.	38.	83.	125.	111.	131.	146.
	129.	144.	120.	122.	113.	103.	94.	87.	81.	69.
	56.	50.	89.	36.	28.	24.	16.			
34	-50.	-93.	-96.	-147.	-207.	-248.	-254.	-248.	-194.	-177.
	-126.	-87.	-24.	12.	46.	79.	119.	99.	112.	125.
	114.	130.	104.	106.	98.	90.	81.	74.	66.	58.
	47.	43.	36.	65.	27.	21.	16.			
35	-40.	-71.	-73.	-121.	-161.	-191.	-194.	-168.	-148.	-127.
	-98.	-69.	-18.	1.	27.	53.	72.	72.	78.	94.
	84.	108.	80.	91.	83.	75.	67.	62.	57.	50.
	40.	36.	28.	27.	82.	20.	13.			
36	-28.	-48.	-52.	-87.	-112.	-137.	-142.	-146.	-121.	-103.
	-79.	-52.	-26.	-6.	11.	28.	58.	50.	59.	74.
	62.	75.	59.	63.	59.	54.	50.	47.	44.	41.
	33.	31.	24.	21.	20.	36.	11.			
37	-19.	-35.	-32.	-60.	-80.	-102.	-101.	-93.	-74.	-68.
	-41.	-32.	-19.	-11.	7.	25.	46.	38.	41.	50.
	41.	51.	40.	38.	37.	36.	35.	35.	34.	26.
	20.	20.	16.	16.	13.	11.	29.			

Table VI-2(c) Correlation Matrix elements C_{ij} for 75 GeV.

1	987.	1067.	957.	1315.	1573.	1562.	1432.	1084.	751.	499.
	185.	-138.	-364.	-630.	-709.	-788.	-851.	-732.	-712.	-728.
	-594.	-692.	-471.	-507.	-450.	-393.	-335.	-291.	-246.	-204.
	-145.	-130.	-96.	-79.	-69.	-50.	-38.			
2	1067.	2386.	1739.	2369.	2947.	2963.	2704.	2167.	1484.	1053.
	465.	-204.	-600.	-1050.	-1254.	-1457.	-1562.	-1410.	-1338.	-1328.
	-1125.	-1247.	-870.	-920.	-823.	-726.	-629.	-553.	-478.	-379.
	-275.	-233.	-180.	-150.	-130.	-90.	-69.			
3	957.	1739.	2135.	2413.	3084.	3154.	2902.	2404.	1597.	1185.
	552.	-142.	-600.	-1085.	-1292.	-1499.	-1660.	-1502.	-1438.	-1508.
	-1200.	-1338.	-958.	-1005.	-894.	-783.	-671.	-594.	-517.	-411.
	-295.	-255.	-195.	-151.	-140.	-98.	-72.			
4	1315.	2369.	2413.	4439.	4751.	4936.	4652.	3988.	2712.	2103.
	1092.	-51.	-840.	-1564.	-1920.	-2277.	-2553.	-2338.	-2230.	-2341.
	-1941.	-2099.	-1513.	-1587.	-1426.	-1265.	-1103.	-965.	-827.	-646.
	-480.	-395.	-319.	-254.	-226.	-167.	-125.			
5	1573.	2947.	3084.	4751.	7891.	6986.	6771.	5951.	4124.	3365.
	1965.	322.	-906.	-1932.	-2548.	-3165.	-3594.	-3231.	-3164.	-3356.
	-2756.	-3043.	-2234.	-2290.	-2065.	-1840.	-1615.	-1419.	-1224.	-956.
	-730.	-607.	-476.	-380.	-336.	-255.	-197.			
6	1562.	2963.	3154.	4936.	6986.	9683.	7883.	7115.	5134.	4248.
	2696.	769.	-686.	-1916.	-2685.	-3453.	-4056.	-3705.	-3634.	-3864.
	-3251.	-3693.	-2666.	-2758.	-2477.	-2195.	-1913.	-1699.	-1485.	-1140.
	-874.	-724.	-586.	-459.	-408.	-294.	-223.			
7	1432.	2704.	2902.	4652.	6771.	7883.	10267.	7792.	5627.	4966.
	3515.	1277.	-244.	-1625.	-2511.	-3397.	-4117.	-3826.	-3800.	-4041.
	-3456.	-3833.	-2939.	-2983.	-2689.	-2395.	-2101.	-1862.	-1624.	-1265.
	-959.	-789.	-646.	-500.	-448.	-322.	-259.			
8	1084.	2167.	2404.	3988.	5951.	7115.	7792.	9890.	5973.	5483.
	4043.	1783.	406.	-1023.	-1982.	-2940.	-3755.	-3589.	-3615.	-4046.
	-3397.	-3788.	-2928.	-3058.	-2750.	-2441.	-2132.	-1912.	-1692.	-1329.
	-1009.	-832.	-673.	-538.	-460.	-359.	-280.			
9	751.	1484.	1597.	2712.	4124.	5134.	5627.	5973.	6758.	4767.
	3775.	1952.	762.	-419.	-1222.	-2026.	-2733.	-2706.	-2754.	-3135.
	-2607.	-3055.	-2193.	-2482.	-2241.	-2000.	-1760.	-1576.	-1393.	-1101.
	-822.	-672.	-589.	-459.	-394.	-301.	-231.			
10	499.	1053.	1185.	2103.	3365.	4248.	4966.	5483.	4767.	7082.
	4179.	2549.	1331.	128.	-729.	-1585.	-2254.	-2324.	-2505.	-2951.
	-2554.	-2946.	-2293.	-2451.	-2216.	-1981.	-1747.	-1579.	-1412.	-1134.
	-858.	-702.	-607.	-486.	-416.	-318.	-256.			
11	185.	465.	552.	1092.	1965.	2696.	3515.	4043.	3775.	4179.
	7016.	2794.	1859.	929.	123.	-684.	-1430.	-1553.	-1861.	-2230.
	-1936.	-2330.	-1980.	-2124.	-1933.	-1742.	-1551.	-1423.	-1296.	-1065.
	-708.	-672.	-564.	-447.	-399.	-302.	-230.			
12	-138.	-204.	-142.	-51.	322.	769.	1277.	1783.	1952.	2549.
	2778.	4685.	1927.	1445.	877.	308.	-219.	-565.	-760.	-1112.
	-1041.	-1328.	-1178.	-1226.	-1143.	-1061.	-979.	-870.	-762.	-667.
	-491.	-417.	-365.	-300.	-253.	-209.	-160.			
13	-364.	-600.	-600.	-840.	-906.	-686.	-244.	406.	762.	1331.
	1859.	1927.	4193.	1870.	1412.	954.	599.	277.	20.	-234.
	-375.	-593.	-600.	-672.	-645.	-619.	-593.	-569.	-545.	-434.
	-357.	-319.	-253.	-224.	-178.	-158.	-117.			
14	-630.	-1050.	-1085.	-1564.	-1932.	-1916.	-1625.	-1023.	-419.	128.
	929.	1445.	1870.	4065.	1790.	1749.	1470.	1055.	765.	557.
	338.	239.	-17.	-62.	-106.	-150.	-194.	-212.	-230.	-180.
	-181.	-144.	-134.	-122.	-97.	-102.	-63.			
15	-709.	-1254.	-1292.	-1920.	-2548.	-2685.	-2511.	-1982.	-1222.	-729.
	123.	877.	1412.	1790.	4051.	1981.	1957.	1557.	1293.	1150.
	841.	788.	423.	404.	320.	237.	154.	94.	34.	22.
	-22.	-19.	-30.	-40.	-32.	-47.	-25.			
16	-788.	-1457.	-1499.	-2277.	-3165.	-3453.	-3397.	-2940.	-2026.	-1585.
	-684.	308.	954.	1749.	1981.	4038.	2443.	2059.	1821.	1743.
	1344.	1338.	864.	869.	746.	624.	502.	400.	297.	225.
	137.	106.	74.	43.	33.	7.	13.			
17	-851.	-1562.	-1660.	-2553.	-3594.	-4056.	-4117.	-3750.	-2733.	-2254.
	-1430.	-219.	599.	1470.	1957.	2443.	4398.	2428.	2198.	2225.
	1729.	1865.	1297.	1231.	1079.	927.	775.	663.	552.	419.
	262.	235.	162.	115.	93.	62.	46.			
18	-732.	-1410.	-1502.	-2338.	-3231.	-3705.	-3826.	-3589.	-2706.	-2324.
	-1563.	-545.	277.	1055.	1557.	2059.	2428.	3814.	2136.	2238.
	1770.	1864.	1349.	1343.	1183.	1023.	863.	736.	609.	473.
	319.	272.	209.	155.	124.	91.	65.			
19	-712.	-1338.	-1438.	-2230.	-3164.	-3634.	-3800.	-3615.	-2754.	-2505.
	-1861.	-760.	20.	765.	1293.	1821.	2198.	2136.	3018.	2249.
	1798.	1984.	1462.	1491.	1309.	1138.	966.	832.	699.	567.
	388.	325.	265.	195.	160.	116.	90.			

75 GeV

20	-728.	-1328.	-1508.	-2341.	-3356.	-3864.	-4041.	-4046.	-3135.	-2951.
	-2230.	-1112.	-234.	557.	1150.	1743.	2225.	2238.	2249.	3533.
	2103.	2252.	1679.	1717.	1523.	1328.	1133.	981.	828.	700.
	493.	407.	320.	247.	210.	153.	111.			
21	-584.	-1125.	-1220.	-1941.	-2756.	-3251.	-3456.	-3397.	-2687.	-2554.
	-1996.	-1041.	-375.	338.	841.	1344.	1729.	1770.	1798.	2103.
	2569.	2023.	1510.	1541.	1371.	1200.	1030.	908.	787.	626.
	447.	365.	300.	237.	195.	141.	115.			
22	-992.	-1247.	-1338.	-2099.	-3043.	-3633.	-3833.	-3788.	-3055.	-2946.
	-2330.	-1328.	-593.	239.	788.	1338.	1865.	1864.	1984.	2252.
	2023.	3025.	1779.	1832.	1640.	1447.	1254.	1105.	956.	774.
	557.	464.	380.	294.	254.	193.	155.			
23	-471.	-870.	-958.	-1519.	-2234.	-2666.	-2939.	-2928.	-2393.	-2293.
	-1980.	-1178.	-600.	-17.	423.	864.	1297.	1349.	1462.	1679.
	1510.	1779.	1964.	1487.	1338.	1189.	1039.	917.	795.	643.
	463.	384.	315.	253.	215.	163.	124.			
24	-507.	-920.	-1005.	-1587.	-2290.	-2758.	-2983.	-3058.	-2482.	-2451.
	-2124.	-1226.	-672.	-62.	404.	869.	1231.	1343.	1481.	1717.
	1541.	1832.	1487.	2161.	1304.	1212.	1120.	1002.	884.	718.
	531.	422.	364.	284.	248.	188.	143.			
25	-450.	-823.	-894.	-1426.	-2065.	-2477.	-2689.	-2750.	-2241.	-2216.
	-1933.	-1143.	-645.	-106.	320.	746.	1079.	1183.	1309.	1523.
	1371.	1640.	1338.	1304.	1851.	1125.	1036.	930.	823.	669.
	499.	400.	346.	272.	236.	184.	139.			
26	-393.	-726.	-783.	-1265.	-1840.	-2195.	-2395.	-2441.	-2000.	-1981.
	-1742.	-1061.	-619.	-150.	237.	624.	927.	1023.	1138.	1328.
	1200.	1447.	1189.	1212.	1125.	1541.	953.	857.	762.	620.
	466.	378.	329.	261.	224.	180.	134.			
27	-335.	-629.	-671.	-1103.	-1615.	-1913.	-2101.	-2132.	-1760.	-1747.
	-1531.	-979.	-593.	-194.	154.	502.	775.	863.	966.	1133.
	1030.	1254.	1039.	1120.	1036.	953.	1231.	785.	701.	570.
	433.	356.	311.	249.	212.	176.	130.			
28	-291.	-553.	-594.	-965.	-1419.	-1699.	-1862.	-1912.	-1576.	-1579.
	-1423.	-870.	-569.	-212.	94.	400.	663.	736.	832.	981.
	908.	1105.	917.	1002.	930.	857.	785.	1064.	632.	532.
	412.	334.	290.	233.	201.	166.	125.			
29	-246.	-478.	-517.	-827.	-1224.	-1485.	-1624.	-1692.	-1393.	-1412.
	-1296.	-762.	-445.	-230.	34.	297.	552.	609.	699.	828.
	787.	956.	795.	884.	823.	762.	701.	632.	897.	493.
	391.	311.	269.	216.	190.	156.	120.			
30	-204.	-379.	-411.	-646.	-956.	-1140.	-1265.	-1329.	-1101.	-1134.
	-1065.	-667.	-434.	-180.	22.	225.	419.	473.	567.	700.
	626.	774.	643.	718.	669.	620.	570.	532.	493.	638.
	314.	253.	221.	177.	155.	124.	92.			
31	-145.	-275.	-295.	-480.	-730.	-874.	-959.	-1009.	-822.	-858.
	-788.	-491.	-357.	-161.	-22.	137.	262.	319.	388.	493.
	447.	557.	463.	531.	499.	466.	433.	412.	391.	314.
	384.	212.	182.	147.	131.	106.	81.			
32	-130.	-233.	-255.	-395.	-607.	-724.	-789.	-832.	-672.	-702.
	-672.	-417.	-319.	-144.	-19.	106.	235.	272.	325.	407.
	365.	464.	384.	422.	400.	378.	356.	334.	311.	253.
	212.	278.	153.	125.	110.	90.	67.			
33	-96.	-180.	-195.	-319.	-476.	-586.	-646.	-673.	-589.	-607.
	-564.	-365.	-263.	-134.	-30.	74.	162.	209.	265.	320.
	300.	380.	315.	364.	346.	329.	311.	290.	269.	221.
	182.	153.	218.	115.	99.	78.	61.			
34	-79.	-150.	-151.	-254.	-380.	-455.	-500.	-538.	-459.	-486.
	-447.	-300.	-224.	-122.	-40.	43.	115.	155.	195.	247.
	237.	294.	253.	284.	272.	261.	249.	233.	216.	177.
	147.	125.	115.	156.	85.	68.	54.			
35	-69.	-130.	-140.	-226.	-336.	-408.	-448.	-460.	-394.	-416.
	-399.	-253.	-178.	-97.	-32.	33.	93.	124.	180.	210.
	195.	244.	215.	248.	236.	224.	212.	201.	190.	195.
	131.	110.	99.	85.	129.	61.	49.			
36	-50.	-90.	-98.	-167.	-255.	-294.	-322.	-359.	-301.	-318.
	-302.	-209.	-158.	-102.	-47.	7.	62.	91.	116.	153.
	141.	193.	163.	188.	184.	180.	176.	166.	156.	124.
	106.	90.	78.	68.	61.	88.	40.			
37	-38.	-69.	-72.	-125.	-197.	-223.	-259.	-280.	-231.	-256.
	-230.	-160.	-117.	-63.	-25.	13.	46.	62.	90.	111.
	115.	155.	124.	143.	139.	134.	130.	125.	120.	92.
	81.	67.	61.	54.	49.	40.	67.			

Table VI-2(d) Correlation Matrix elements C_{ij} for 100 GeV.

1	1086.	1214.	1126.	1601.	1952.	2034.	1914.	1690.	1064.	868.
	562.	79.	-235.	-479.	-746.	-1013.	-1034.	-1012.	-819.	-985.
	-846.	-900.	-679.	-726.	-642.	-557.	-473.	-425.	-377.	-287.
	-249.	-200.	-171.	-123.	-99.	-73.	-60.			
2	1214.	2847.	2073.	3071.	3753.	4003.	3787.	3317.	2111.	1638.
	972.	165.	-411.	-931.	-1417.	-1904.	-2038.	-1897.	-1795.	-1640.
	-1610.	-1668.	-1282.	-1341.	-1191.	-1041.	-890.	-813.	-736.	-532.
	-472.	-386.	-308.	-233.	-210.	-154.	-118.			
3	1126.	2073.	2553.	3135.	3977.	4310.	4121.	3691.	2499.	2023.
	1290.	316.	-304.	-881.	-1433.	-1986.	-2157.	-2053.	-1936.	-2010.
	-1773.	-1840.	-1420.	-1485.	-1315.	-1144.	-973.	-891.	-809.	-616.
	-533.	-417.	-340.	-254.	-228.	-162.	-138.			
4	1601.	3071.	3135.	5907.	6411.	7080.	6845.	6378.	4467.	3705.
	2443.	852.	-214.	-1226.	-2174.	-3121.	-3580.	-3338.	-3253.	-3462.
	-3028.	-3167.	-2440.	-2538.	-2256.	-1973.	-1691.	-1563.	-1435.	-1063.
	-936.	-712.	-575.	-461.	-390.	-287.	-231.			
5	1952.	3753.	3977.	6411.	10124.	9839.	9764.	9061.	6475.	5540.
	3798.	1533.	-73.	-1504.	-2865.	-4287.	-4851.	-4628.	-4542.	-4871.
	-4247.	-4481.	-3473.	-3709.	-3274.	-2840.	-2406.	-2222.	-2039.	-1506.
	-1319.	-1007.	-830.	-650.	-583.	-413.	-332.			
6	2034.	4003.	4310.	7080.	9839.	13740.	12054.	11404.	8291.	7339.
	5389.	2389.	556.	-1506.	-3216.	-4926.	-5772.	-5609.	-5527.	-5920.
	-5289.	-5585.	-4387.	-4570.	-4059.	-3547.	-3036.	-2801.	-2566.	-1907.
	-1670.	-1252.	-1025.	-790.	-723.	-501.	-424.			
7	1914.	3787.	4121.	6845.	9764.	12054.	14996.	12204.	9154.	8284.
	6354.	3192.	1166.	-1120.	-3013.	-4911.	-6036.	-5770.	-5789.	-6405.
	-5756.	-6027.	-4791.	-5044.	-4483.	-3922.	-3361.	-3076.	-2791.	-2144.
	-1875.	-1377.	-1164.	-888.	-808.	-565.	-475.			
8	1690.	3317.	3691.	6378.	9061.	11404.	12204.	15026.	9542.	9002.
	7121.	3946.	1580.	-543.	-2497.	-4452.	-5859.	-5774.	-5501.	-6474.
	-5829.	-6117.	-4853.	-5181.	-4603.	-4024.	-3445.	-3168.	-2892.	-2220.
	-1914.	-1403.	-1181.	-926.	-813.	-563.	-494.			
9	1064.	2111.	2499.	4467.	6475.	8291.	9154.	9542.	9778.	7739.
	6398.	3760.	2103.	269.	-1406.	-3080.	-4338.	-4278.	-4551.	-5174.
	-4703.	-4940.	-3952.	-4215.	-3754.	-3293.	-2833.	-2615.	-2397.	-1846.
	-1616.	-1178.	-995.	-781.	-692.	-490.	-402.			
10	868.	1638.	2023.	3705.	5540.	7339.	8284.	9002.	7739.	10922.
	7148.	4540.	2830.	1024.	-681.	-2385.	-3905.	-4011.	-4342.	-4959.
	-4586.	-4893.	-3924.	-4315.	-3826.	-3338.	-2850.	-2661.	-2473.	-1918.
	-1688.	-1182.	-1021.	-825.	-690.	-498.	-403.			
11	562.	972.	1290.	2443.	3798.	5389.	6354.	7121.	6398.	7148.
	10002.	4867.	3516.	1897.	250.	-1397.	-2759.	-2936.	-3414.	-4240.
	-3919.	-4376.	-3536.	-3837.	-3431.	-3025.	-2619.	-2439.	-2259.	-1802.
	-1549.	-1087.	-949.	-738.	-636.	-469.	-406.			
12	79.	165.	316.	852.	1533.	2389.	3192.	3946.	3760.	4540.
	4867.	6631.	3286.	2121.	1058.	-5.	-1202.	-1352.	-1919.	-2448.
	-2408.	-2709.	-2252.	-2452.	-2192.	-1932.	-1673.	-1616.	-1560.	-1216.
	-1062.	-764.	-656.	-511.	-453.	-334.	-282.			
13	-235.	-411.	-304.	-214.	-43.	556.	1166.	1580.	2103.	2830.
	3516.	3286.	5735.	2633.	1819.	1006.	75.	-298.	-792.	-1347.
	-1483.	-1586.	-1428.	-1562.	-1441.	-1339.	-1228.	-1148.	-1068.	-872.
	-745.	-552.	-479.	-397.	-299.	-247.	-217.			
14	-479.	-931.	-881.	-1226.	-1504.	-1506.	-1120.	-543.	269.	1024.
	1897.	2121.	2633.	5360.	2022.	1716.	1309.	818.	338.	-46.
	-225.	-406.	-492.	-742.	-685.	-627.	-570.	-596.	-622.	-495.
	-435.	-321.	-273.	-232.	-210.	-155.	-129.			
15	-746.	-1417.	-1433.	-2174.	-2895.	-3216.	-3015.	-2497.	-1406.	-681.
	250.	1058.	1819.	2022.	5232.	2221.	2270.	1799.	1425.	1151.
	844.	734.	464.	295.	227.	158.	90.	18.	-53.	-47.
	-50.	-42.	-46.	-38.	-41.	-39.	-31.			
16	-1013.	-1904.	-1986.	-3121.	-4287.	-4926.	-4911.	-4452.	-3080.	-2385.
	-1397.	-5.	1006.	1716.	2221.	5103.	3231.	2780.	2512.	2347.
	1912.	1874.	1420.	1133.	1138.	944.	750.	633.	515.	401.
	336.	236.	181.	156.	128.	78.	66.			
17	-1034.	-2038.	-2157.	-3580.	-4851.	-5772.	-6036.	-5859.	-4338.	-3905.
	-2755.	-1202.	75.	1309.	2270.	3231.	6006.	3514.	3181.	3305.
	2744.	2924.	2131.	2087.	1811.	1536.	1260.	1130.	1000.	756.
	657.	483.	341.	289.	262.	175.	153.			
18	-1012.	-1897.	-2053.	-3338.	-4628.	-5609.	-5770.	-5774.	-4278.	-4011.
	-2416.	-1352.	-298.	818.	1799.	2780.	3514.	4738.	3181.	3283.
	2802.	2898.	2202.	2203.	1926.	1649.	1372.	1234.	1096.	851.
	739.	520.	402.	321.	263.	191.	168.			
19	-918.	-1795.	-1936.	-3253.	-4542.	-5527.	-5789.	-5901.	-4551.	-4342.
	-3414.	-1919.	-792.	338.	1425.	2512.	3181.	3181.	4443.	3475.
	3011.	3159.	2409.	2464.	2163.	1862.	1562.	1410.	1258.	928.
	854.	594.	473.	373.	329.	227.	197.			

100 GeV

20	-985.	-1840.	-2010.	-3462.	-4871.	-5920.	-6405.	-6474.	-5174.	-4959.
	-4240.	-2448.	-1347.	-46.	1151.	2347.	3302.	3283.	3475.	3376.
	3459.	3616.	2787.	2938.	2576.	2215.	1854.	1694.	1535.	1174.
	1000.	724.	602.	460.	399.	289.	252.			
21	-846.	-1610.	-1773.	-3028.	-4247.	-5289.	-5726.	-5829.	-4703.	-4586.
	-3919.	-2488.	-1483.	-225.	844.	1912.	2744.	2802.	3011.	3459.
	4149.	3349.	2644.	2766.	2449.	2132.	1816.	1668.	1520.	1153.
	1009.	727.	596.	468.	408.	292.	253.			
22	-900.	-1668.	-1840.	-3167.	-4481.	-5585.	-6027.	-6117.	-4940.	-4893.
	-4376.	-2709.	-1586.	-406.	734.	1874.	2924.	2898.	3159.	3616.
	3340.	4781.	2828.	2995.	2650.	2305.	1960.	1803.	1645.	1282.
	1092.	801.	660.	507.	450.	318.	253.			
23	-679.	-1282.	-1420.	-2440.	-3473.	-4387.	-4791.	-4853.	-3952.	-3924.
	-3536.	-2252.	-1428.	-492.	464.	1420.	2131.	2202.	2409.	2787.
	2644.	2828.	2975.	2459.	2177.	1894.	1612.	1487.	1363.	1071.
	908.	654.	548.	423.	382.	264.	219.			
24	-726.	-1341.	-1485.	-2538.	-3709.	-4570.	-5044.	-5181.	-4215.	-4315.
	-3837.	-2452.	-1562.	-742.	295.	1333.	2087.	2203.	2464.	2938.
	2766.	2995.	2456.	3482.	2127.	1961.	1796.	1676.	1556.	1185.
	1013.	735.	631.	475.	433.	307.	252.			
25	-642.	-1191.	-1315.	-2256.	-3274.	-4059.	-4483.	-4603.	-3754.	-3826.
	-3431.	-2192.	-1451.	-685.	227.	1138.	1811.	1926.	2163.	2576.
	2449.	2650.	2177.	2127.	2513.	1819.	1665.	1541.	1418.	1084.
	934.	680.	583.	440.	398.	287.	234.			
26	-557.	-1041.	-1144.	-1973.	-2840.	-3547.	-3922.	-4024.	-3293.	-3338.
	-3025.	-1932.	-1339.	-627.	158.	944.	1536.	1649.	1862.	2215.
	2132.	2305.	1894.	1961.	1819.	2345.	1534.	1406.	1279.	983.
	856.	625.	536.	404.	364.	268.	216.			
27	-473.	-890.	-973.	-1691.	-2406.	-3036.	-3361.	-3445.	-2833.	-2850.
	-2619.	-1673.	-1228.	-570.	90.	790.	1269.	1372.	1562.	1854.
	1816.	1960.	1612.	1796.	1665.	1534.	1777.	1272.	1141.	882.
	777.	570.	488.	369.	329.	248.	198.			
28	-425.	-813.	-891.	-1563.	-2222.	-2801.	-3076.	-3168.	-2615.	-2661.
	-2439.	-1616.	-1149.	-596.	18.	833.	1130.	1234.	1410.	1694.
	1698.	1803.	1487.	1676.	1541.	1406.	1272.	1616.	1027.	840.
	742.	542.	469.	361.	322.	241.	198.			
29	-377.	-736.	-809.	-1435.	-2039.	-2566.	-2791.	-2892.	-2397.	-2473.
	-2259.	-1560.	-1068.	-622.	-53.	515.	1000.	1096.	1258.	1535.
	1520.	1645.	1363.	1556.	1418.	1279.	1141.	1027.	1456.	709.
	707.	514.	450.	354.	314.	233.	199.			
30	-287.	-532.	-616.	-1063.	-1506.	-1907.	-2144.	-2220.	-1846.	-1918.
	-1802.	-1216.	-872.	-495.	-147.	401.	736.	851.	928.	1174.
	1153.	1282.	1071.	1185.	1084.	1084.	882.	840.	799.	944.
	555.	404.	339.	275.	236.	187.	138.			
31	-249.	-472.	-533.	-936.	-1319.	-1670.	-1875.	-1914.	-1616.	-1688.
	-1549.	-1062.	-745.	-435.	-50.	336.	657.	739.	854.	1000.
	1009.	1092.	908.	1813.	934.	856.	777.	742.	707.	555.
	720.	368.	307.	249.	223.	163.	133.			
32	-200.	-386.	-417.	-712.	-1007.	-1252.	-1377.	-1403.	-1178.	-1182.
	-1087.	-766.	-552.	-321.	-42.	236.	483.	520.	594.	724.
	727.	801.	654.	735.	680.	625.	570.	542.	514.	404.
	368.	433.	245.	196.	172.	131.	110.			
33	-171.	-308.	-340.	-575.	-830.	-1025.	-1164.	-1181.	-995.	-1021.
	-949.	-656.	-479.	-273.	-46.	181.	341.	402.	473.	262.
	596.	660.	548.	631.	583.	536.	488.	469.	450.	339.
	307.	245.	332.	175.	143.	111.	91.			
34	-123.	-233.	-254.	-461.	-650.	-790.	-888.	-926.	-781.	-825.
	-738.	-511.	-397.	-232.	-38.	156.	289.	321.	373.	460.
	468.	507.	423.	475.	440.	404.	369.	361.	354.	275.
	249.	196.	175.	216.	120.	88.	77.			
35	-99.	-210.	-228.	-390.	-583.	-723.	-808.	-815.	-692.	-690.
	-636.	-453.	-299.	-210.	-41.	128.	262.	263.	329.	399.
	408.	450.	382.	433.	398.	364.	329.	322.	314.	236.
	223.	172.	143.	120.	181.	82.	64.			
36	-73.	-154.	-162.	-287.	-413.	-501.	-565.	-563.	-490.	-498.
	-469.	-334.	-247.	-155.	-39.	78.	175.	191.	227.	289.
	292.	318.	264.	307.	287.	268.	248.	241.	233.	187.
	163.	131.	111.	88.	82.	109.	47.			
37	-60.	-118.	-138.	-231.	-332.	-424.	-475.	-494.	-402.	-403.
	-406.	-282.	-217.	-129.	-31.	66.	153.	168.	197.	252.
	253.	253.	219.	252.	234.	216.	198.	198.	199.	138.
	133.	110.	91.	77.	64.	47.	157.			

Table VI-3(a)

Eigenvalues λ_i and Corresponding Eigenvectors x_i of the Correlation Matrix C for 25 GeV.

I= 1	EVAL(I)=	12236.3							
.104	.181	.178	.281	.371	.391	.352	.289	.158	.110
-.004	-.071	-.134	-.168	-.186	-.203	-.214	-.172	-.143	-.151
-.116	-.122	-.085	-.094	-.082	-.070	-.058	-.048	-.038	-.030
-.024	-.018	-.014	-.009	-.011	-.006	-.007			
I= 2	EVAL(I)=	3587.2							
.130	.212	.160	.175	.168	.018	-.131	-.286	-.352	-.443
-.434	-.305	-.246	-.190	-.105	-.024	.031	.049	.043	.070
.066	.070	.064	.075	.068	.061	.054	.040	.026	.020
.025	.009	.014	.008	.006	.003	.003			
I= 3	EVAL(I)=	1315.5							
-.219	-.308	-.219	-.301	-.160	.085	.402	.360	.126	-.064
-.312	-.398	-.165	-.134	-.049	.019	.126	.064	.079	.082
.065	.081	.060	.085	.071	.058	.046	.038	.030	.027
.030	.024	.019	.015	.011	.015	.010			
I= 4	EVAL(I)=	1089.0							
.137	.118	.047	.054	-.179	-.411	-.443	.153	.353	.332
-.004	-.304	-.309	-.226	-.181	-.139	-.108	-.048	-.003	.008
.001	.011	-.012	.002	.008	.013	.018	.016	.014	.004
.019	.018	.010	.007	.003	.006	.006			
I= 5	EVAL(I)=	1042.5							
.064	.108	.062	.083	.079	-.160	-.194	.492	.096	-.064
-.634	.317	.216	.151	.153	.143	.113	-.039	.000	-.087
-.044	-.064	-.041	-.034	-.028	-.022	-.017	-.013	-.009	-.019
-.009	-.003	.001	-.003	-.004	-.006	-.002			
I= 6	EVAL(I)=	987.1							
.071	.102	.037	-.061	.018	-.228	.433	-.558	.211	.410
-.412	.007	-.040	.108	.095	.080	.008	-.011	-.050	-.052
-.041	-.041	-.034	-.044	-.040	-.037	-.034	-.028	-.022	-.005
-.011	.003	.001	-.003	-.002	-.005	-.001			
I= 7	EVAL(I)=	899.1							
.012	.122	.045	-.027	.209	-.582	.324	.283	-.558	.171
.199	-.015	-.022	-.136	-.006	.060	.088	.037	-.014	-.032
-.017	.010	.004	-.008	-.005	-.003	-.002	-.003	-.005	-.018
-.013	-.007	-.006	-.001	-.005	-.010	-.002			
I= 8	EVAL(I)=	866.0							
.061	.131	.071	.165	.141	-.210	.112	.058	.333	-.356
.255	-.467	.000	.419	.300	.212	.129	.009	-.019	-.030
-.016	-.037	-.050	-.046	-.043	-.041	-.040	-.042	-.044	-.031
-.019	-.013	-.014	-.012	-.003	-.006	-.007			
I= 9	EVAL(I)=	803.0							
.094	.106	.021	-.199	-.271	-.330	.274	-.032	.222	-.565
.045	.324	-.020	-.114	-.217	-.222	-.252	-.111	-.037	-.084
-.027	-.005	-.013	-.085	-.053	-.026	-.004	.007	.017	.016
.006	.005	.014	.008	.010	-.000	.006			
I= 10	EVAL(I)=	715.5							
-.123	-.271	-.076	-.032	.631	-.148	-.071	-.093	.326	-.105
.078	.330	-.304	-.253	.071	.072	.162	.107	.099	-.114
.040	.068	.040	.026	.028	.029	.030	.024	.017	-.001
.004	.007	.013	.010	.003	.007	.001			
I= 11	EVAL(I)=	678.0							
.021	.088	.011	.371	-.413	.085	.133	.007	-.045	-.037
.077	.139	-.150	-.528	.483	.190	.225	.020	-.022	-.045
-.028	-.034	-.013	-.004	-.012	-.019	-.024	-.016	-.009	-.020
-.017	-.010	-.012	-.009	-.014	-.006	-.002			
I= 12	EVAL(I)=	656.5							
-.133	-.222	-.013	.265	.135	-.186	.011	-.106	.117	-.035
-.050	-.238	.722	-.369	.028	-.120	-.189	-.054	.053	.066
.020	.026	.014	.025	.021	.018	.015	.023	.031	.011
.025	.011	.004	.009	.008	.008	.009			

Table VI-3(b)

Eigenvalues λ_i and Corresponding Eigenvectors x_i of the Correlation Matrix C for 50 GeV.

I= 1	EVAL(I)=	35753.4							
.080	.146	.148	.235	.321	.366	.362	.333	.240	.185
.111	.021	-.051	-.107	-.143	-.178	-.210	-.176	-.172	-.181
-.148	-.158	-.118	-.116	-.101	-.086	-.072	-.064	-.056	-.043
-.035	-.027	-.022	-.020	-.015	-.011	-.007			
I= 2	EVAL(I)=	8599.9							
-.098	-.177	-.159	-.186	-.198	-.122	-.026	.129	.234	.381
.442	.374	.326	.269	.193	.118	.043	-.010	-.032	-.059
-.077	-.087	-.078	-.093	-.084	-.075	-.067	-.059	-.052	-.046
-.035	-.031	-.023	-.019	-.014	-.014	-.008			
I= 3	EVAL(I)=	2703.3							
-.106	-.224	-.167	-.245	-.289	-.162	-.003	.278	.201	.230
.140	-.163	-.277	-.404	-.317	-.225	-.157	-.069	-.010	.049
.098	.094	.103	.124	.113	.102	.091	.084	.076	.058
.054	.042	.037	.027	.032	.021	.017			
I= 4	EVAL(I)=	2257.8							
.135	.218	.161	.159	.108	-.204	-.367	-.479	-.160	.173
.502	-.009	-.055	-.094	-.164	-.183	-.194	-.143	-.108	-.087
-.073	-.013	-.013	-.018	-.006	.006	.017	.016	.016	.024
.019	.012	.015	.011	.008	.011	.009			
I= 5	EVAL(I)=	1822.6							
-.066	-.100	-.073	-.074	-.007	.093	.339	-.026	-.107	-.669
.607	.028	-.018	.052	-.035	-.056	.005	-.007	.010	.036
.057	.055	.028	.034	.029	.023	.018	.023	.028	.030
.017	.014	.005	.006	.003	.004	.004			
I= 6	EVAL(I)=	1698.2							
.027	.048	.001	-.037	-.088	-.178	-.130	.131	.022	-.299
-.294	.290	.477	.182	-.325	-.328	-.367	-.170	-.088	-.061
-.030	.009	.023	.044	.040	.037	.033	.031	.029	.023
.027	.025	.019	.011	.018	.012	.004			
I= 7	EVAL(I)=	1661.9							
-.055	-.086	-.092	-.065	-.176	.098	.595	-.673	.117	.192
-.154	.044	.098	.031	-.126	-.108	-.084	.000	.014	-.010
-.014	-.002	.020	.047	.043	.039	.035	.016	-.003	.012
.007	.012	.006	.006	-.000	.008	-.001			
I= 8	EVAL(I)=	1503.3							
.021	.038	.012	-.003	.049	-.039	.061	-.027	-.064	-.055
-.005	.156	.433	-.772	.407	-.087	.040	.018	-.002	.002
.012	.015	.020	-.001	-.001	-.002	-.002	-.002	-.001	.004
-.007	.003	.006	-.001	.000	-.000	.002			
I= 9	EVAL(I)=	1465.0							
-.006	.021	-.019	.019	.070	-.105	-.043	-.104	.217	-.159
-.124	.727	-.566	-.100	.123	-.031	-.053	.008	.046	-.034
.006	.005	-.003	-.006	-.008	-.009	-.011	-.005	.000	-.010
.007	-.006	-.001	-.005	-.008	-.000	.002			
I= 10	EVAL(I)=	1380.8							
.035	.048	.019	.037	-.129	-.284	.031	-.046	.392	-.174
-.039	-.391	-.118	.161	.591	-.199	-.291	-.120	-.095	-.077
-.086	-.058	-.048	-.007	-.002	.003	.007	.003	-.000	.007
.003	.001	-.000	.007	.006	-.001	-.001			
I= 11	EVAL(I)=	1349.5							
.083	.181	.092	.128	.184	-.669	.262	.040	.318	-.076
.020	-.069	.094	-.075	-.308	.215	.283	.142	.046	.011
.031	-.009	-.022	-.058	-.048	-.038	-.030	-.030	-.029	-.018
-.037	-.023	-.010	-.010	-.014	-.012	-.000			
I= 12	EVAL(I)=	1304.1							
.041	.077	.035	.030	-.094	-.389	.395	.236	-.676	.218
-.038	.095	-.162	.107	.171	-.118	-.113	-.066	-.005	-.064
.004	-.018	-.004	-.016	-.013	-.010	-.007	-.002	.004	.008
.002	-.004	.005	-.001	.005	.004	-.001			

Table VI-3(c)

Eigenvalues λ_i and Corresponding Eigenvectors x_i of the Correlation Matrix C for 75 GeV.

I= 1	EVAL(I)=	64726.4							
.063	.120	.128	.203	.293	.340	.357	.343	.261	.239
.178	.076	.006	-.060	-.104	-.147	-.182	-.173	-.171	-.187
-.158	-.177	-.134	-.138	-.124	-.110	-.096	-.085	-.074	-.059
-.044	-.036	-.030	-.023	-.020	-.015	-.012			
I= 2	EVAL(I)=	16708.1							
-.085	-.145	-.139	-.188	-.209	-.162	-.065	.070	.155	.271
.389	.363	.356	.327	.267	.203	.140	.074	.022	-.026
-.047	-.080	-.092	-.104	-.100	-.096	-.091	-.087	-.083	-.070
-.055	-.046	-.042	-.035	-.029	-.025	-.019			
I= 3	EVAL(I)=	4498.7							
.119	.210	.184	.250	.298	.227	.054	-.128	-.202	-.287
-.258	.010	.162	.275	.297	.287	.268	.177	.081	.049
-.013	-.071	-.081	-.101	-.107	-.113	-.118	-.113	-.109	-.085
-.078	-.063	-.053	-.047	-.043	-.038	-.026			
I= 4	EVAL(I)=	3226.1							
-.121	.193	.150	.153	-.112	-.077	-.292	-.545	-.214	-.133
.372	.272	.146	-.003	-.131	-.196	-.222	-.210	-.143	-.133
-.079	-.080	-.036	-.029	-.020	-.011	-.003	.009	.021	.001
.022	.009	.014	.012	.012	.012	.011			
I= 5	EVAL(I)=	2891.4							
-.020	-.039	-.023	-.052	-.079	-.046	-.097	.041	.030	.109
-.737	.324	.341	.154	-.038	-.147	-.186	-.243	-.108	-.148
-.086	-.083	-.023	.008	.013	.017	.021	.034	.047	.038
.034	.028	.026	.021	.028	.017	.014			
I= 6	EVAL(I)=	2519.3							
.073	.113	.079	.119	.116	-.010	-.328	-.265	.198	.614
-.194	.164	-.332	-.265	.003	.112	.238	.150	.064	.017
.001	-.035	-.005	-.041	-.039	-.037	-.035	-.031	-.027	-.035
-.025	-.013	-.026	-.023	-.021	-.015	-.015			
I= 7	EVAL(I)=	2379.8							
-.063	-.124	-.084	-.096	-.017	.164	.369	-.066	-.164	-.184
-.013	.726	-.423	-.083	.039	.052	.014	.026	.032	.057
.047	.052	.016	.052	.040	.029	.020	.029	.038	.019
.010	.014	.009	.009	.003	.005	.002			
I= 8	EVAL(I)=	2161.1							
-.008	-.008	-.018	-.019	.038	.051	.179	-.125	-.111	.193
-.004	-.003	.059	.437	-.793	.120	.100	.164	.067	.108
.052	.047	.031	.017	.007	-.001	-.008	-.011	-.013	-.006
-.015	-.009	-.011	-.009	-.011	-.006	-.008			
I= 9	EVAL(I)=	2120.8							
-.003	.009	.019	.038	.003	.003	-.463	.250	.268	-.285
.019	.041	-.493	.441	-.098	.201	-.032	-.190	-.082	-.165
-.060	-.038	-.034	-.028	-.017	-.007	.001	.007	.013	.004
.013	.015	.012	.009	.011	.004	.010			
I= 10	EVAL(I)=	2016.7							
-.036	-.056	-.044	-.063	-.099	.011	.354	-.451	-.023	.269
-.050	-.310	-.308	.419	.328	-.034	-.147	-.213	-.107	-.104
-.067	-.042	-.028	.004	.008	.011	.014	.016	.017	.023
.018	.021	.014	.016	.013	.013	.012			
I= 11	EVAL(I)=	1976.3							
-.030	-.064	-.070	-.103	-.145	.418	.017	-.412	.686	-.279
-.030	-.020	.171	-.089	-.072	.028	-.029	.061	.059	.105
.028	-.006	-.004	.015	.009	.003	-.001	-.003	-.005	.008
.003	.002	-.010	-.002	-.004	.001	.002			
I= 12	EVAL(I)=	1880.1							
.095	.113	.077	.080	-.098	-.625	.358	-.105	.236	-.204
-.081	-.006	-.020	-.216	-.165	.324	.177	-.188	-.078	-.110
-.111	-.117	-.112	-.090	-.071	-.056	-.043	-.027	-.010	-.027
.000	.002	-.004	-.001	.001	.002	-.000			

Table VI-4 Diagonal Elements C^s_{ii} of the Correlation Matrix of Shower Fluctuation.

25 GeV	563.	548.	690.	1040.	1502.	1638.	1429.	1037.	738.	585.
	442.	402.	450.	467.	486.	545.	539.	420.	325.	288.
	249.	206.	165.	135.	117.	97.	76.	55.	37.	28.
	23.	15.	11.	9.	7.	5.	4.			
50 GeV	925.	1032.	1453.	2373.	3686.	4487.	4417.	3608.	2653.	2050.
	1534.	1056.	934.	977.	1093.	1358.	1491.	1311.	1183.	1135.
	1010.	879.	722.	576.	469.	374.	291.	224.	174.	131.
	90.	61.	43.	31.	23.	15.	9.			
75 GeV	1177.	1403.	2076.	3582.	5868.	7434.	7837.	6883.	5370.	4473.
	3486.	2360.	1899.	1830.	1885.	2212.	2436.	2282.	2192.	2176.
	2063.	1901.	1633.	1395.	1215.	1039.	869.	709.	563.	404.
	263.	182.	134.	100.	73.	51.	32.			
100 GeV	1302.	1643.	2604.	4773.	8125.	10946.	12129.	10873.	8640.	7444.
	6008.	4077.	2959.	2293.	2122.	2726.	3372.	3347.	3328.	3467.
	3399.	3084.	2643.	2293.	1973.	1676.	1403.	1149.	913.	677.
	462.	307.	210.	148.	101.	65.	30.			

Table VI-3(d)

Eigenvalues λ_i and Corresponding Eigenvectors x_i of the Correlation Matrix C for 100 GeV.

I= 1	EVAL(I)= 101720.9									
.053	.189	.328	.349	.270	.259					
.211	.008	-.128	-.170	-.170	-.189					
-.240	-.150	-.116	-.100	-.084	-.064					
-.056	-.027	-.017	-.014							
I= 2	EVAL(I)= 22038.3									
.077	.191	.196	.117	.104	.235					
-.354	-.344	-.228	-.146	-.026	-.029					
.557	.100	.087	.081	.080	.066					
-.057	.029	.019	.016							
I= 3	EVAL(I)= 5582.7									
.111	.261	.209	.089	.127	.336					
-.244	-.287	-.284	-.309	-.167	-.051					
.014	.170	.209	.113	.116	.081					
-.072	-.058	-.104	-.024							
I= 4	EVAL(I)= 3835.6									
.106	.152	.100	.259	.438	.228					
-.177	-.251	-.144	-.375	-.211	-.192					
.098	.147	.225	.045	.047	.036					
-.033	-.041	-.036	-.011							
I= 5	EVAL(I)= 3170.3									
.077	.088	.108	.057	.274	.083					
-.744	-.096	-.049	-.015	-.123	-.074					
.660	.305	.039	.041	.041	.036					
-.029	-.007	-.012	-.012							
I= 6	EVAL(I)= 3050.9									
.059	.082	.122	.093	.205	.666					
-.314	-.117	-.283	-.054	-.108	-.053					
.918	.150	.024	.011	.007	.001					
-.010	-.008	-.001	-.001							
I= 7	EVAL(I)= 3049.8									
.014	.026	.010	.002	.015	.092					
-.044	-.016	-.006	.110	.016	.034					
.031	.007	.009	.008	.007	.005					
-.004	.003	.004	.001	.000						
I= 8	EVAL(I)= 2836.7									
.040	.086	.120	.057	.249	.335					
-.181	-.367	-.389	-.306	-.138	-.118					
.805	.002	.009	.014	.030	.024					
-.028	-.017	-.013	-.013							
I= 9	EVAL(I)= 2789.4									
.066	.123	.074	.167	.516	.161					
.031	.154	.016	.066	.012	.019					
-.015	-.046	-.029	-.016	-.019	-.015					
-.011	-.003	-.008	-.002							
I= 10	EVAL(I)= 2479.7									
.029	.089	.001	.007	.288	.066					
.039	-.117	-.180	-.381	-.083	-.133					
-.084	-.339	-.001	.013	-.005	.009					
.015	.006	.017	-.007							
I= 11	EVAL(I)= 2278.6									
.001	.009	.046	.340	.288	.235					
.001	.068	.007	.404	.023	.338					
.181	.094	.069	.052	.028	.009					
.009	-.013	.001	.000							
I= 12	EVAL(I)= 2181.9									
-.034	.008	.093	.167	.137	.173					
.063	.023	.054	.418	.082	.014					
-.017	.030	.022	.017	.012	.016					
.011	.003	.001	.001							

Table VI-6(a)

Eigenvalues λ_i^S and Corresponding Eigenvectors x_i^S of the Correlation Matrix of Shower Fluctuation C^S for 25 GeV.

I= 1	EVAL(I)=	11507.9						
.111	.185	.188	.283	.365	.382	.343	.279	.158	.107
-.004	-.071	-.135	-.168	-.187	-.206	-.217	-.178	-.150	-.156
-.122	-.127	-.090	-.099	-.086	-.073	-.061	-.051	-.040	-.032
-.025	-.019	-.015	-.009	-.012	-.006	-.007			
I= 2	EVAL(I)=	2787.4						
.169	.231	.200	.178	.154	.006	-.132	-.261	-.362	-.418
-.394	-.301	-.255	-.193	-.108	-.024	.038	.063	.056	.086
.085	.088	.083	.092	.085	.077	.070	.052	.034	.027
.032	.012	.019	.011	.008	.004	.003			
I= 3	EVAL(I)=	710.6						
-.484	-.333	-.342	-.156	-.004	.180	.278	.183	.070	-.040
-.118	-.307	-.215	-.208	-.151	-.095	.031	.034	.091	.122
.101	.118	.122	.123	.112	.102	.091	.078	.066	.057
.060	.045	.036	.033	.023	.032	.019			
I= 4	EVAL(I)=	362.4						
.578	-.015	.162	.182	.228	.196	.163	-.019	-.357	-.197
-.067	.161	.272	.170	.210	.249	.164	-.038	-.012	-.060
-.066	-.103	-.024	-.033	-.047	-.061	-.075	-.068	-.061	-.061
-.066	-.057	-.038	-.030	-.020	-.026	-.022			
I= 5	EVAL(I)=	255.1						
.277	.026	-.165	-.106	.036	-.011	.249	.111	.241	-.027
-.270	-.305	-.168	.120	.262	.404	.356	.193	.032	-.080
-.070	-.085	-.167	-.016	-.054	-.091	-.128	-.140	-.152	-.110
-.079	-.036	-.040	-.045	-.041	-.021	-.025			
I= 6	EVAL(I)=	174.2						
-.434	.096	.543	.125	-.100	-.250	-.219	.001	.440	.134
-.023	-.244	-.219	.013	.043	.074	.029	-.041	.115	.030
.021	-.043	-.088	-.055	-.033	-.012	.009	.006	.002	-.028
.054	.071	.044	.015	.023	.029	.026			
I= 7	EVAL(I)=	143.5						
-.090	.071	-.166	-.104	-.130	-.141	-.023	-.005	-.027	-.100
-.286	.002	-.016	.024	.066	.107	-.041	-.418	-.368	-.288
-.374	-.203	-.133	-.011	.039	.089	.139	.146	.152	.161
.168	.155	.141	.108	.107	.068	.092			
I= 8	EVAL(I)=	108.0						
.206	-.136	.032	.315	.118	.213	-.069	.172	.360	-.130
-.194	.098	.319	.212	.161	.111	.060	-.190	.191	.097
.222	.039	.180	.149	.156	.163	.170	.153	.135	.112
.139	.071	.060	.064	.054	.075	.022			
I= 9	EVAL(I)=	88.7						
-.072	.020	-.277	.405	-.025	.011	-.152	-.147	.038	.061
.226	-.191	-.212	.152	.129	.106	-.015	-.258	-.478	.204
.073	.044	.217	.159	.080	-.000	-.080	-.091	-.102	-.082
-.093	-.092	-.131	-.101	-.108	-.048	-.077			
I= 10	EVAL(I)=	73.4						
.096	-.027	.358	-.093	.069	-.037	.149	.131	-.094	.306
.089	.068	-.016	-.130	.023	.177	.225	.244	-.311	-.033
-.263	.198	-.313	.239	.227	.214	.202	.147	.093	-.013
-.034	.009	-.011	.003	-.043	-.016	-.006			
I= 11	EVAL(I)=	67.2						
-.022	-.036	-.288	.411	.057	-.057	-.299	.131	-.044	.135
.037	.183	-.078	-.389	-.104	.180	.148	.084	.301	.055
-.328	-.151	-.216	.054	.051	.048	.045	.085	.125	-.192
-.019	-.042	-.040	.016	-.068	.009	.015			
I= 12	EVAL(I)=	37.2						
-.029	.065	-.021	-.058	-.077	-.144	.016	.078	.072	-.037
-.240	.183	-.048	-.093	-.065	-.038	.101	-.307	.233	-.128
-.169	.068	.665	-.059	-.118	-.176	-.235	-.109	.016	-.160
-.132	-.024	.023	-.036	-.073	-.144	-.078			

Table VI-5 Diagonal Elements C_{ii}^D of the Correlation Matrix of Detector Fluctuation.

25 GeV	50 GeV	75 GeV	100 GeV
51.	-195.	-191.	-216.
1061.	2113.	3530.	3994.
147.	483.	506.	749.
30.	128.	121.	259.
529.	853.	983.	1204.
8331.	1437.	2324.	2555.
2333.	607.	1124.	1697.
22.	77.	96.	127.
84.	81.	58.	-51.
661.	1520.	2284.	-2776.
88.	185.	331.	331.
17.	46.	85.	122.
664.	690.	857.	1134.
7007.	16000.	22355.	30333.
238.	424.	766.	1188.
10.	34.	56.	68.
909.	1474.	2023.	2000.
6301.	14499.	21666.	31101.
186.	369.	637.	940.
11.	59.	56.	79.
997.	1645.	2249.	2794.
5145.	11505.	18265.	23777.
135.	302.	502.	669.
7.	21.	38.	44.
1010.	1730.	2430.	2868.
5666.	13117.	19633.	26933.
85.	223.	362.	374.
7.	20.	35.	127.
1136.	2113.	3007.	4153.
3056.	5966.	15333.	13903.
73.	215.	356.	467.
755.	1130.	1388.	1137.
2095.	5566.	8266.	11155.
59.	188.	335.	543.
970.	1859.	2609.	3479.
3146.	7322.	13577.	19105.
56.	126.	234.	267.

Table VI-6(b)

Eigenvalues λ_i^s and Corresponding Eigenvectors x_i^s of the Correlation Matrix of Shower Fluctuation C^s for 50 GeV.

I= 1	EVAL(I)=	34470.9							
.084	.148	.153	.239	.319	.362	.358	.324	.241	.182
.108	.021	-.051	-.106	-.142	-.179	-.210	-.179	-.175	-.184
-.151	-.161	-.122	-.118	-.104	-.089	-.074	-.066	-.057	-.045
-.036	-.028	-.023	-.020	-.015	-.011	-.008			
I= 2	EVAL(I)=	7158.5							
-.123	-.192	-.191	-.204	-.195	-.113	-.019	.123	.248	.360
.401	.374	.322	.263	.193	.122	.043	-.011	-.037	-.066
-.089	-.099	-.093	-.107	-.098	-.089	-.079	-.071	-.062	-.055
-.043	-.037	-.028	-.023	-.018	-.016	-.010			
I= 3	EVAL(I)=	1619.0							
.272	.281	.312	.277	.172	.015	-.112	-.209	-.247	-.125
-.058	.115	.200	.284	.265	.246	.175	.123	.038	-.031
-.109	-.100	-.149	-.168	-.157	-.146	-.135	-.124	-.112	-.089
-.083	-.070	-.057	-.044	-.050	-.035	-.025			
I= 4	EVAL(I)=	902.3							
-.419	-.182	-.196	.003	.134	.304	.342	.179	.092	-.169
-.254	-.068	-.057	.055	.151	.248	.236	.323	.207	.135
.114	-.006	-.031	-.027	-.049	-.071	-.093	-.088	-.083	-.091
-.086	-.065	-.065	-.047	-.050	-.043	-.033			
I= 5	EVAL(I)=	482.2							
.729	.026	-.145	-.118	-.103	-.050	.040	.124	.334	.139
-.045	-.076	-.134	-.164	-.038	.087	.118	.286	.159	.120
.195	.016	.034	-.020	-.028	-.037	-.045	-.058	-.072	-.090
-.067	-.058	-.040	-.038	-.035	-.040	-.014			
I= 6	EVAL(I)=	352.2							
-.341	.066	.662	.045	-.017	-.175	-.199	.011	.265	.274
.135	-.044	-.161	-.162	-.082	-.002	.081	.206	.147	.136
.179	.046	.018	-.007	-.014	-.020	-.027	-.032	-.037	-.062
-.060	-.075	-.033	-.035	-.029	-.030	.012			
I= 7	EVAL(I)=	245.9							
-.056	-.052	-.088	-.058	-.127	-.056	-.147	-.033	.019	.155
-.014	-.400	-.365	-.135	.077	.288	.136	.048	-.149	-.118
-.445	-.190	-.390	-.144	-.100	-.056	-.013	.031	.074	.077
.084	.050	.066	.071	.050	.043	.055			
I= 8	EVAL(I)=	157.8							
-.065	-.032	-.264	.123	.080	-.032	-.118	.018	-.449	.185
.265	-.037	-.257	-.194	-.065	.064	.041	-.074	-.258	.015
.355	.084	.154	-.109	-.161	-.213	-.265	-.153	-.042	-.105
-.129	-.148	-.052	-.049	-.071	-.026	-.010			
I= 9	EVAL(I)=	133.9							
-.021	.012	.023	-.019	.006	.008	-.049	-.030	.125	.061
-.099	-.121	.052	-.039	.048	.135	.037	.053	-.247	-.067
-.495	.113	.706	.108	.055	.002	-.051	-.092	-.133	-.140
-.116	-.092	-.078	-.046	-.026	-.070	-.047			
I= 10	EVAL(I)=	110.4							
-.096	.117	-.393	.544	.187	-.119	-.128	-.193	.152	.125
.100	.249	-.202	-.024	-.047	-.070	-.027	.192	.344	-.047
-.171	.034	.100	-.087	-.000	.086	.173	.088	.003	.033
.046	.018	.050	.051	-.035	.033	.047			
I= 11	EVAL(I)=	86.0							
.019	.006	.076	-.195	.050	.058	.119	.029	-.268	.002
.117	.182	.121	-.141	-.182	-.224	.060	.640	-.103	-.027
-.176	-.012	.093	-.078	-.096	-.114	-.132	.007	.146	.135
.199	.203	.156	.030	.080	.142	.128			
I= 12	EVAL(I)=	71.0							
.038	-.017	.075	-.273	-.104	.085	.086	.039	-.368	.111
.033	.129	-.177	-.102	-.092	-.082	-.044	-.204	.627	.003
-.335	-.079	.012	.052	.011	-.030	-.070	-.092	-.115	-.083
-.041	-.147	-.016	-.175	-.132	-.024	-.054			

Table VI-6(c)

Eigenvalues λ_i^s and Corresponding Eigenvectors x_i^s of the Correlation Matrix of Shower Fluctuation C^s for 75 GeV.

I= 1	EVAL(I)=	62877.2							
.066	.122	.132	.207	.293	.338	.353	.337	.263	.235
.173	.075	.006	-.060	-.104	-.147	-.181	-.173	-.174	-.189
-.161	-.179	-.137	-.141	-.127	-.113	-.098	-.087	-.076	-.060
-.045	-.037	-.030	-.024	-.021	-.016	-.012			
I= 2	EVAL(I)=	14627.9							
-.099	-.156	-.159	-.203	-.208	-.157	-.061	.069	.165	.263
.352	.357	.351	.324	.265	.206	.141	.076	.023	-.028
-.053	-.086	-.105	-.115	-.111	-.107	-.103	-.099	-.094	-.080
-.063	-.053	-.048	-.040	-.033	-.029	-.022			
I= 3	EVAL(I)=	3004.5							
.232	.270	.302	.303	.228	.120	-.023	-.139	-.256	-.218
-.124	-.013	.106	.192	.227	.262	.249	.202	.125	.081
.015	-.052	-.090	-.111	-.125	-.139	-.153	-.150	-.146	-.122
-.113	-.092	-.078	-.071	-.065	-.057	-.039			
I= 4	EVAL(I)=	1385.2							
-.264	-.167	-.219	-.057	.080	.214	.279	.256	.272	.042
-.075	-.249	-.215	-.080	.042	.164	.200	.311	.296	.241
.236	.140	.092	.037	.006	-.025	-.055	-.084	-.113	-.062
-.105	-.068	-.078	-.066	-.071	-.058	-.049			
I= 5	EVAL(I)=	823.8							
-.619	-.186	-.149	.005	.111	.193	.195	.059	-.488	-.203
-.130	.006	.063	.169	.109	.050	-.012	-.100	-.130	-.104
-.225	-.074	-.138	-.016	-.012	-.008	-.005	.014	.032	.048
.029	.030	.050	.044	.041	.029	.026			
I= 6	EVAL(I)=	524.5							
-.322	.060	.308	.056	.088	.003	-.007	-.024	-.193	.101
.157	.246	.162	.043	-.084	-.211	-.168	-.109	-.033	.082
.514	.177	.370	.118	.064	.010	-.044	-.067	-.090	-.087
-.105	-.118	-.091	-.078	-.079	-.076	-.051			
I= 7	EVAL(I)=	483.4							
-.512	.084	.570	.094	-.037	-.106	-.247	-.054	.437	.027
-.053	-.117	-.062	-.021	.057	.135	.112	.009	.034	-.083
-.202	-.026	-.032	-.025	.007	.038	.069	.055	.041	.038
.061	.062	.028	.027	.025	.026	.027			
I= 8	EVAL(I)=	315.8							
.086	.040	-.183	.208	.106	.117	.001	.041	.149	-.013
-.098	.055	.176	.204	.137	.071	.024	-.056	.067	-.094
-.395	.045	.694	.152	.143	.133	.124	.071	.018	.096
-.035	-.042	-.022	-.046	-.022	-.040	-.024			
I= 9	EVAL(I)=	284.4							
-.105	.006	.017	-.012	-.051	-.145	-.090	-.064	-.336	.257
.182	.025	-.185	-.315	-.245	-.174	.077	.228	.217	.035
-.497	-.032	.167	-.081	-.084	-.087	-.090	-.097	-.103	-.205
-.114	-.051	-.090	-.075	-.083	-.028	-.074			
I= 10	EVAL(I)=	209.6							
-.153	.086	-.378	.248	-.062	-.172	-.278	-.097	.155	-.101
-.025	-.370	-.006	.005	-.027	-.059	.034	-.277	-.353	-.027
.058	.013	.073	-.056	-.119	-.181	-.244	-.206	-.169	-.200
-.117	-.025	-.113	-.068	-.006	-.064	-.011			
I= 11	EVAL(I)=	191.1							
-.154	.090	-.348	.530	.162	.015	-.177	-.160	.087	.084
.036	.474	-.188	-.104	-.038	.028	.032	.035	.220	.017
.122	.008	-.182	.039	.013	-.013	-.039	.078	.195	.087
.148	.124	.042	-.005	-.013	-.006	-.004			
I= 12	EVAL(I)=	154.0							
.062	-.092	.055	.010	.017	.001	.028	.022	-.116	.138
.091	.143	-.432	-.097	.117	.331	.224	.178	-.612	-.176
.122	-.006	.207	-.059	-.004	.051	.105	.109	.112	-.093
-.011	.026	-.045	-.004	-.065	-.007	-.016			

Table VI-6(d)

Eigenvalues λ_i^s and Corresponding Eigenvectors x_i^s of the Correlation Matrix of Shower Fluctuation C^s for 100 GeV.

I= 1	EVAL(I)=	99427.5						
.054	.103	.114	.191	.267	.326	.347	.343	.273	.256
.208	.118	.056	-.009	-.068	-.128	-.169	-.167	-.172	-.190
-.173	-.181	-.145	-.152	-.135	-.118	-.102	-.094	-.086	-.066
-.057	-.042	-.035	-.027	-.024	-.017	-.014			
I= 2	EVAL(I)=	19504.0						
-.089	-.163	-.158	-.205	-.232	-.192	-.113	-.011	.113	.225
.329	.352	.365	.335	.283	.230	.145	.096	.028	-.030
-.063	-.081	-.087	-.107	-.102	-.096	-.090	-.089	-.088	-.074
-.064	-.044	-.041	-.032	-.027	-.021	-.018			
I= 3	EVAL(I)=	3701.6						
.207	.268	.294	.301	.257	.114	.006	-.114	-.275	-.227
-.132	-.043	.114	.207	.206	.206	.272	.216	.159	.083
.011	-.017	-.063	-.100	-.119	-.137	-.156	-.157	-.158	-.119
-.105	-.100	-.088	-.063	-.060	-.050	-.036			
I= 4	EVAL(I)=	1792.6						
.260	.180	.206	.107	-.028	-.167	-.261	-.164	-.391	-.061
.083	.254	.199	.111	-.006	-.124	-.238	-.291	-.297	-.214
-.193	-.137	-.084	.005	.043	.080	.118	.115	.112	.094
.086	.072	.086	.061	.071	.046	.031			
I= 5	EVAL(I)=	880.3						
.531	.110	.333	.080	-.093	-.200	-.258	-.058	.604	.139
.071	-.019	-.074	-.006	-.008	-.010	-.001	.032	.070	.045
.131	.076	.190	.036	.035	.034	.033	.020	.007	-.009
-.017	-.024	-.033	-.033	-.007	-.014	-.000			
I= 6	EVAL(I)=	656.1						
-.690	.009	.488	.184	.089	-.015	-.113	-.068	-.287	-.075
-.097	.003	.171	.134	.081	.029	.010	.001	-.104	-.048
-.037	.032	.113	.039	.066	.093	.120	.079	.038	.073
.043	.012	.041	.009	.012	.005	.000			
I= 7	EVAL(I)=	584.9						
-.097	.010	.194	-.022	.017	.048	.079	.059	-.313	.176
.159	.393	.016	-.067	-.096	-.125	-.192	-.096	.133	.173
.437	.115	.434	.086	.057	.028	-.001	-.050	-.100	-.140
-.133	-.117	-.108	-.114	-.078	-.078	-.067			
I= 8	EVAL(I)=	427.8						
-.045	-.051	.484	-.217	-.135	-.031	.060	.019	-.104	.079
.135	.165	-.192	-.221	-.113	.005	-.006	.194	.281	.117
.001	-.025	-.606	-.058	-.013	.033	.078	.060	.043	-.046
.047	.071	.014	.059	.009	.040	.032			
I= 9	EVAL(I)=	369.7						
.107	.051	-.232	.174	.157	.109	.143	-.006	.125	-.142
-.064	.500	.157	-.131	-.057	.017	.014	.419	.197	-.005
-.210	.016	.097	.006	.114	.222	.331	.183	.036	.143
.114	.007	-.006	-.007	-.019	.000	-.014			
I= 10	EVAL(I)=	325.7						
.029	.028	-.213	.145	.129	-.068	.014	-.039	-.126	-.065
-.014	-.032	.172	.275	.063	-.149	-.058	-.094	-.027	.025
.675	.062	-.456	-.030	.045	.121	.196	.113	.030	.014
.048	.003	.026	-.030	-.022	.003	.015			
I= 11	EVAL(I)=	216.6						
.223	-.161	.277	-.393	-.013	.215	.387	.039	-.050	-.064
.001	-.180	.380	.166	.055	-.057	.121	.001	.080	-.071
.092	.042	.235	-.017	-.011	-.004	.002	.088	.173	.206
.209	.153	.050	.126	.101	.104	.009			
I= 12	EVAL(I)=	171.9						
-.002	-.006	.042	.009	.068	-.007	-.054	.059	-.085	.116
.068	.137	-.254	-.065	-.004	.057	.191	.451	-.581	-.055
.309	-.074	.089	-.088	-.085	-.082	-.079	-.044	-.009	.269
.051	.197	.018	.150	.006	.089	.086			

Table VI-7

Optimized Coefficient Values [in unit of (No. of electrons)^2] of the Fit of Correlation Matrix C^s to the two Dimensional 2nd Order Fourier Series.

Coefficient	Energy			
	25 GeV	50 GeV	75 GeV	100 GeV
a_{00}	2	-13	-21	-61
a_{01}	-1	-36	-50	-142
a_{02}	-9	-15	-3	-16
a_{11}	315	830	1341	1802
a_{12}	72	335	633	1017
a_{22}	75	269	503	833
b_{10}	-10	-46	-104	-205
b_{20}	-5	2	-10	-2
b_{11}	158	589	1094	1786
b_{12}	88	374	789	1390
b_{21}	-221	-506	-737	-898
b_{22}	-31	-139	-209	-279
d_{11}	153	689	1692	2931
d_{12}	84	-252	-333	-452
d_{22}	175	373	542	659

Table C-1

Non-Interacting (No Hadronic Interaction) Pion Pulse Height Obtained by the Gaussian Fit.

Chamber Plane No.	Pulse Height (Arbitrary Unit)	Error (Same Unit as PH)
1	1.81	.25
2	1.61	.24
3	2.32	.25
4	2.07	.25
5	1.75	.22
6	1.72	.32
7	1.69	.21
8	1.72	.24
9	2.05	.25
10	1.82	.22
11	1.69	.23
12	1.95	.26
13	1.88	.27
14	1.84	.20
15		
16	1.89	.26
17	1.82	.24
18	2.12	.30
19	2.17	.25
20	1.99	.25
21	2.36	.24
22	2.05	.24
23	2.57	.27
24	2.14	.31
25		
26		
27	2.14	.22
28		
29	2.03	.25
30	2.00	.21
31	2.18	.26
32	2.48	.24
33	2.44	.25
34	2.95	.30
35	2.61	.26
36	2.90	.26
37	2.86	.27

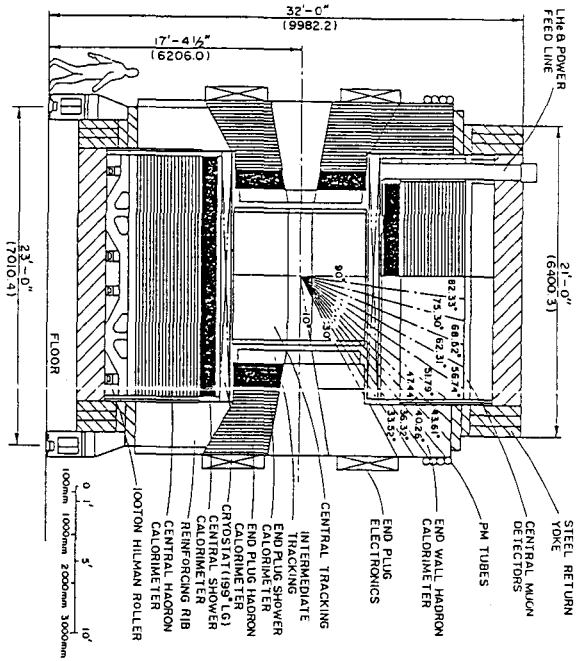

Fig. I-1

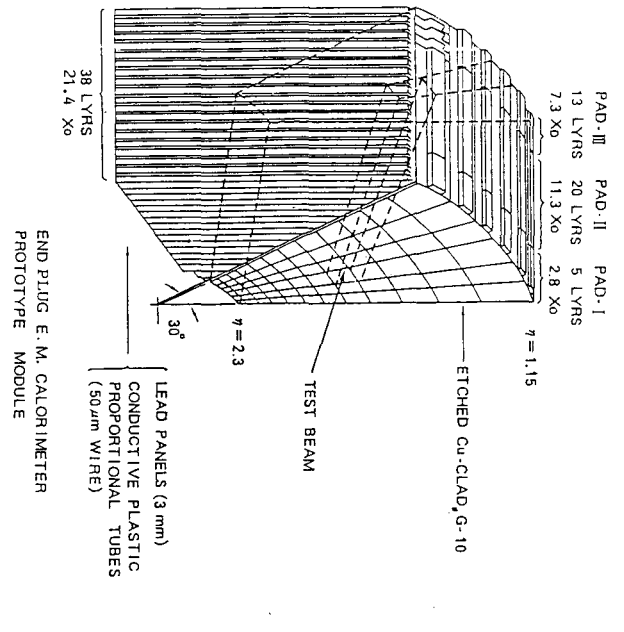

END PLUG E.M. CALORIMETER PROTOTYPE MODULE

Fig. I-2

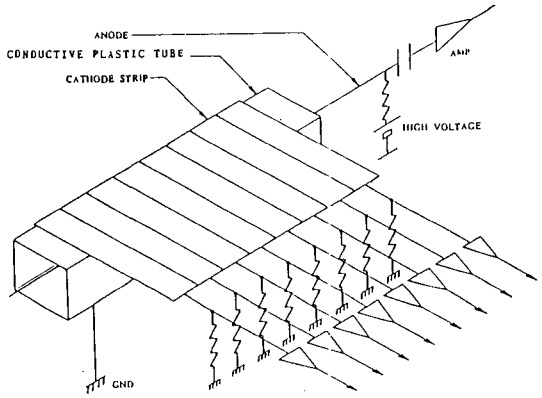

Fig. II-4(b)

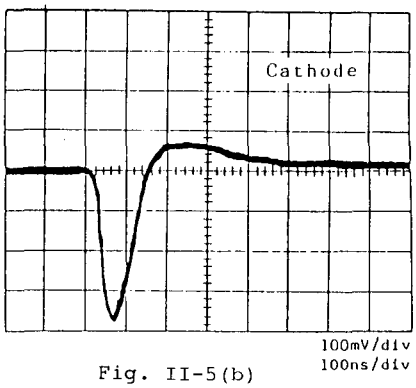

Fig. II-5(b)

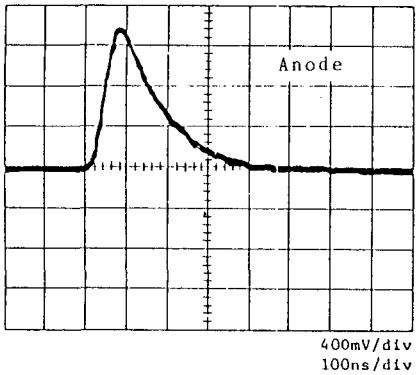

Fig. II-5(a)

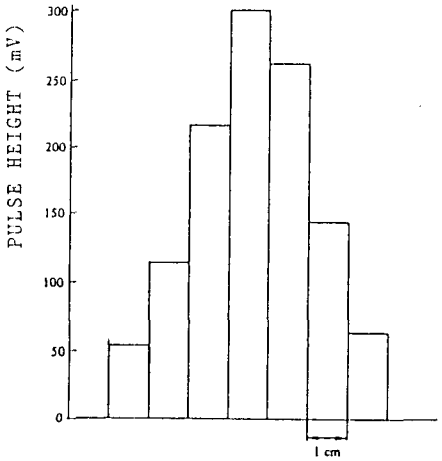

Fig. II-6

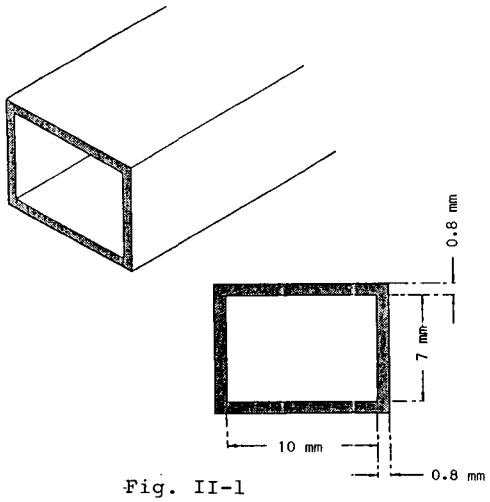

Fig. II-1

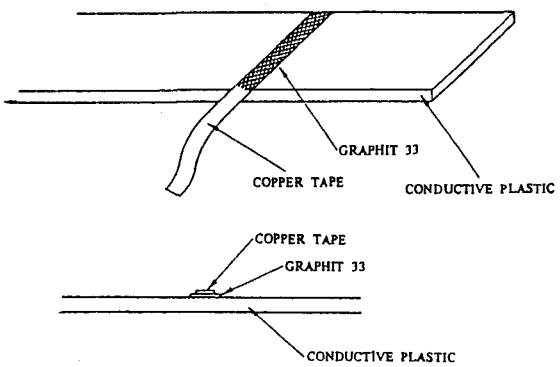

Fig. II-3

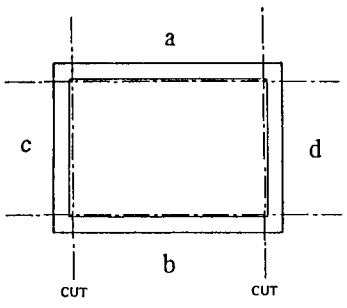

Fig. II-2

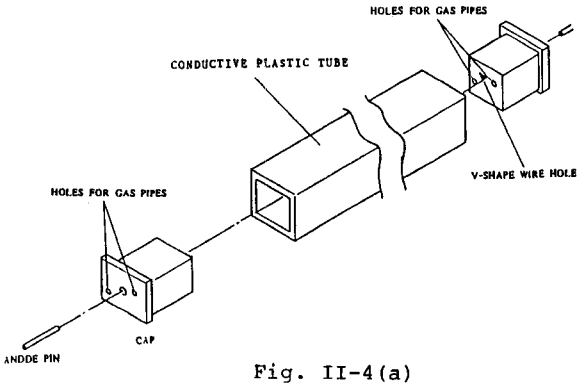

Fig. II-4(a)

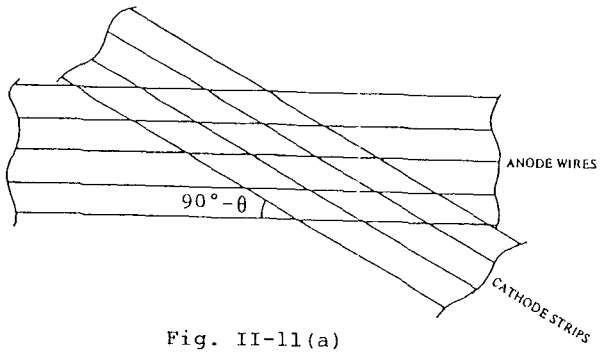

Fig. II-11(a)

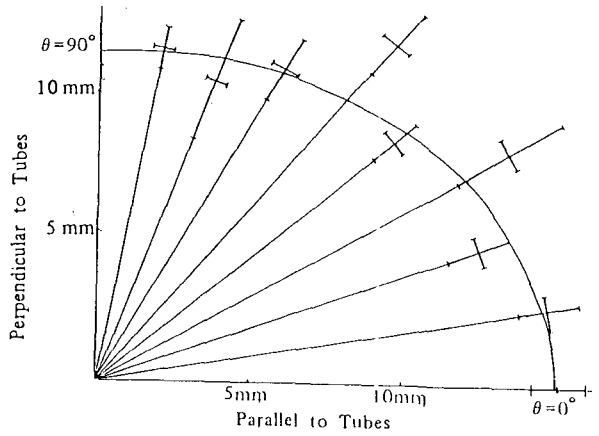

Fig. II-11(b)

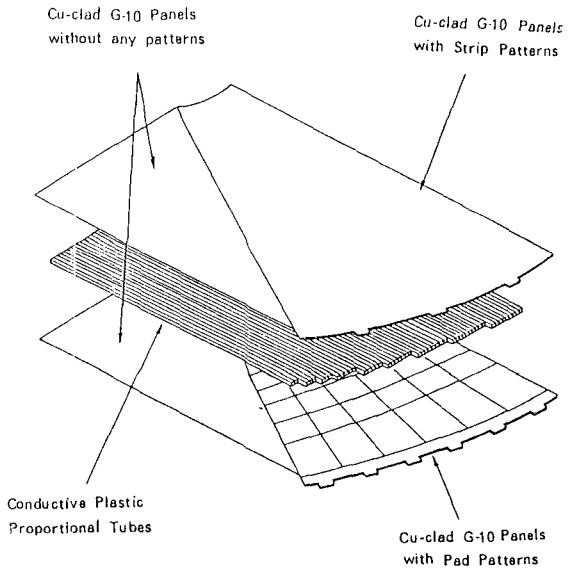

Fig. III-1

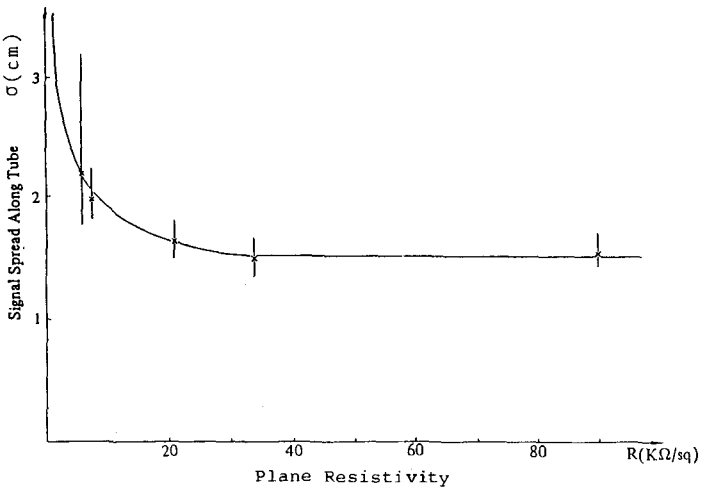

Fig. II-7

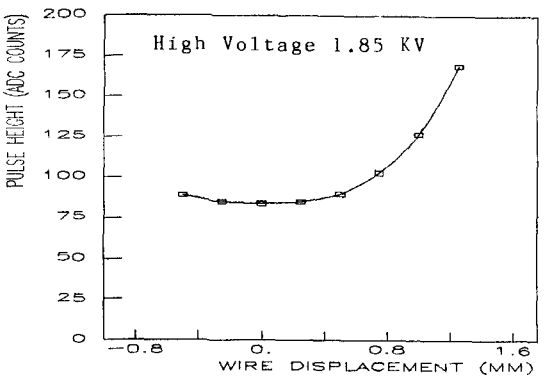

Fig. II-9

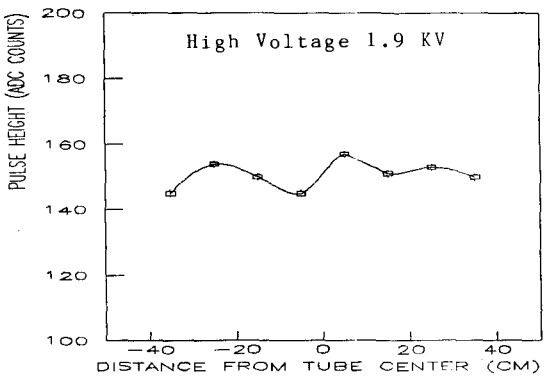

Fig. II-8

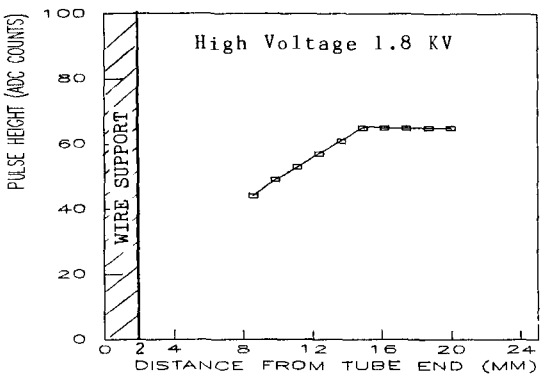

Fig. II-10

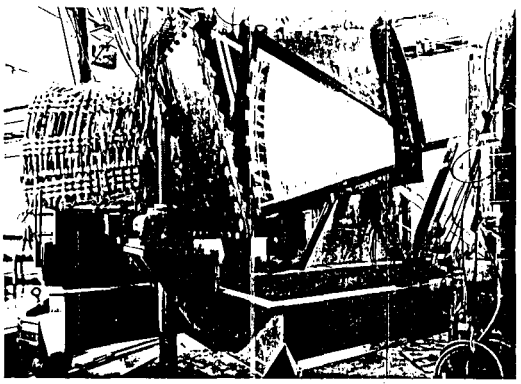

Fig. III-4

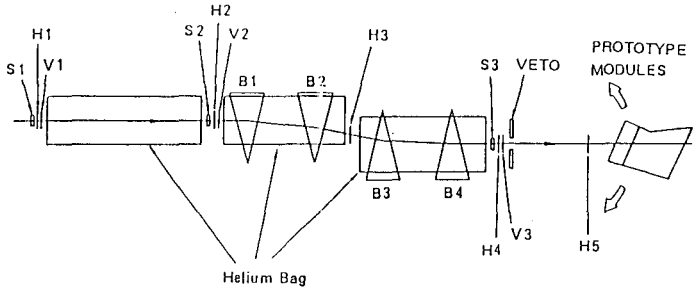

S1, S2, S3 : Scintillation Counters.
VETO : Scintillation Counter for vitoing halo beam.
H1, H2, H3, H4, H5 : X-Multiwira Proportional Chamber.
V1, V2, V3 : Y-Multiwira Proportional Chamber.
B1, B2, B3, B4 : Banding Magnets.

Fig. IV-1

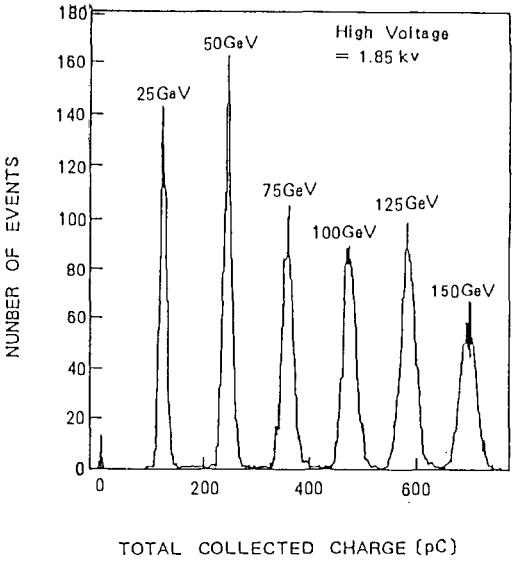

Fig. IV-2

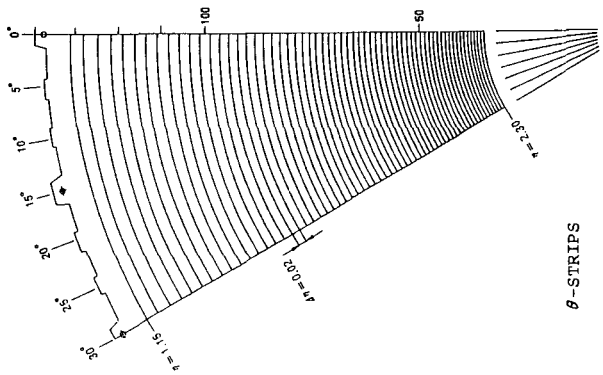

Fig. III-3(b)

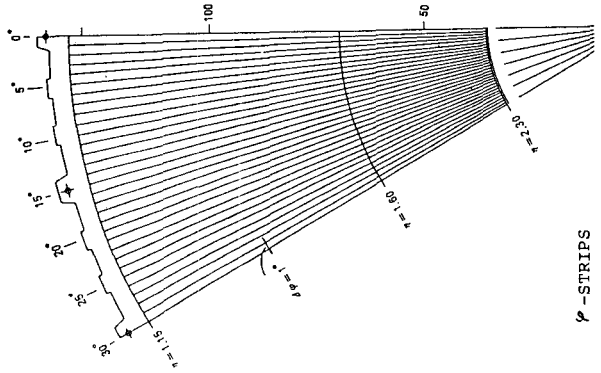

Fig. III-3(c)

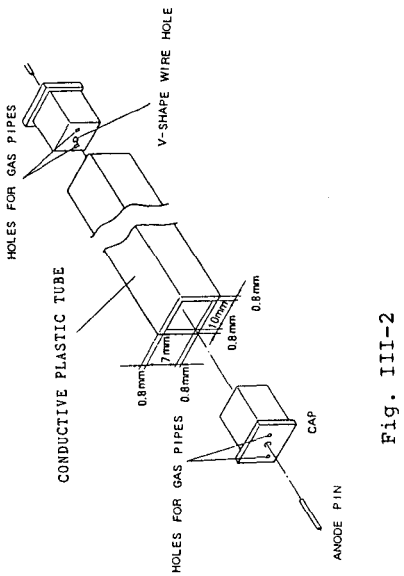

Fig. III-2

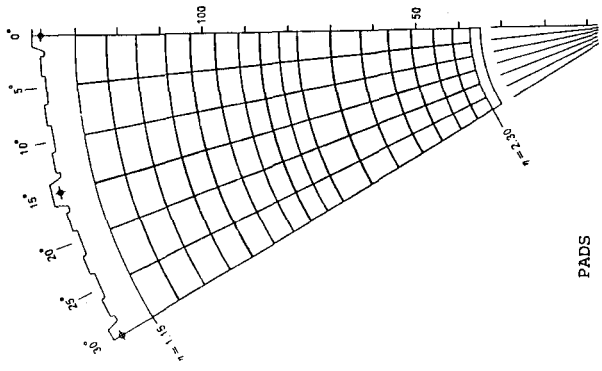

Fig. III-3(a)

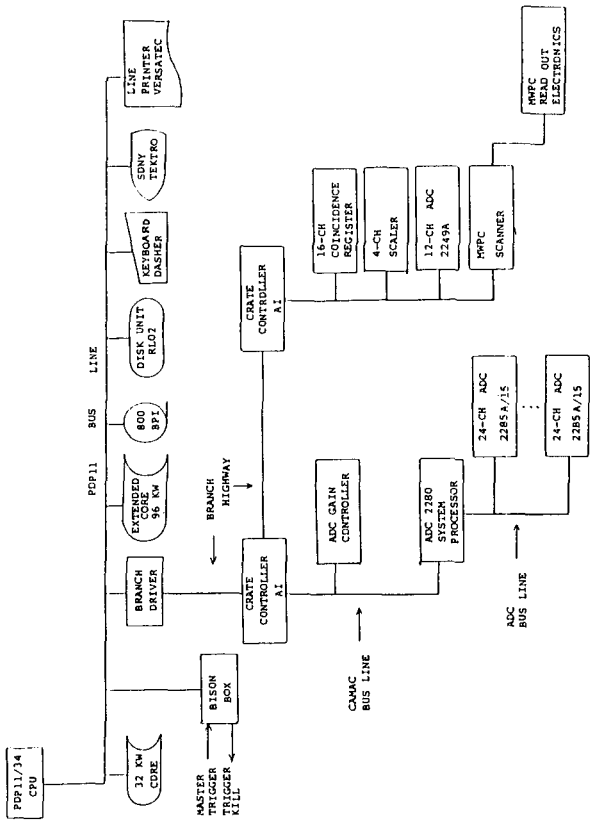

Fig. IV-4

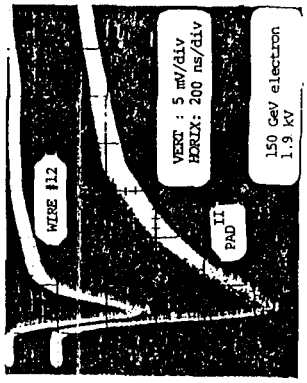

Fig. V-1(b)

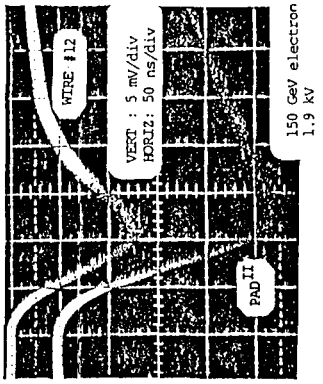

Fig. V-1(a)

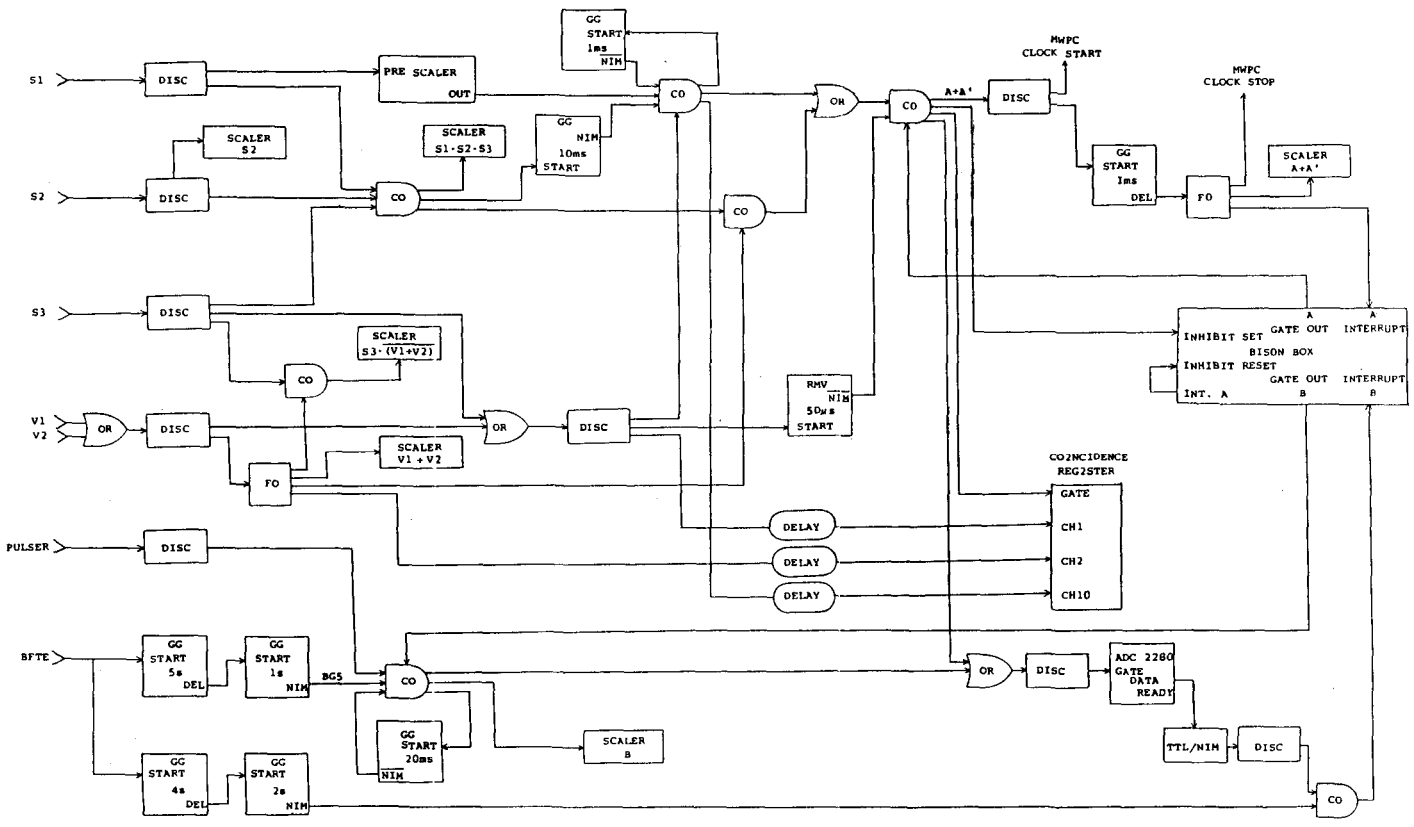

Fig. IV-3

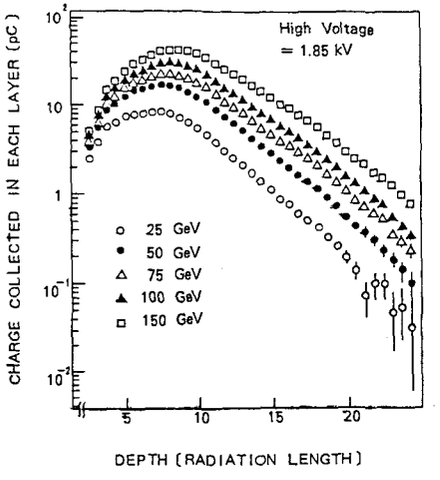

Fig. V-2

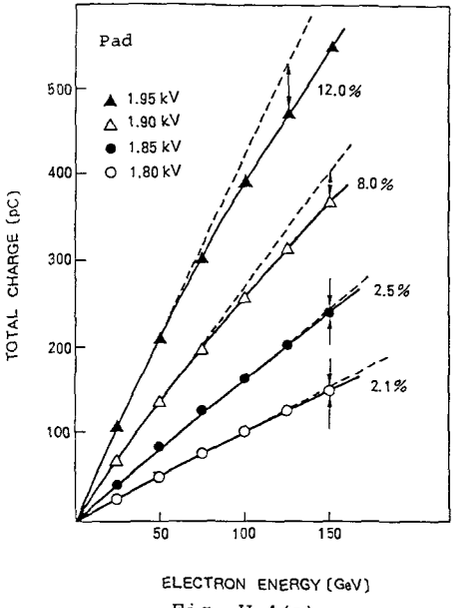

Fig. V-4(a)

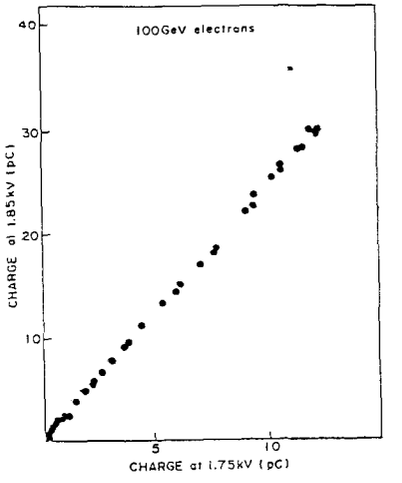

Fig. V-5(a)

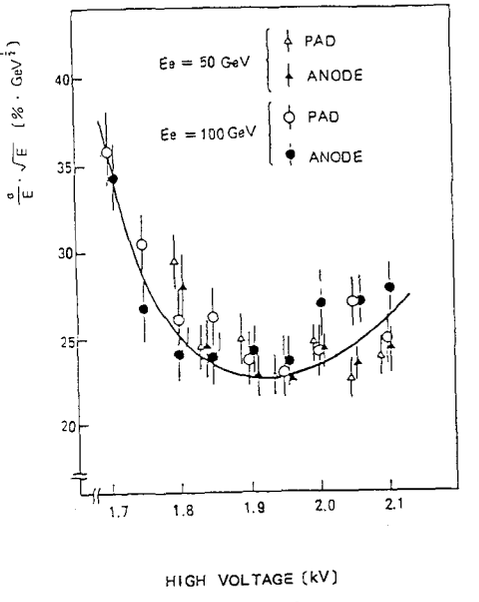

Fig. V-6

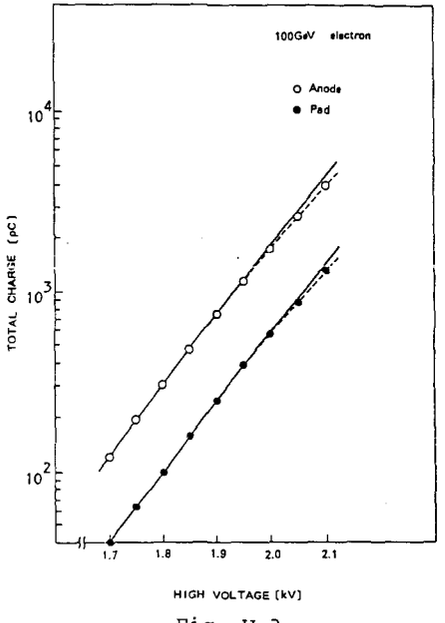

Fig. V-3

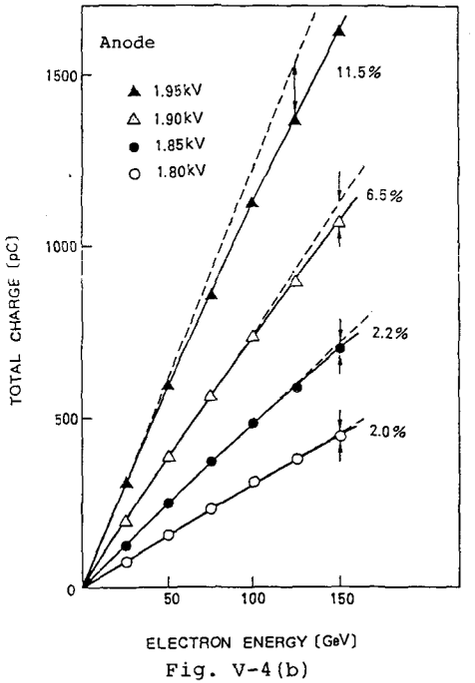

Fig. V-4(b)

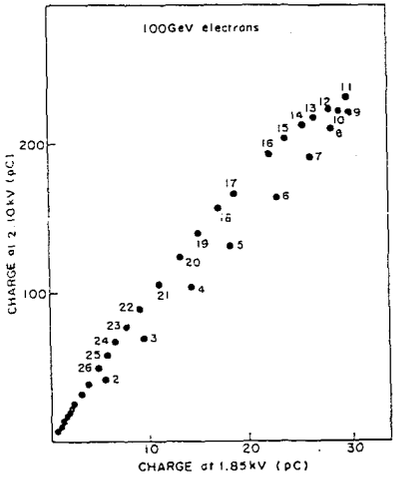

Fig. V-5(b)

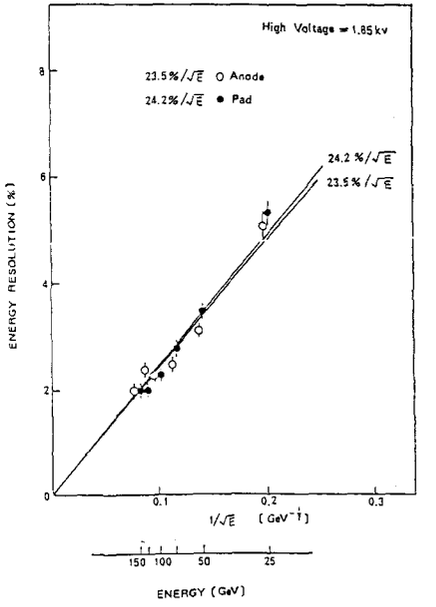

Fig. V-7

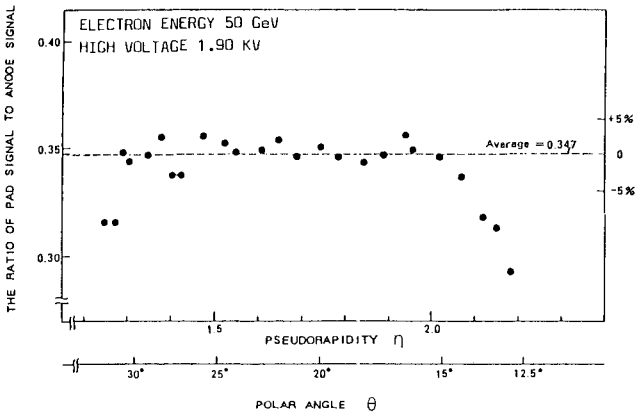

Fig. V-11

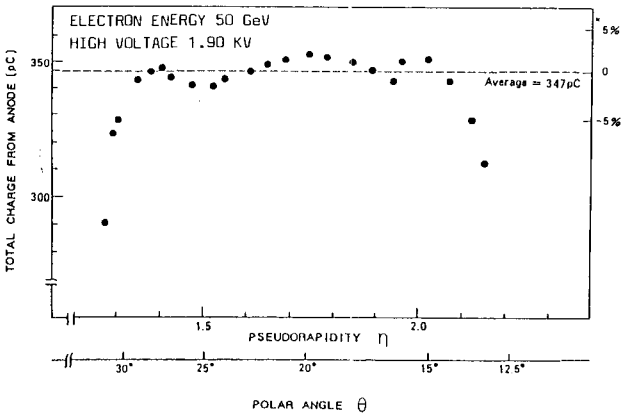

Fig. V-12

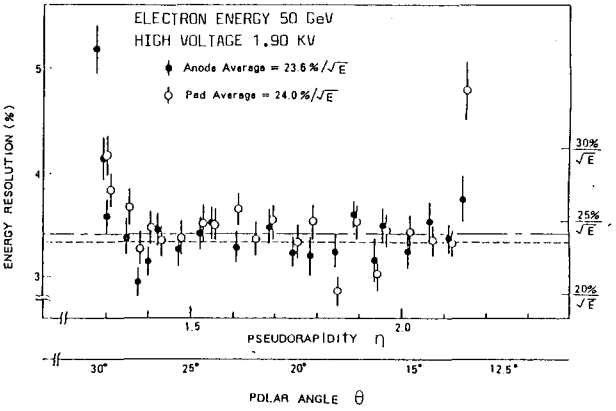

Fig. V-13

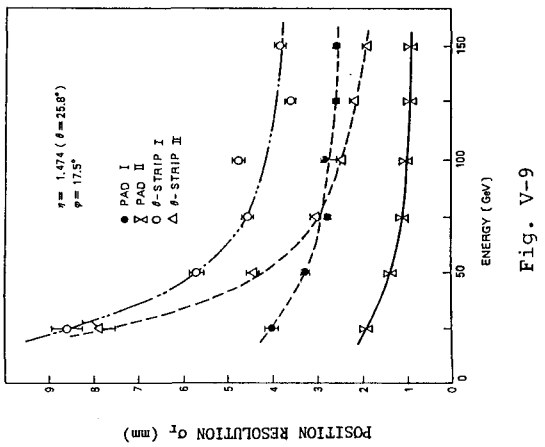

Fig. V-9

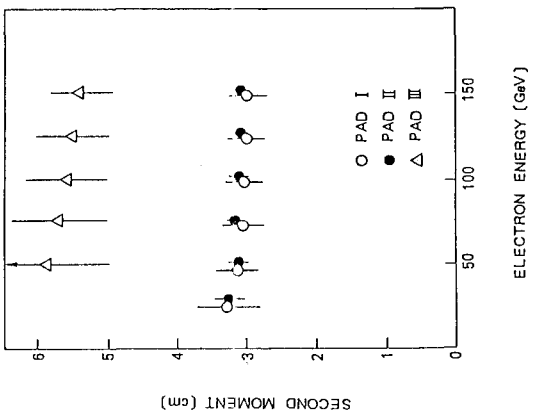

Fig. V-10

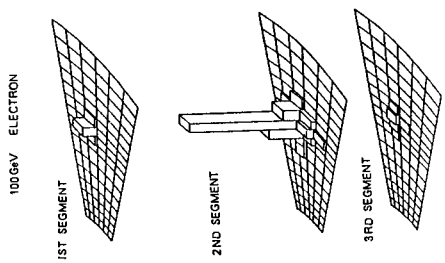

Fig. V-8(a)

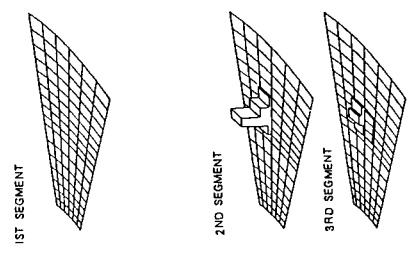

Fig. V-8(b)

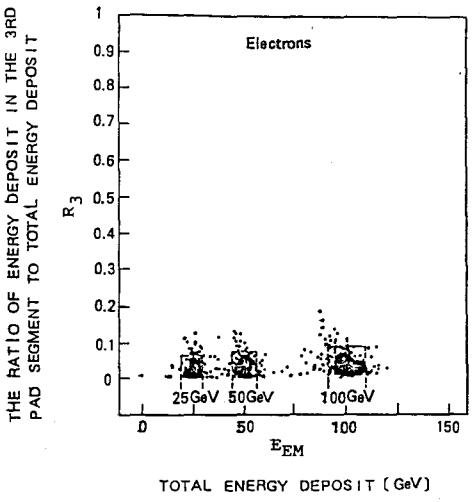

Fig. V-14(a)

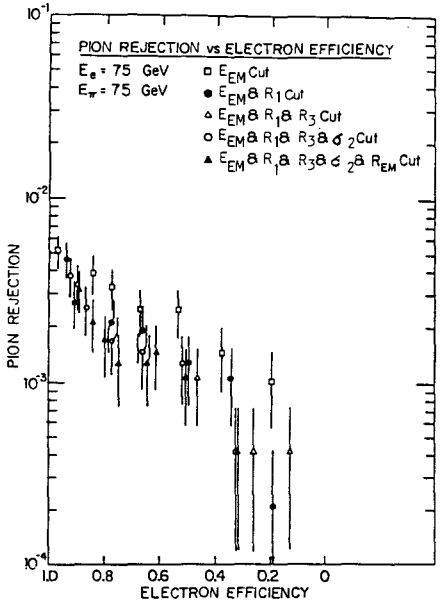

Fig. V-15(a)

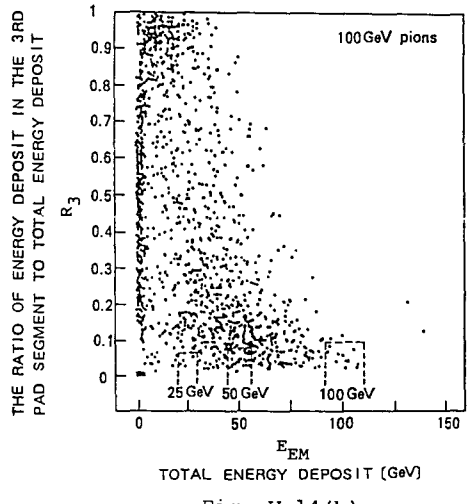

Fig. V-14(b)

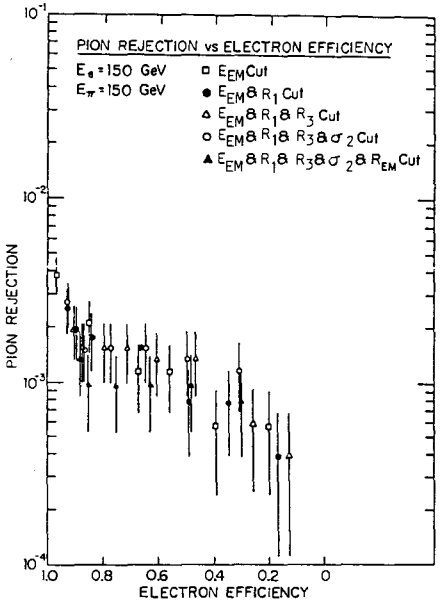

Fig. V-15(b)

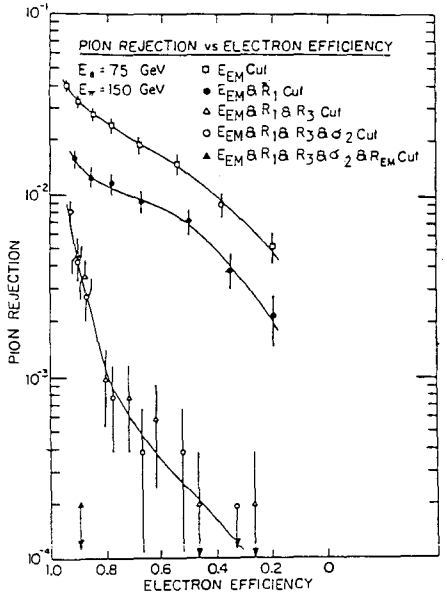

Fig. V-15(c)

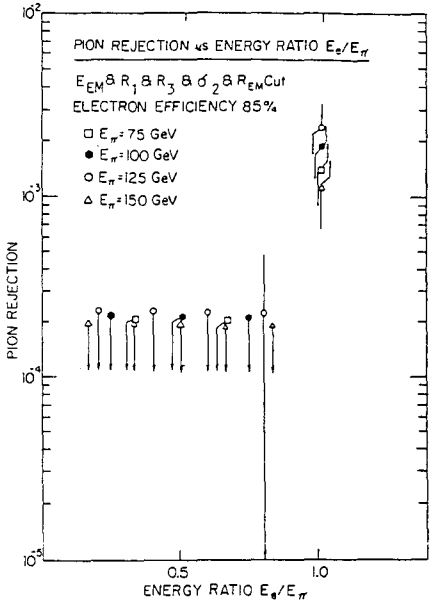

Fig. V-16(b)

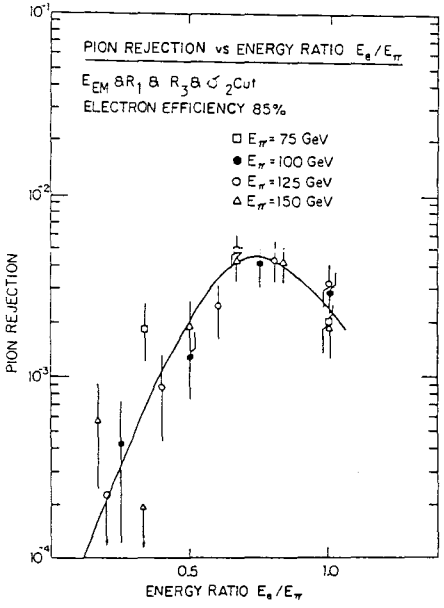

Fig. V-16(a)

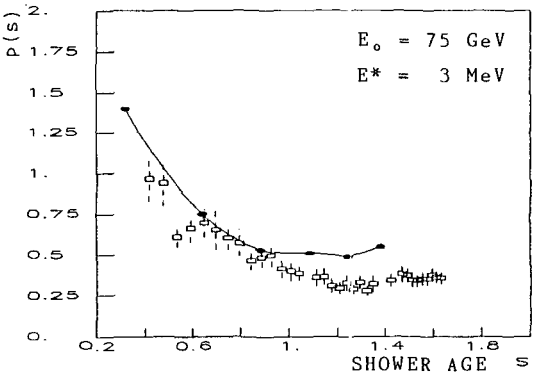

Fig. VI-2(a)

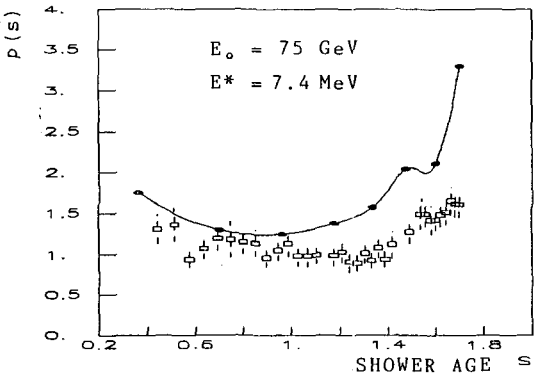

Fig. VI-2(b)

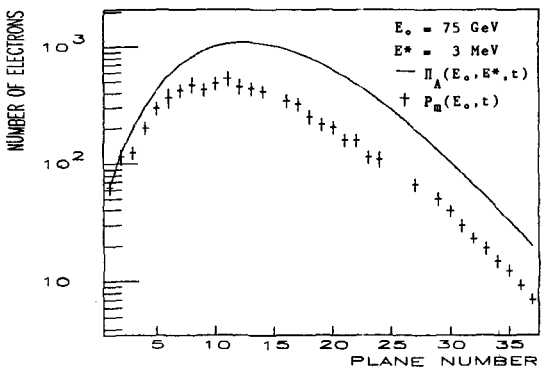

Fig. VI-1(a)

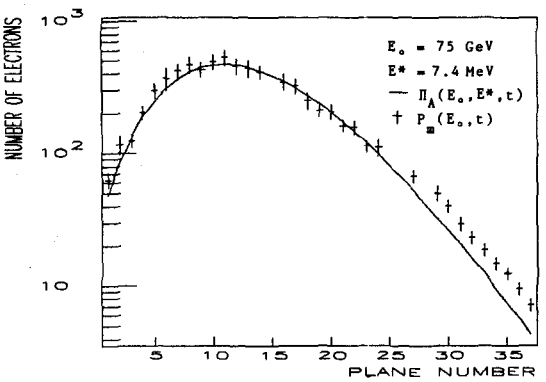

Fig. VI-1(b)

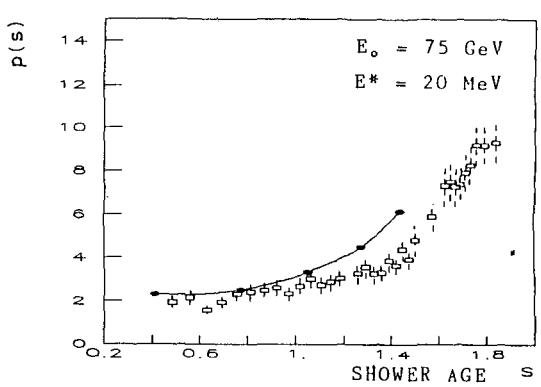

Fig. VI-2(c)

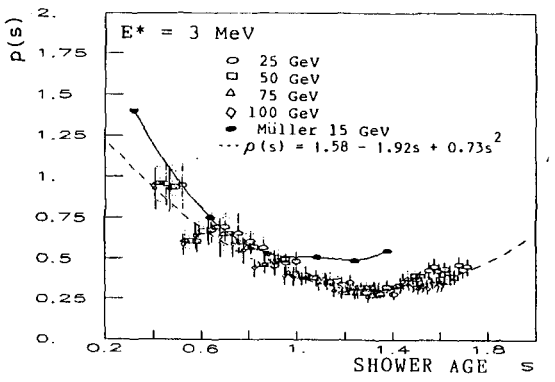

Fig. VI-3

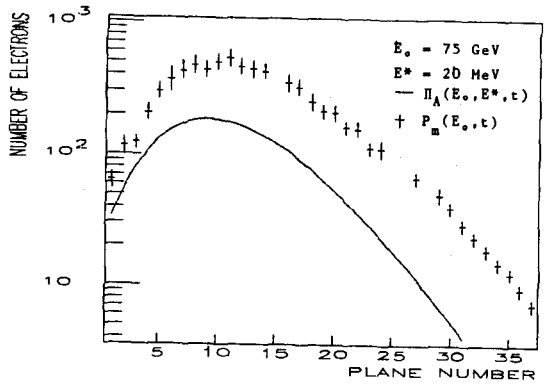

Fig. VI-1(c)

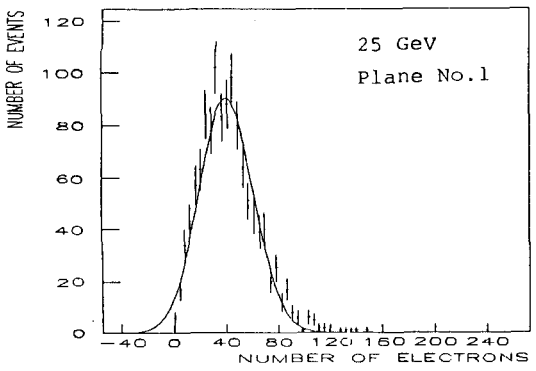

Fig. VI-5(a)

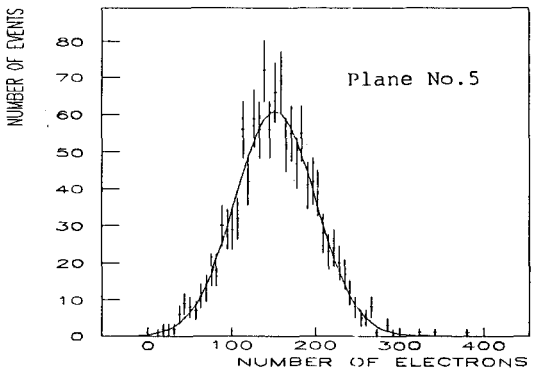

Fig. VI-5(b)

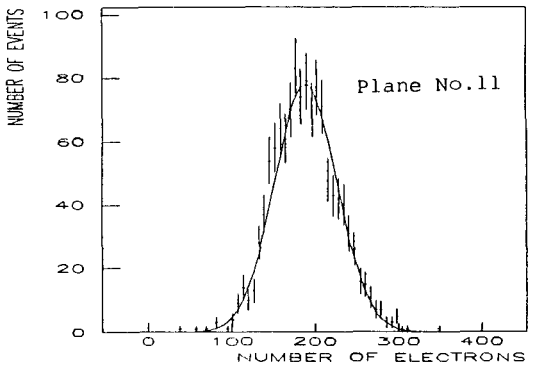

Fig. VI-5(c)

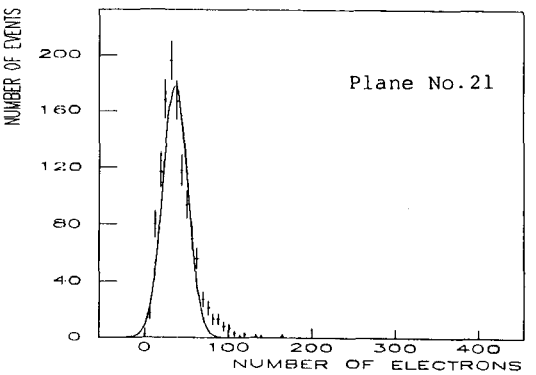

Fig. VI-5(d)

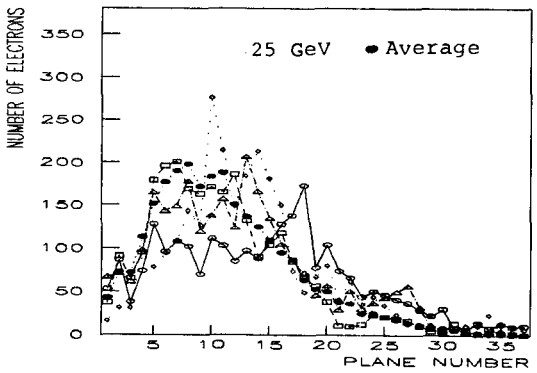

Fig. VI-4(a)

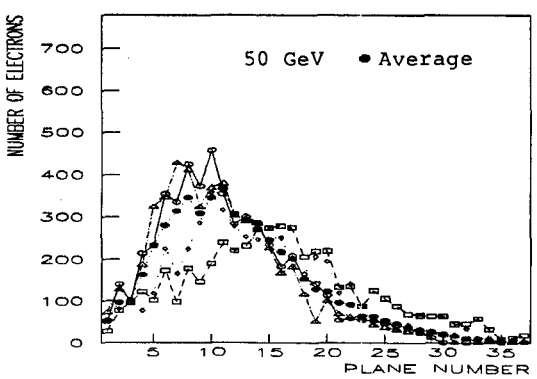

Fig. VI-4(b)

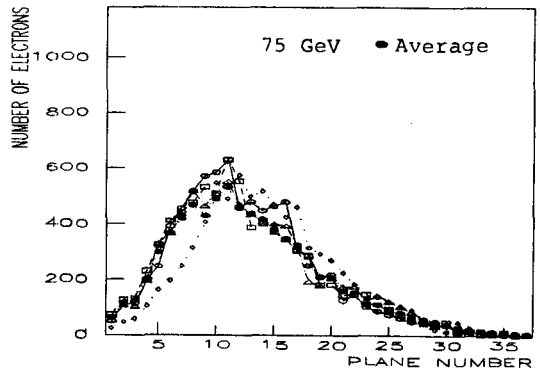

Fig. VI-4(c)

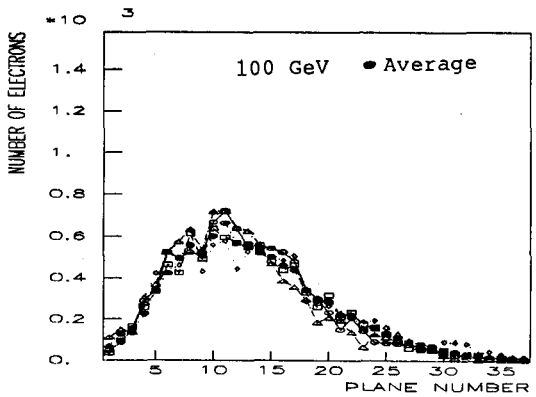

Fig. VI-4(d)

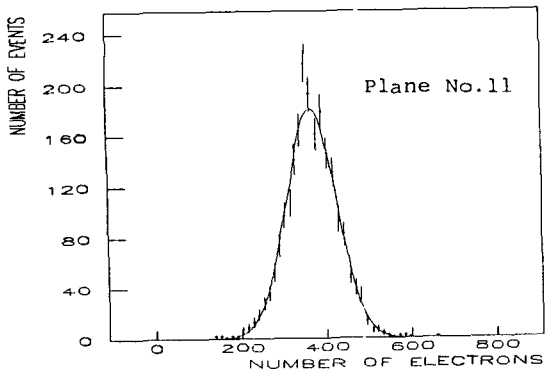

Fig. VI-6(c)

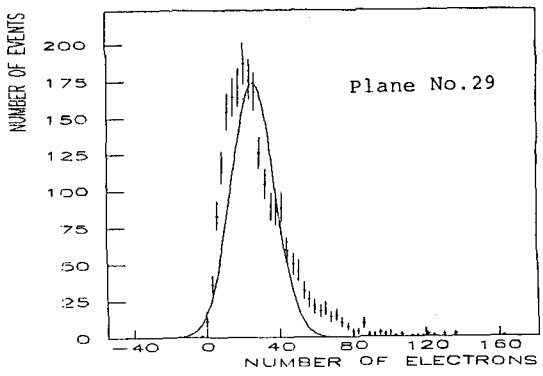

Fig. VI-6(e)

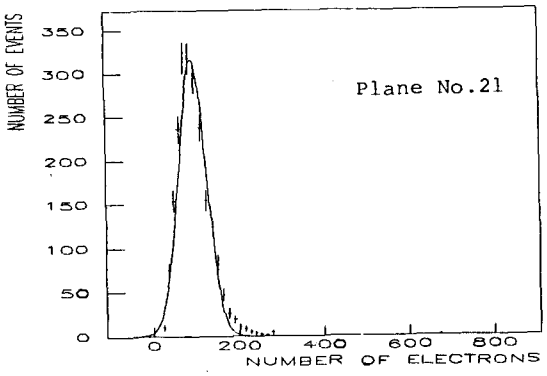

Fig. VI-6(d)

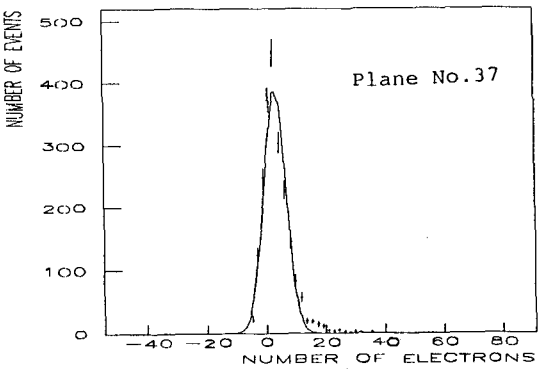

Fig. VI-6(f)

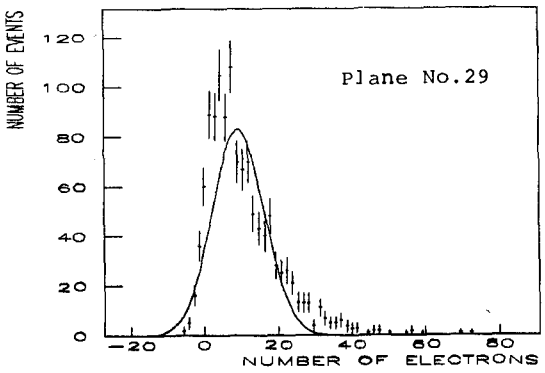

Fig. VI-5(e)

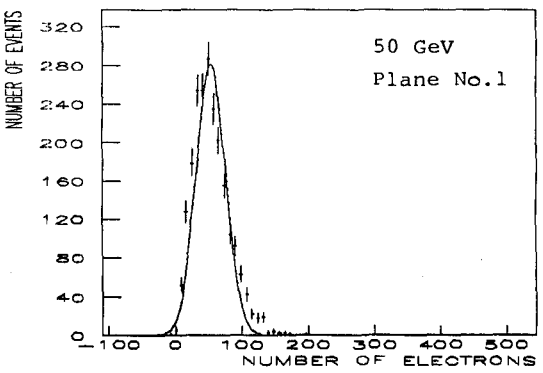

Fig. VI-6(a)

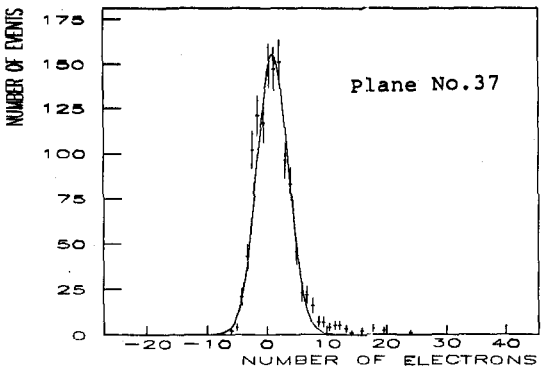

Fig. VI-5(f)

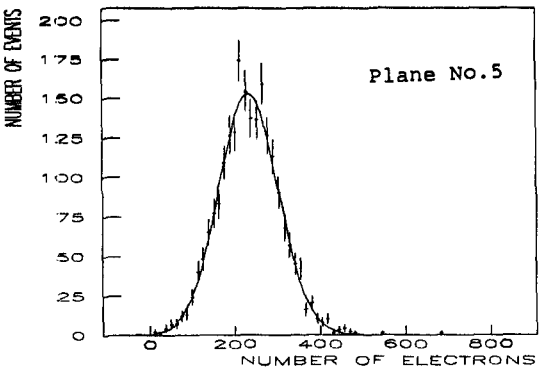

Fig. VI-6(b)

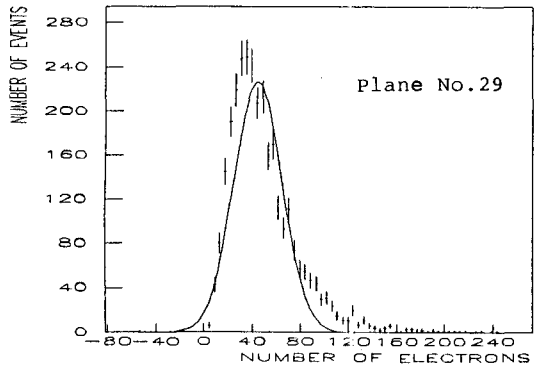

Fig. VI-7(e)

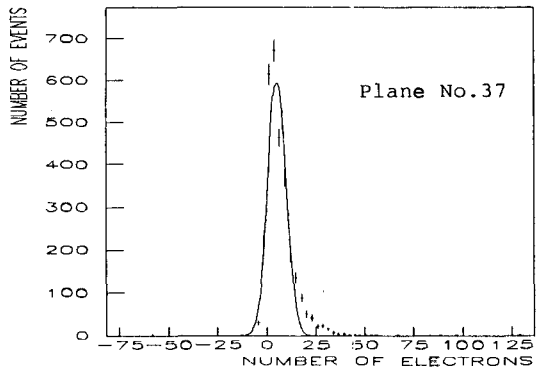

Fig. VI-7(f)

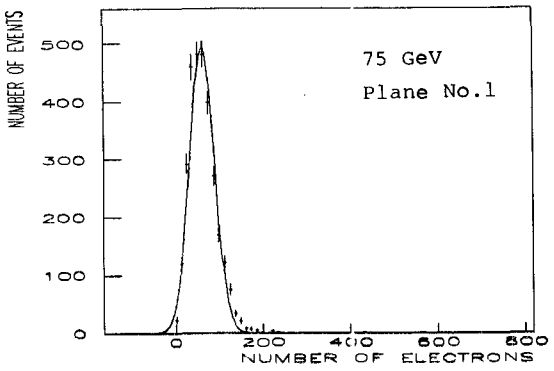

Fig. VI-7(a)

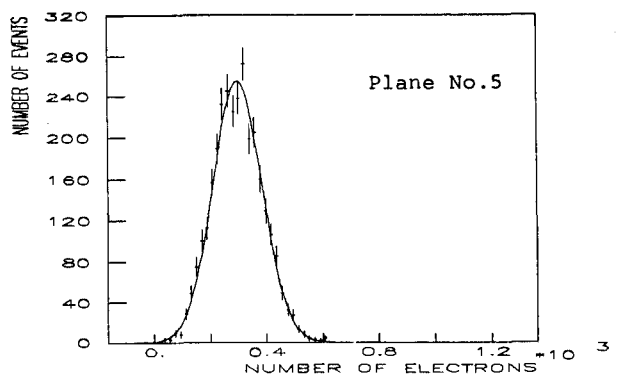

Fig. VI-7(b)

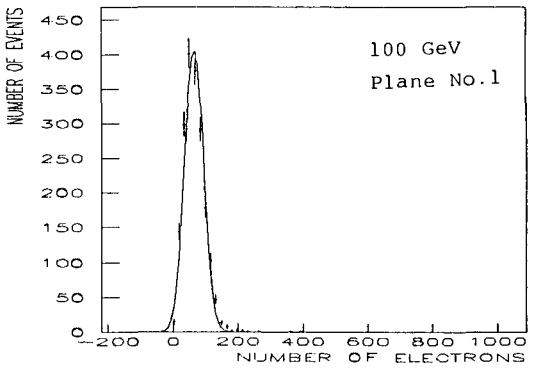

Fig. VI-8(a)

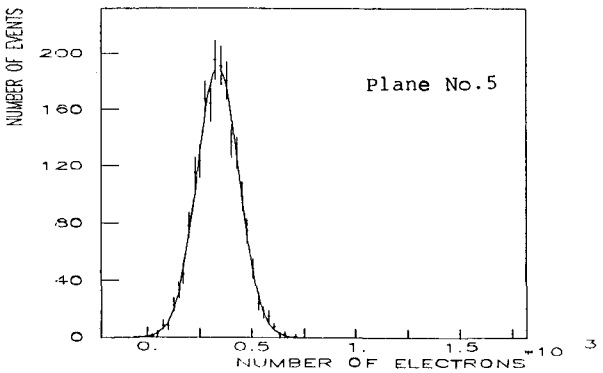

Fig. VI-8(b)

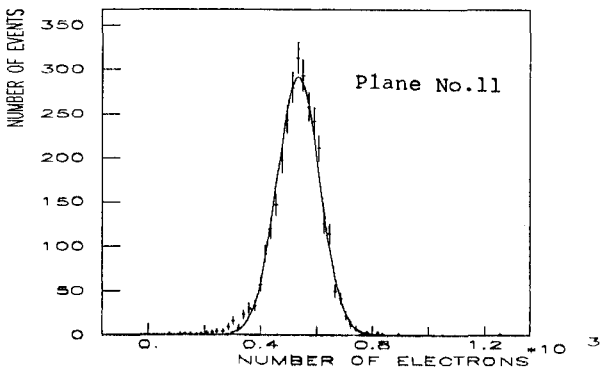

Fig. VI-7(c)

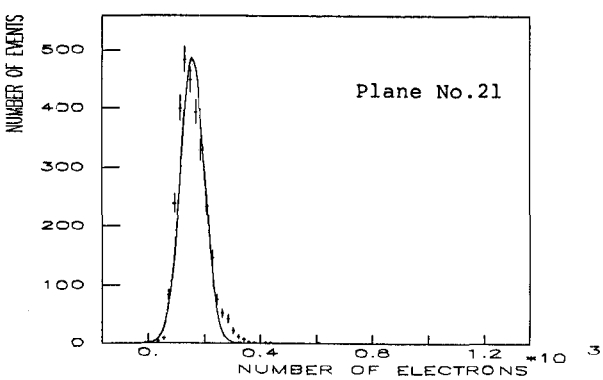

Fig. VI-7(d)

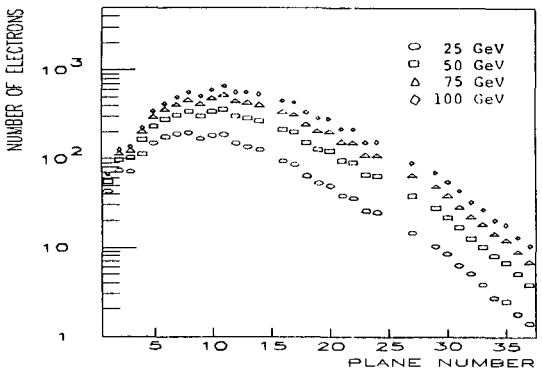

Fig. VI-9

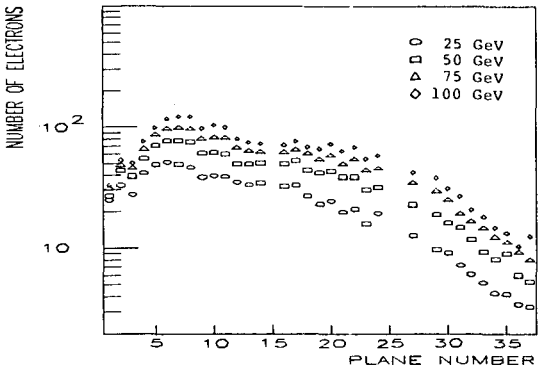

Fig. VI-10

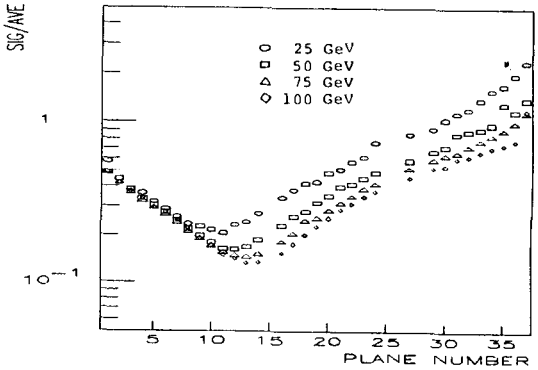

Fig. VI-11

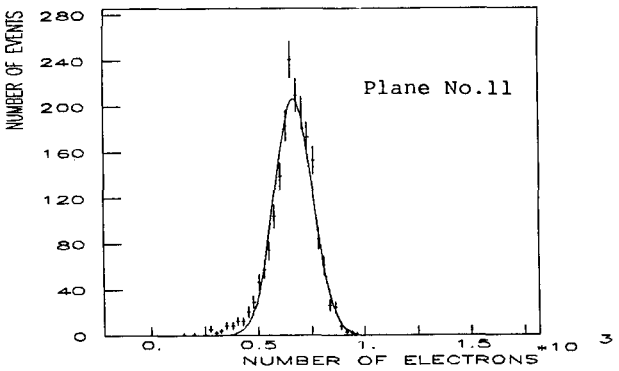

Fig. VI-8(c)

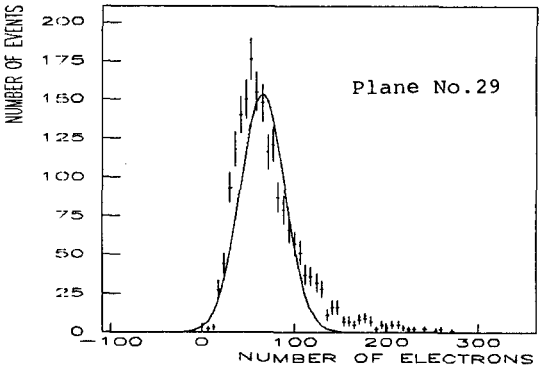

Fig. VI-8(e)

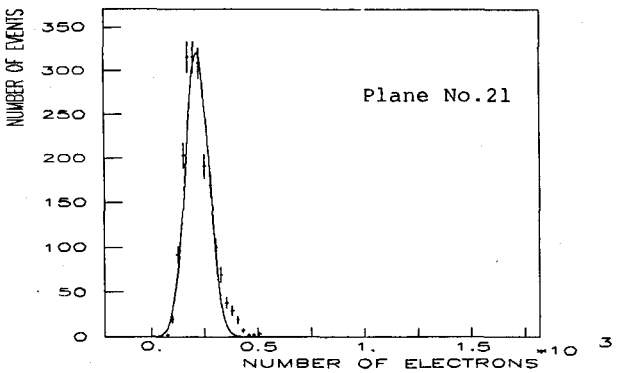

Fig. VI-8(d)

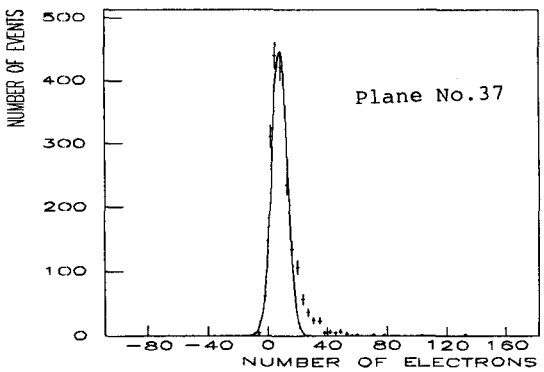

Fig. VI-8(f)

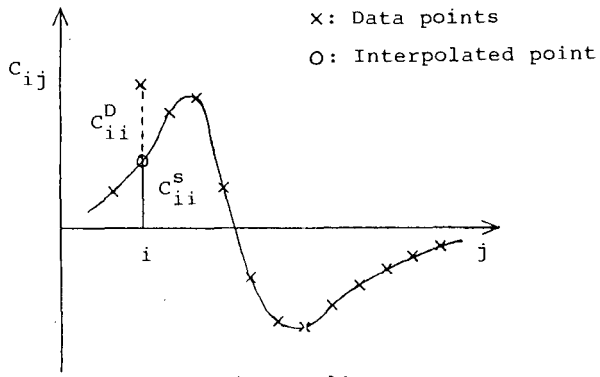

Fig. VI-19

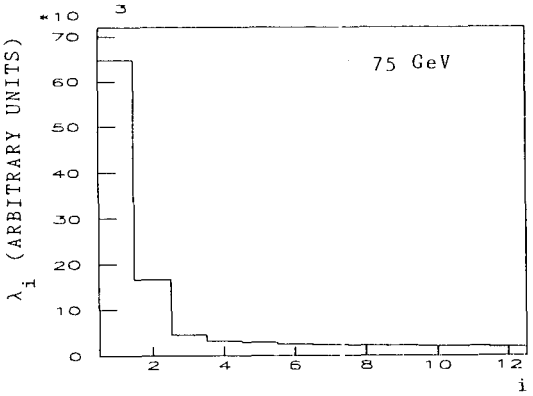

Fig. VI-20

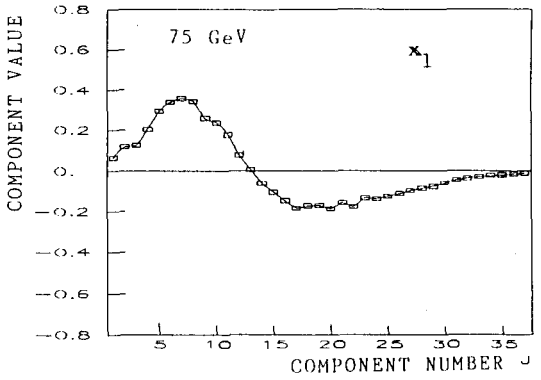

Fig. VI-21(a)

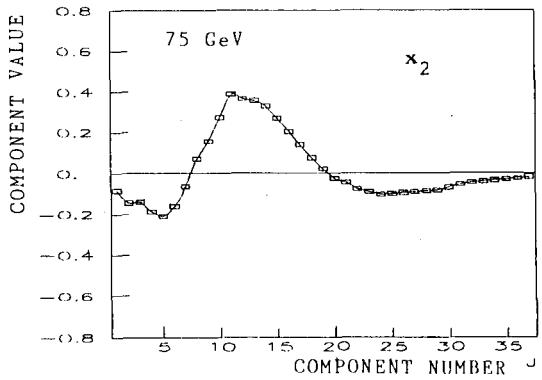

Fig. VI-21(b)

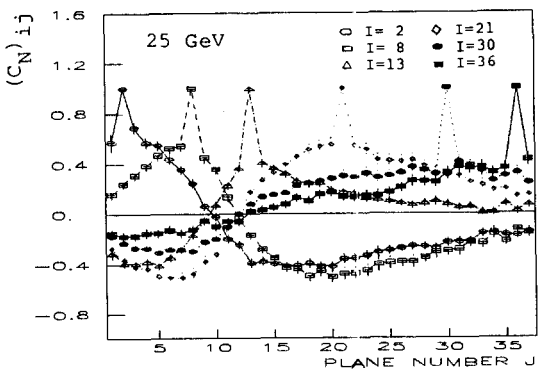

Fig. VI-18(a)

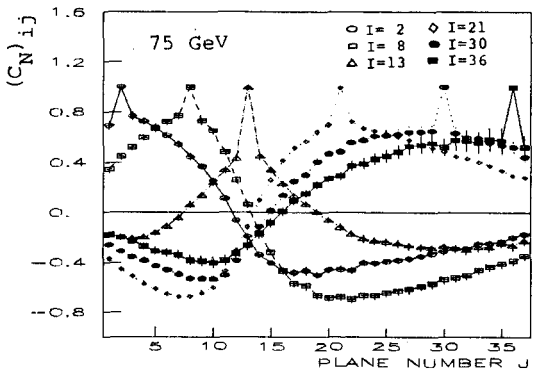

Fig. VI-18(c)

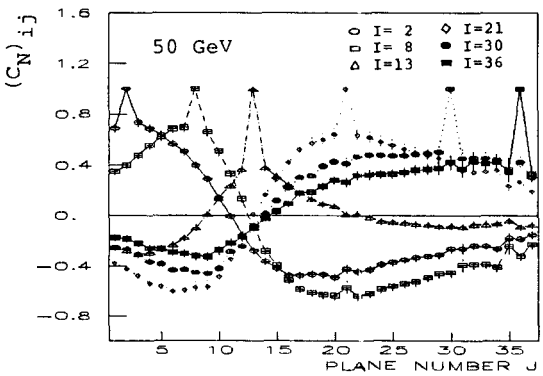

Fig. VI-18(b)

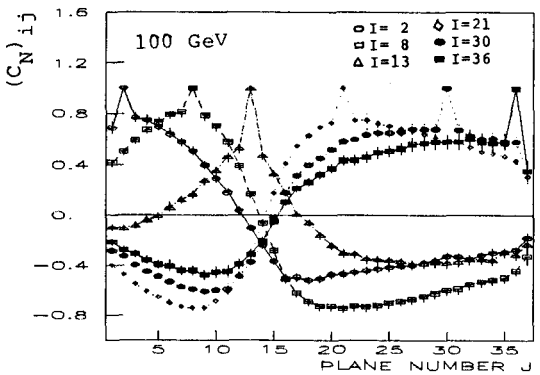

Fig. VI-18(d)

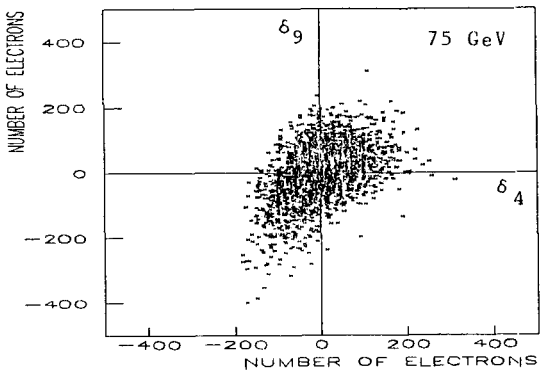

Fig. VI-22(a)

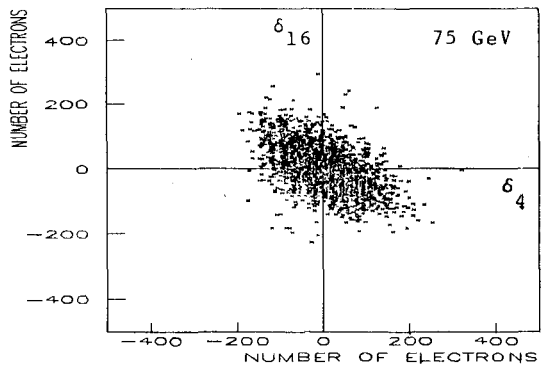

Fig. VI-22(b)

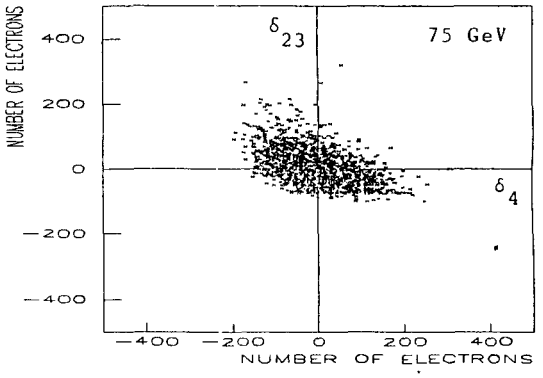

Fig. VI-22(c)

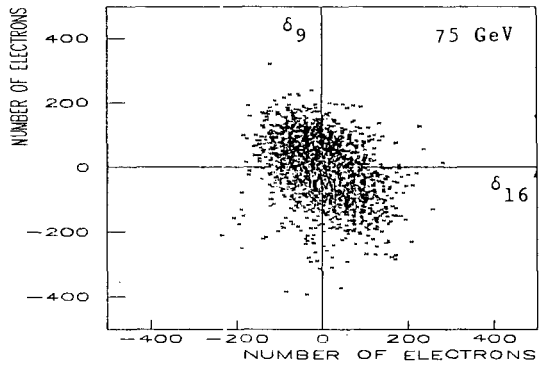

Fig. VI-22(d)

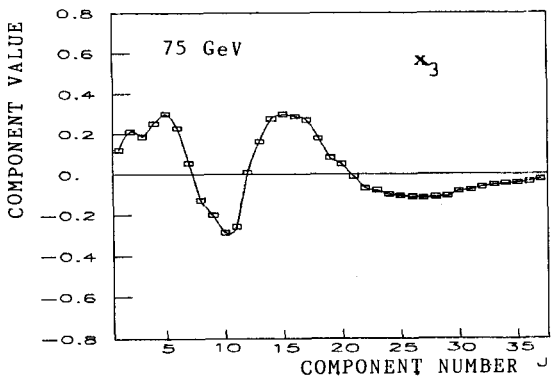

Fig. VI-21(c)

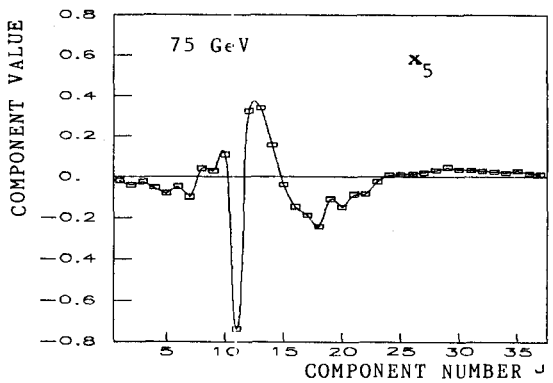

Fig. VI-21(e)

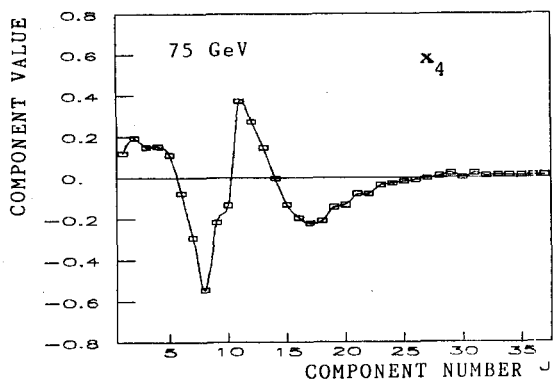

Fig. VI-21(d)

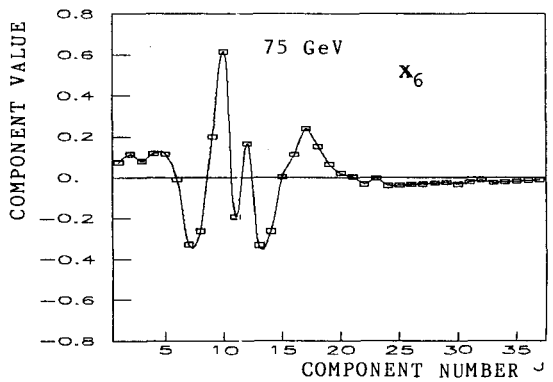

Fig. VI-21(f)

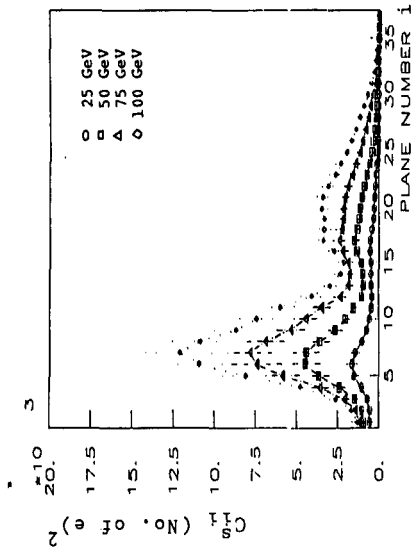

Fig. VI-24

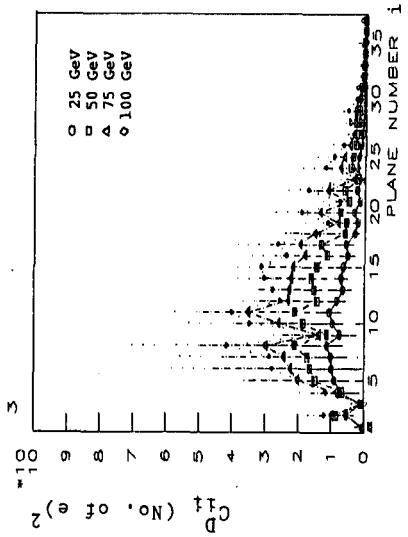

Fig. VI-25

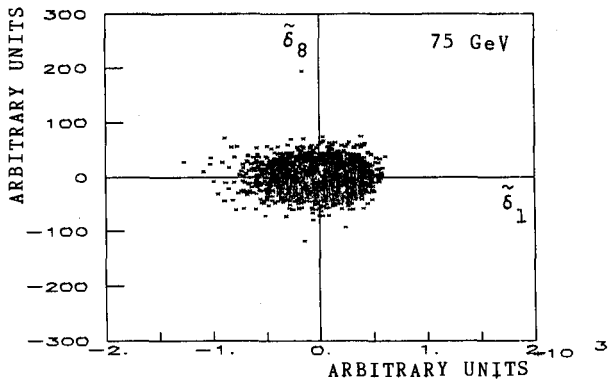

Fig. VI-23(a)

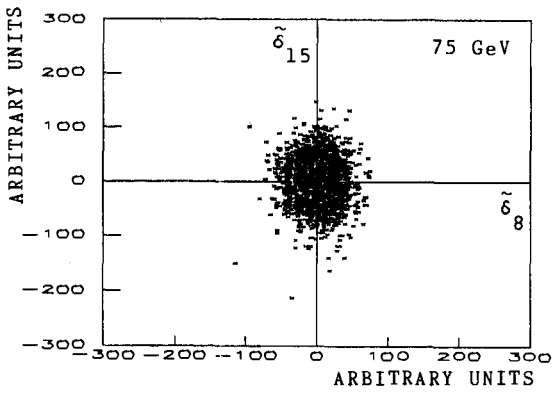

Fig. VI-23(c)

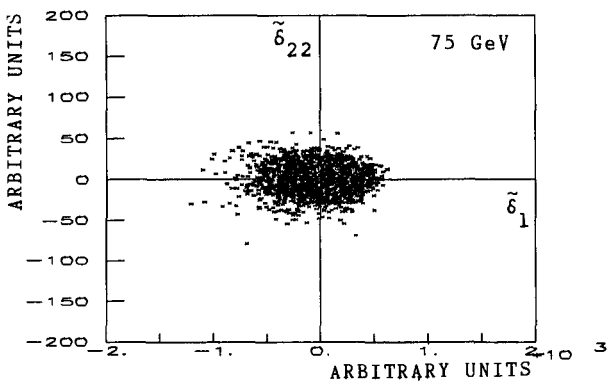

Fig. VI-23(b)

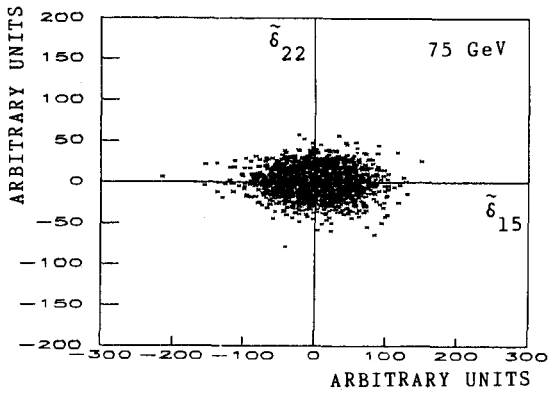

Fig. VI-23(d)

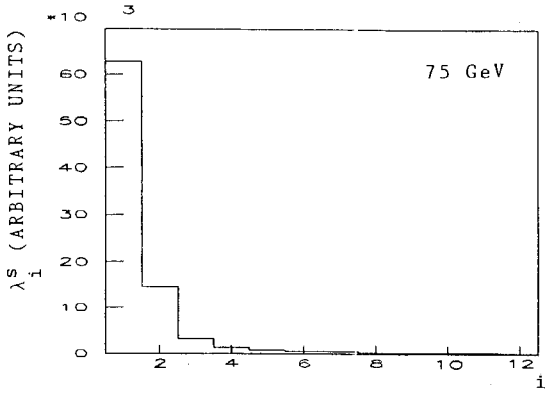

Fig. VI-27

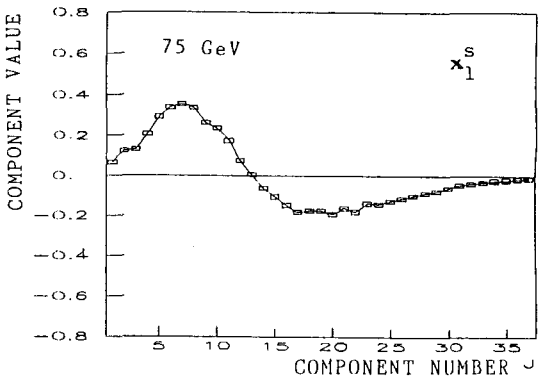

Fig. VI-28(a)

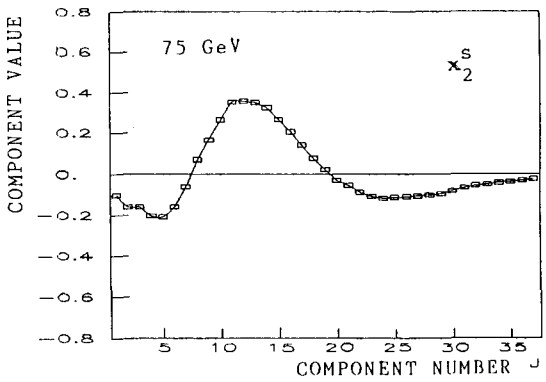

Fig. VI-28(b)

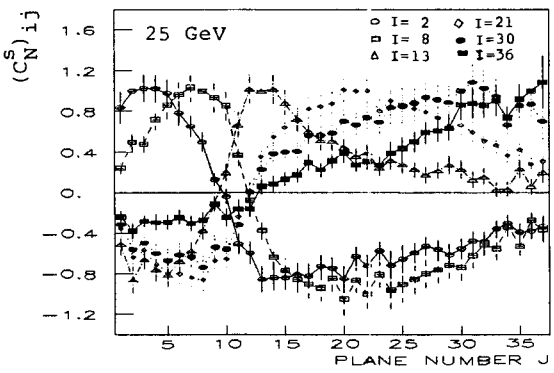

Fig. VI-26(a)

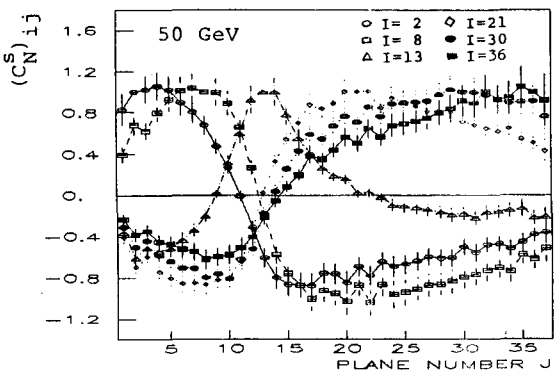

Fig. VI-26(b)

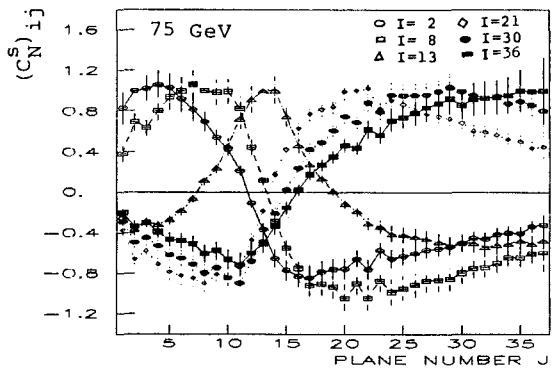

Fig. VI-26(c)

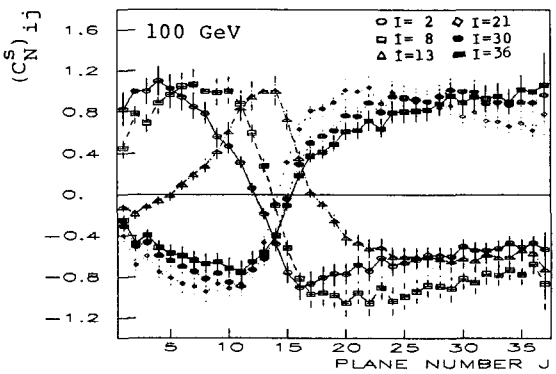

Fig. VI-26(d)

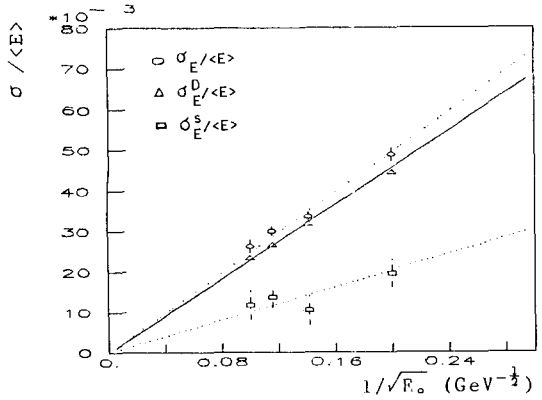

Fig. VI-29

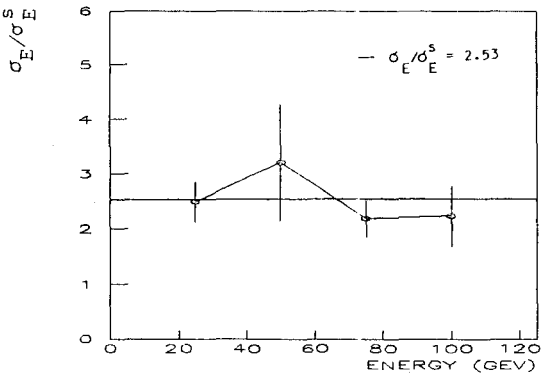

Fig. VI-30

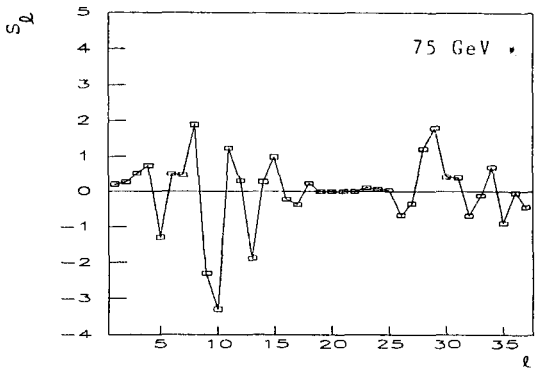

Fig. VI-31

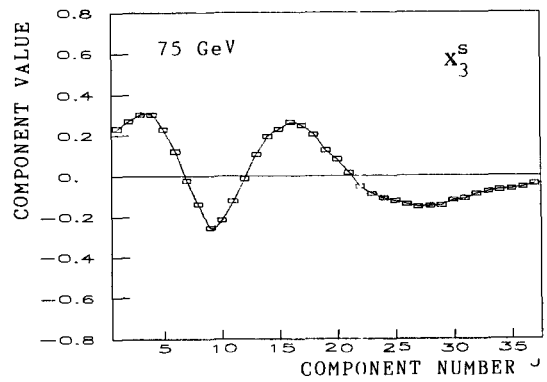

Fig. VI-28(c)

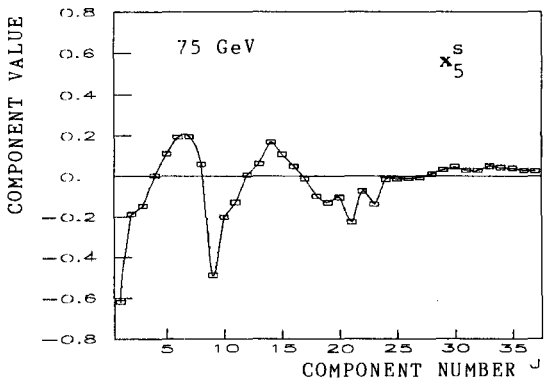

Fig. VI-28(e)

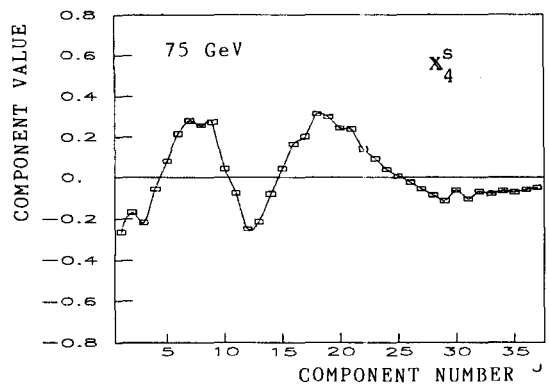

Fig. VI-28(d)

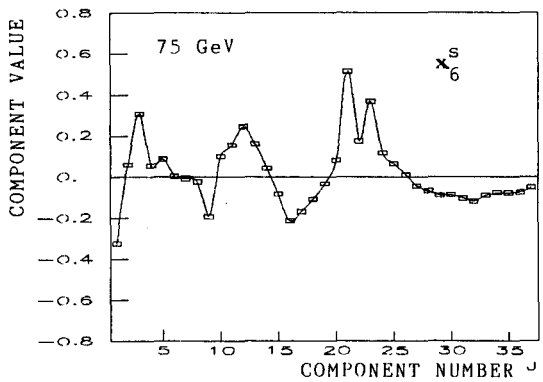

Fig. VI-28(f)

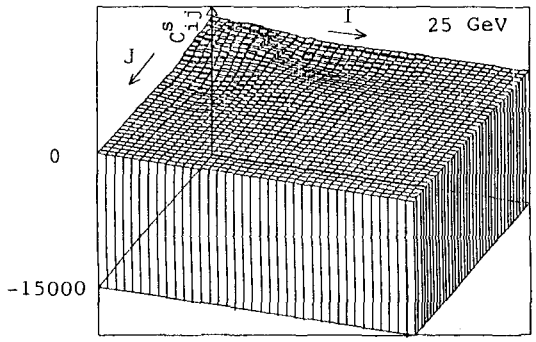

Fig. VI-33(a)

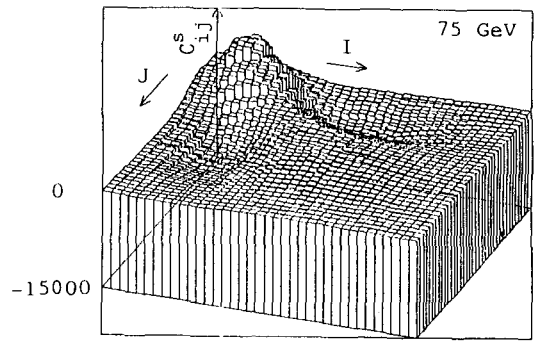

Fig. VI-33(c)

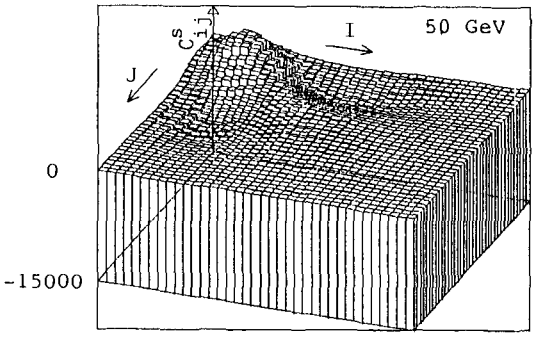

Fig. VI-33(b)

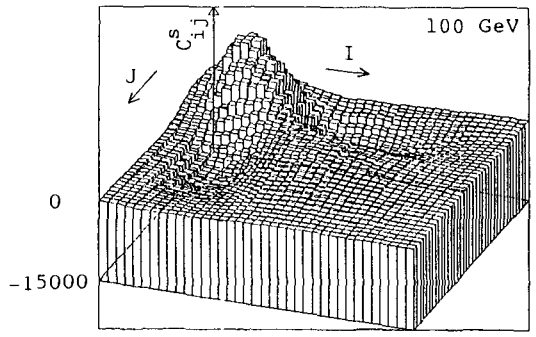

Fig. VI-33(d)

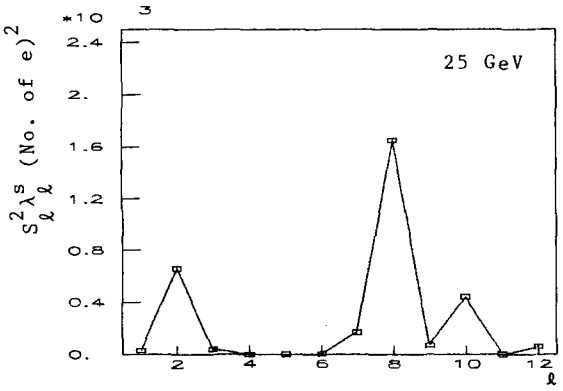

Fig. VI-32(a)

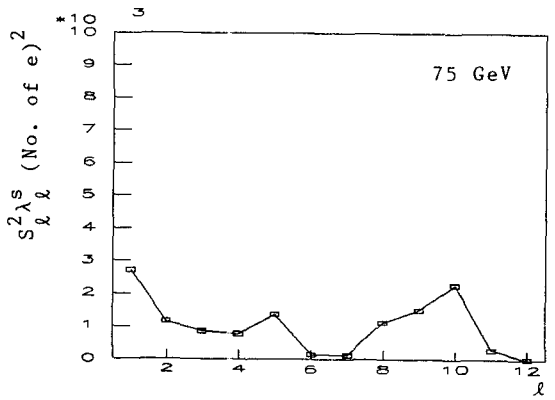

Fig. VI-32(c)

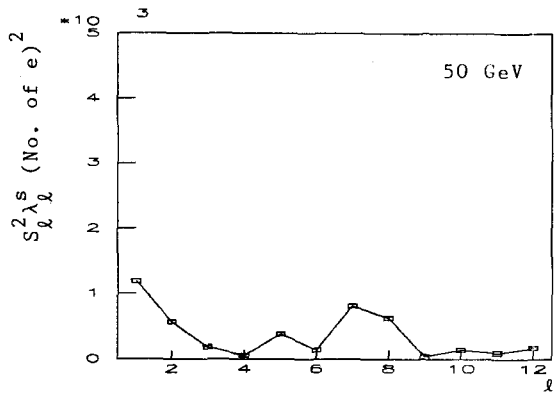

Fig. VI-32(b)

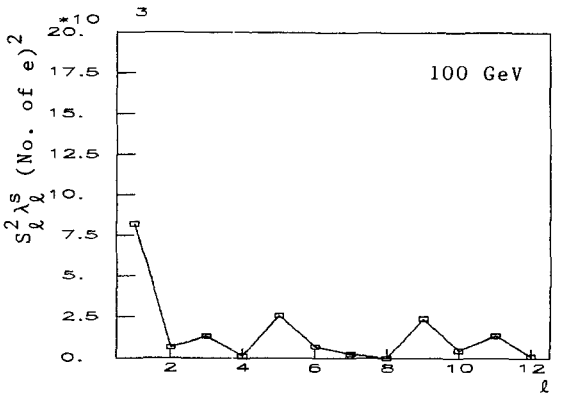

Fig. VI-32(d)

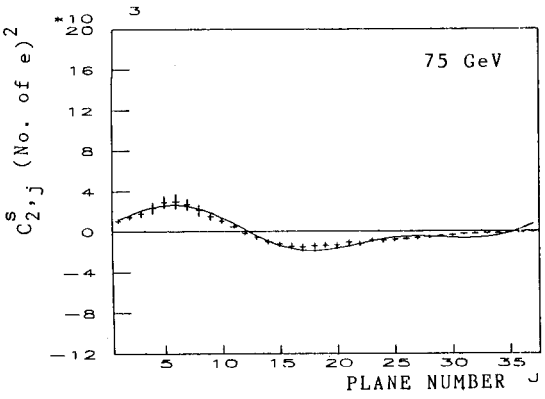

Fig. VI-35(a)

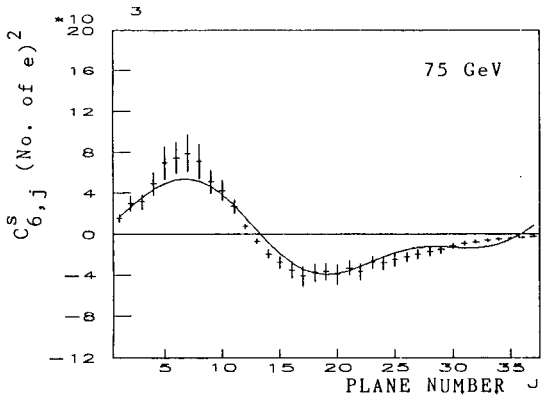

Fig. VI-35(b)

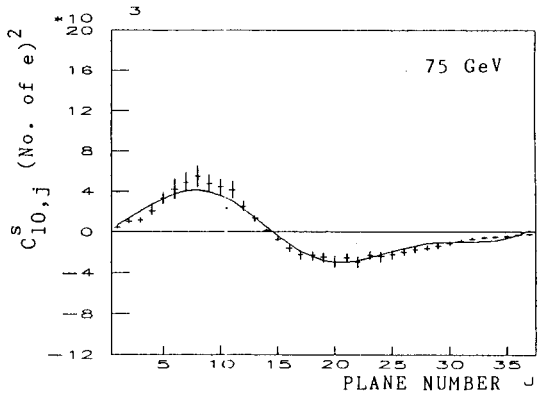

Fig. VI-35(c)

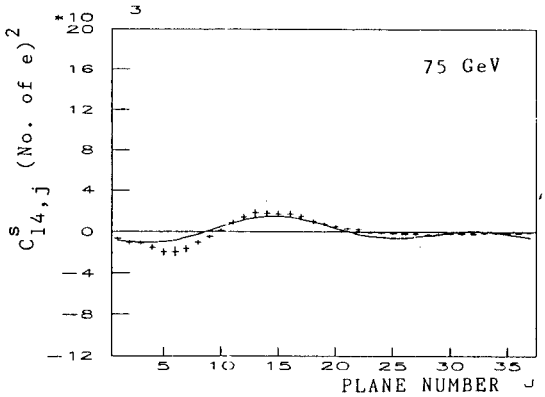

Fig. VI-35(d)

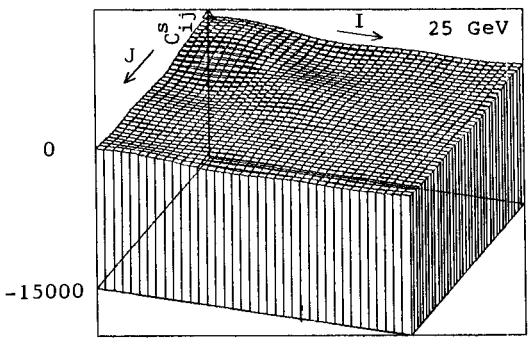

Fig. VI-34(a)

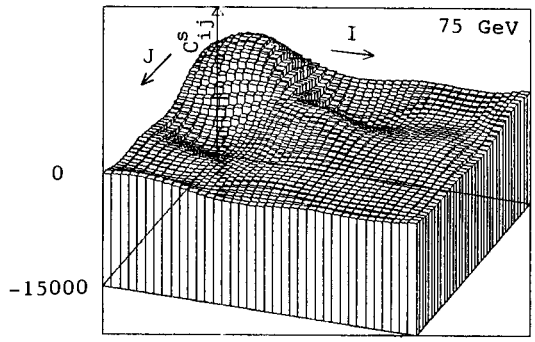

Fig. VI-34(c)

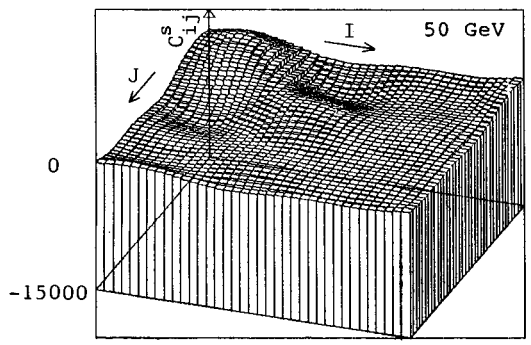

Fig. VI-34(b)

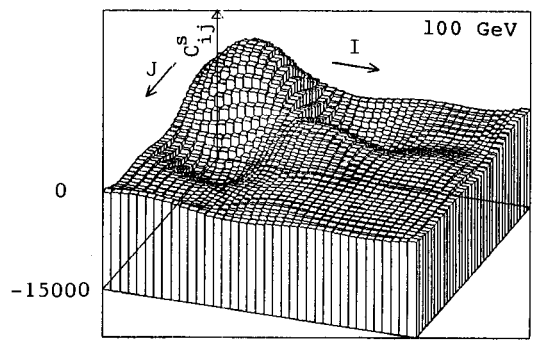

Fig. VI-34(d)

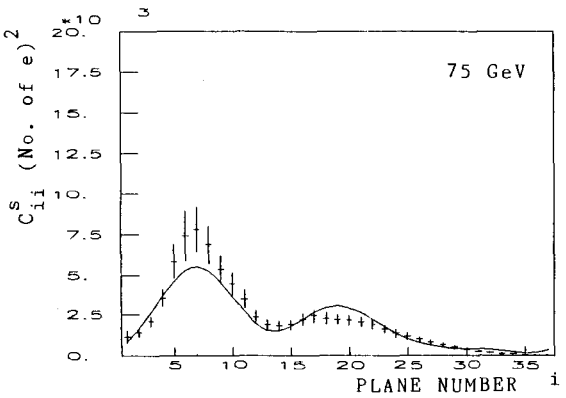

Fig. VI-36

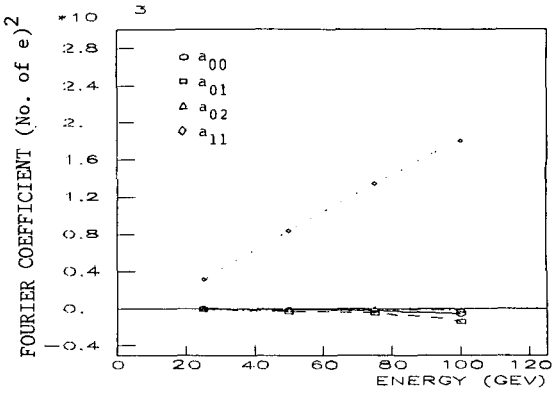

Fig. VI-37(a)

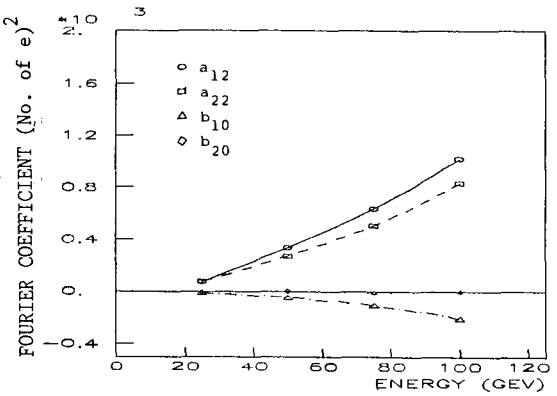

Fig. VI-37(b)

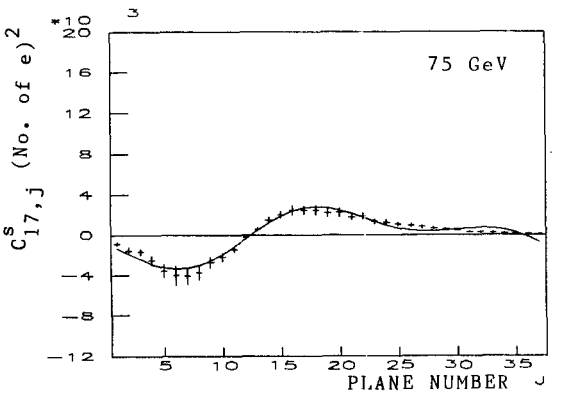

Fig. VI-35(e)

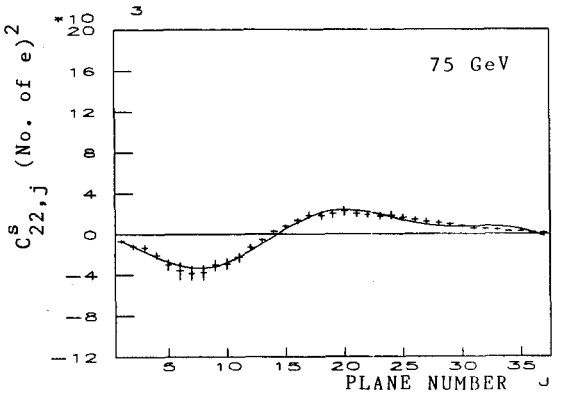

Fig. VI-35(f)

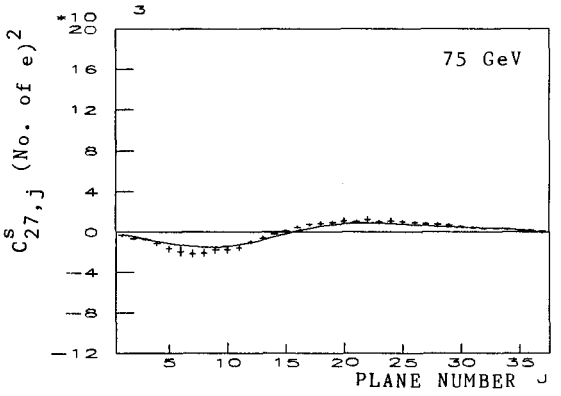

Fig. VI-35(g)

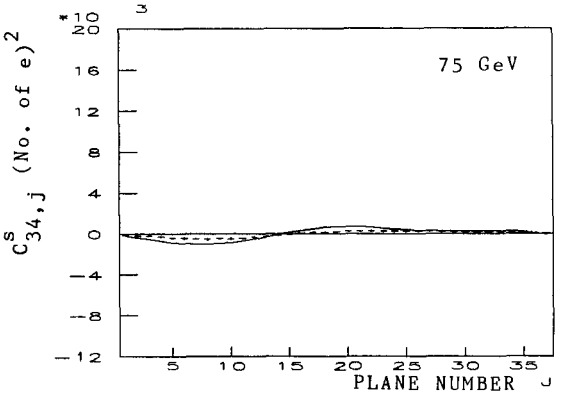

Fig. VI-35(h)

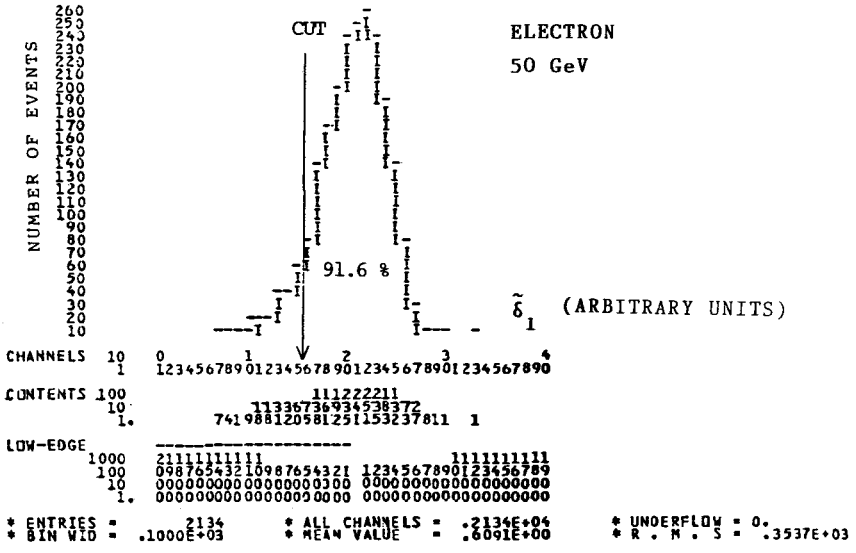

Fig. VI-38(a)

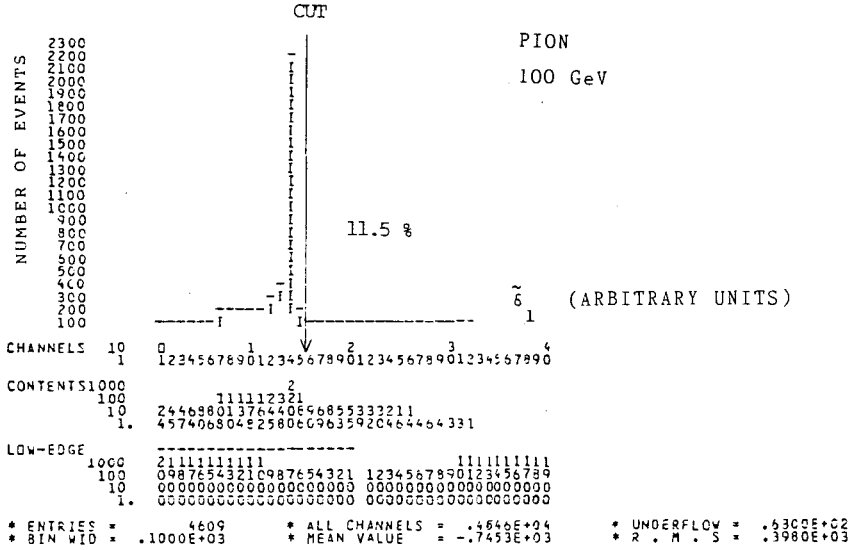

Fig. VI-38(b)

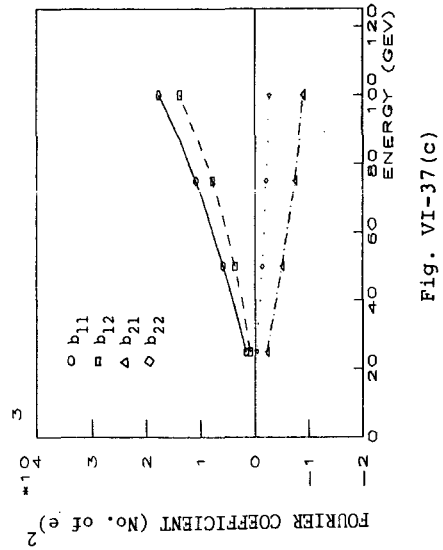

Fig. VI-37(c)

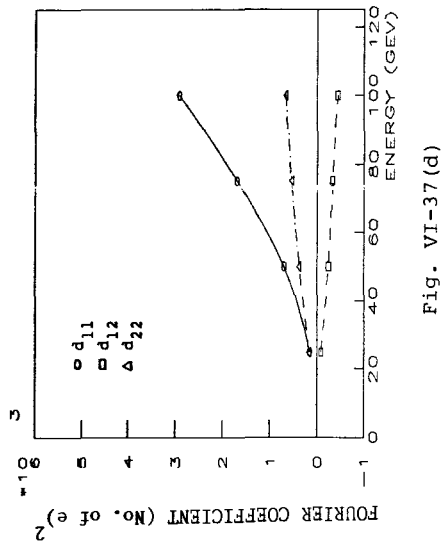

Fig. VI-37(d)

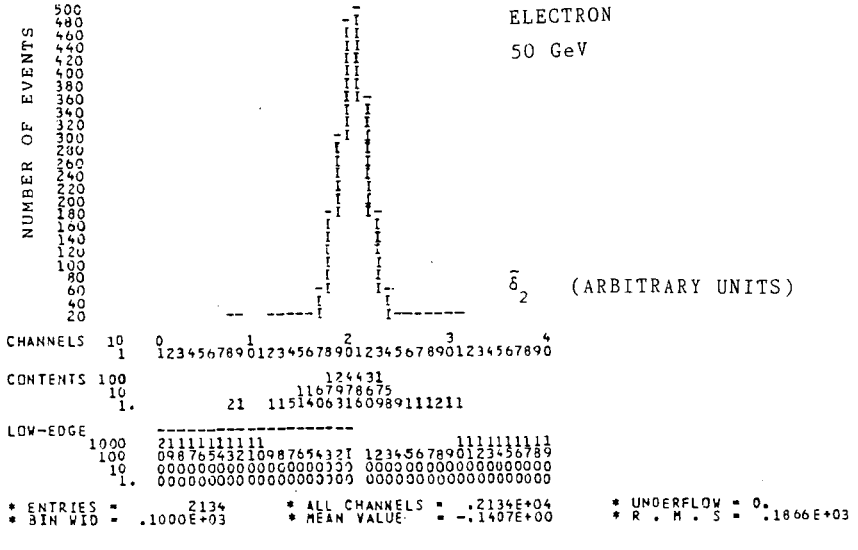

Fig. VI-39(a)

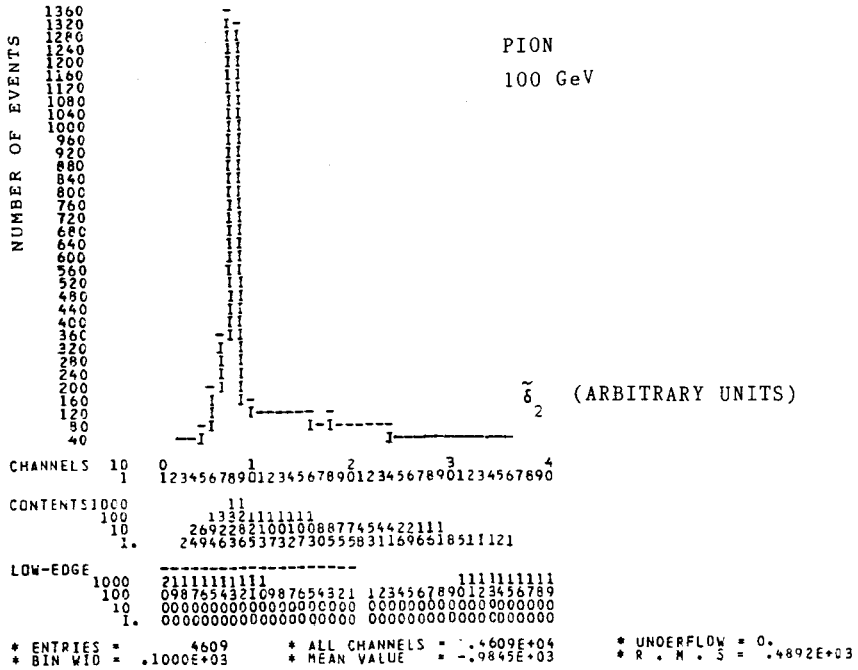

Fig. VI-39(b)

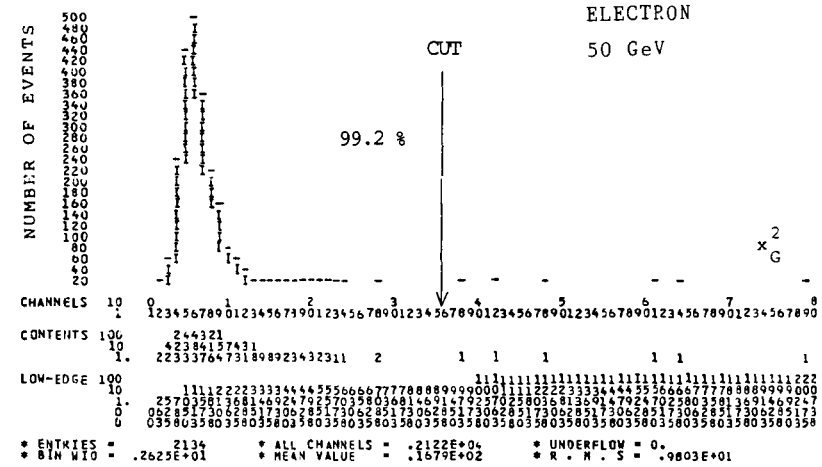

Fig. VI-40(a)

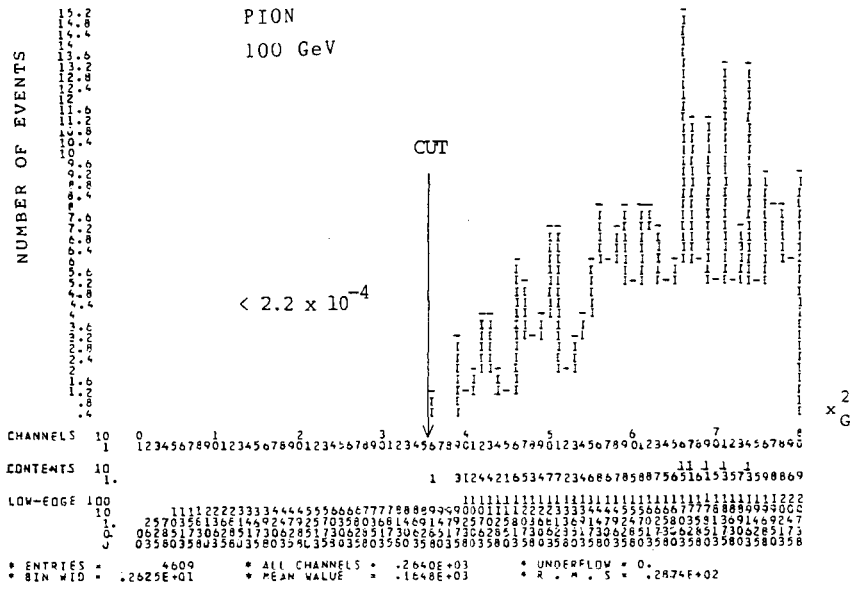

Fig. VI-40(b)

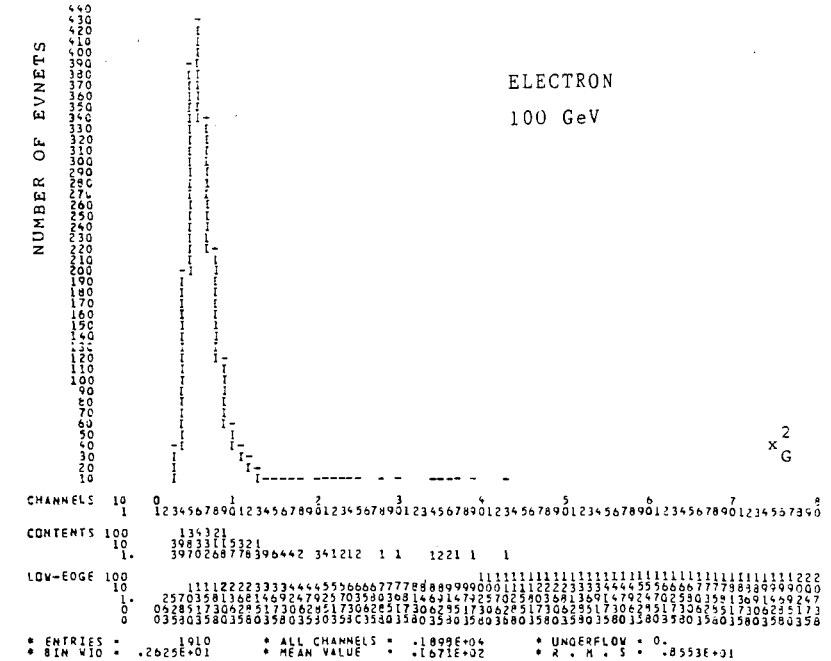

Fig. VI-41(a)

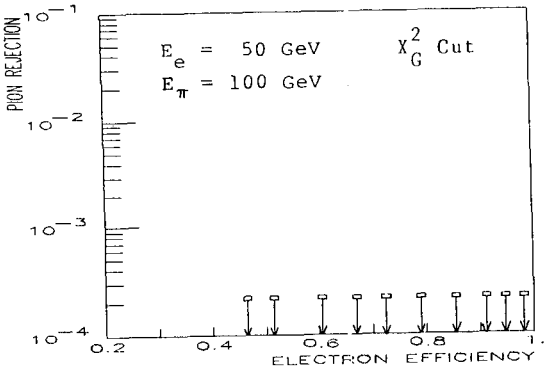

Fig. VI-42(c)

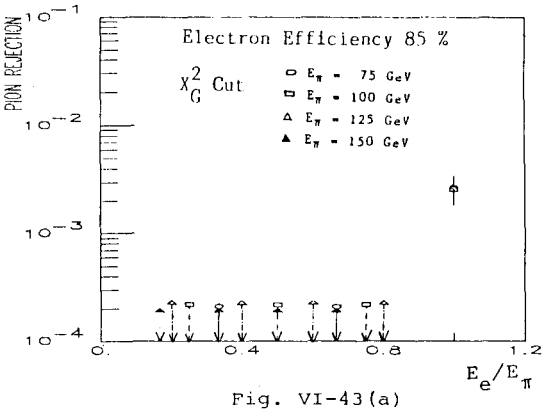

Fig. VI-43(a)

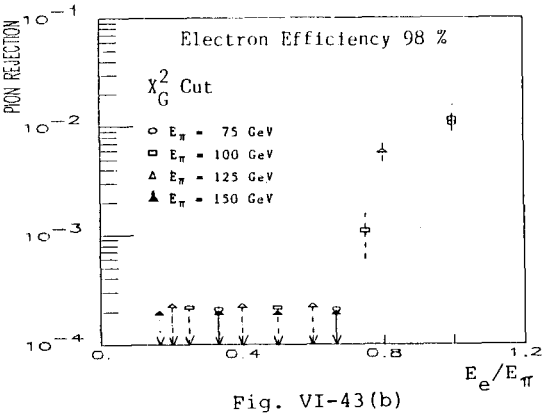

Fig. VI-43(b)

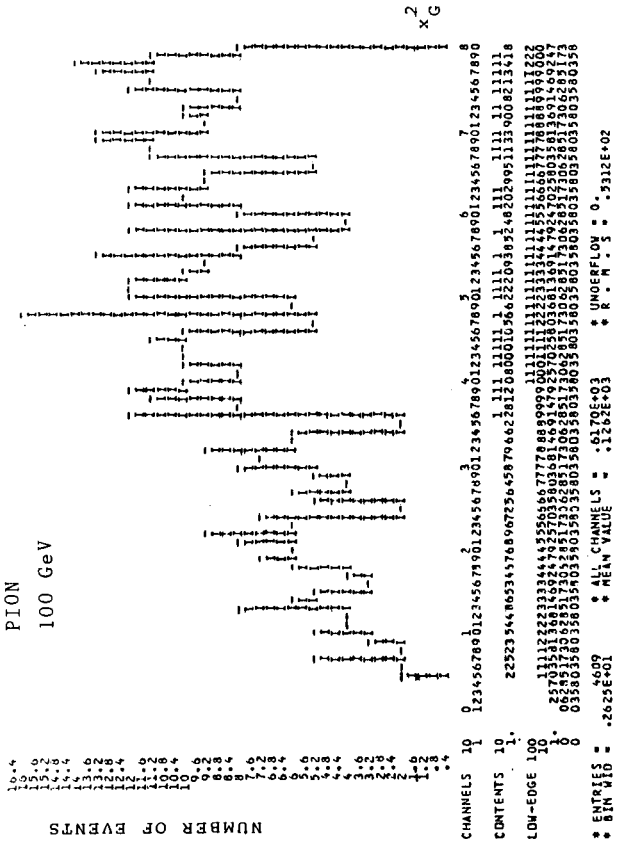

Fig. VI-41(b)

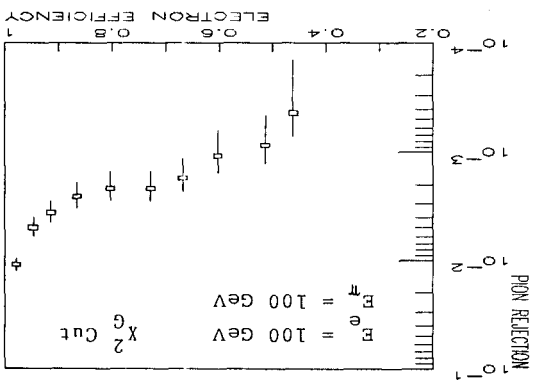

Fig. VI-42(b)

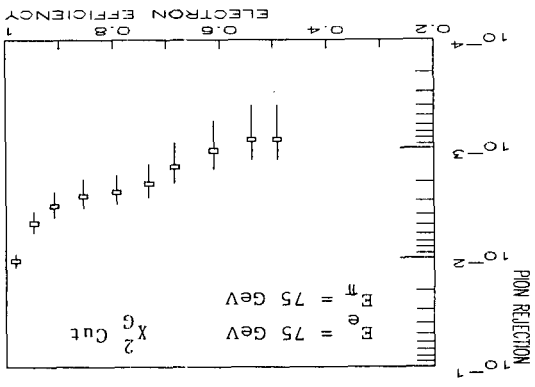

Fig. VI-42(a)

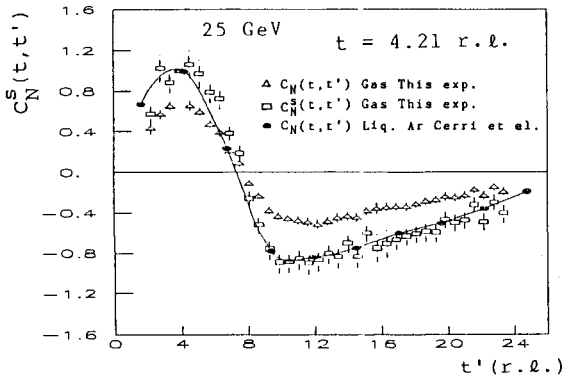

Fig. VII-2(a)

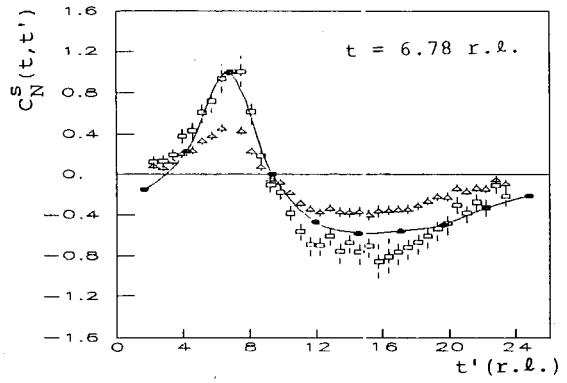

Fig. VII-2(b)

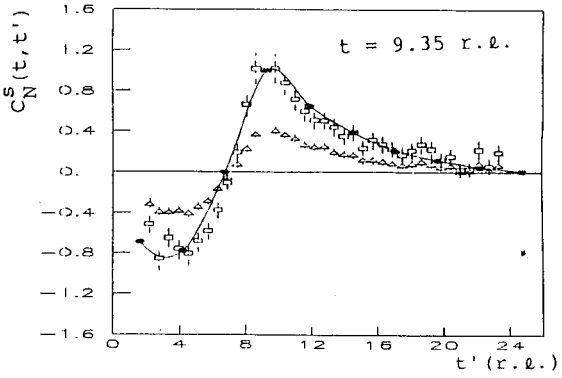

Fig. VII-2(c)

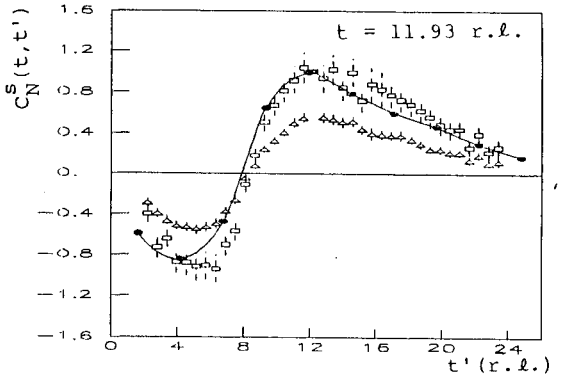

Fig. VII-2(d)

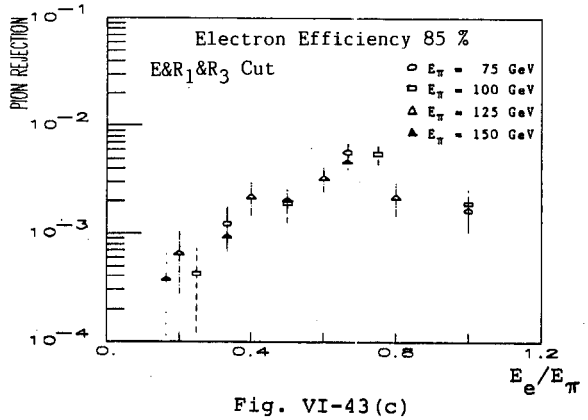

Fig. VI-43(c)

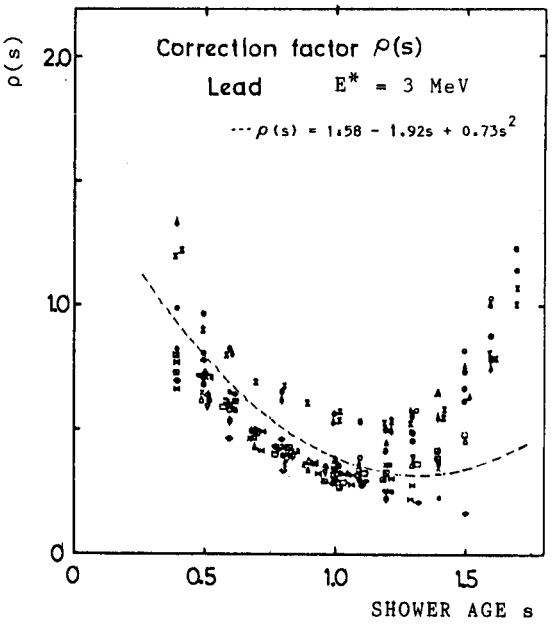

Fig. VII-1

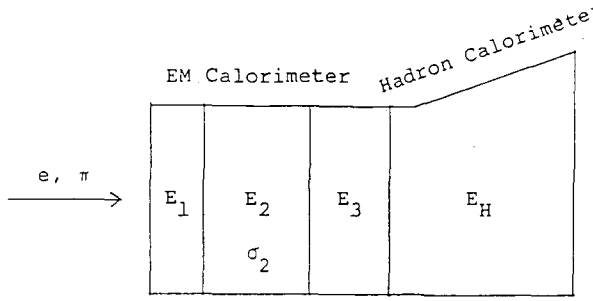

Fig. A-1

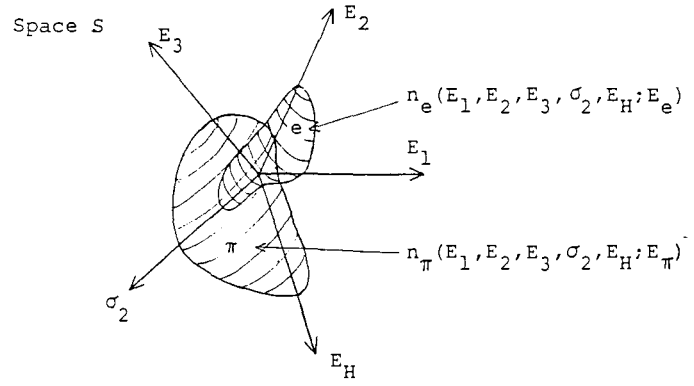

Fig. A-2

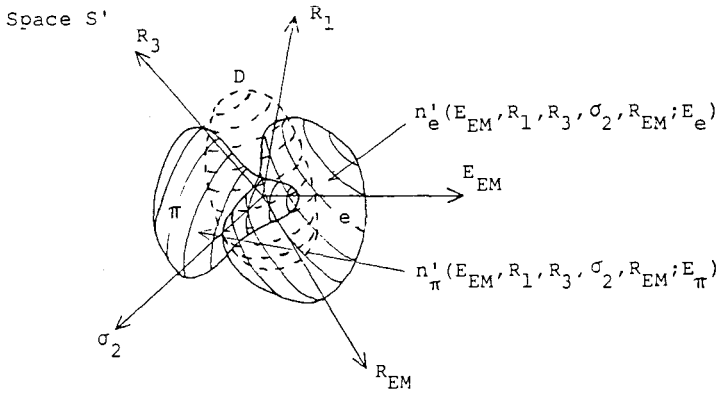

Fig. A-3

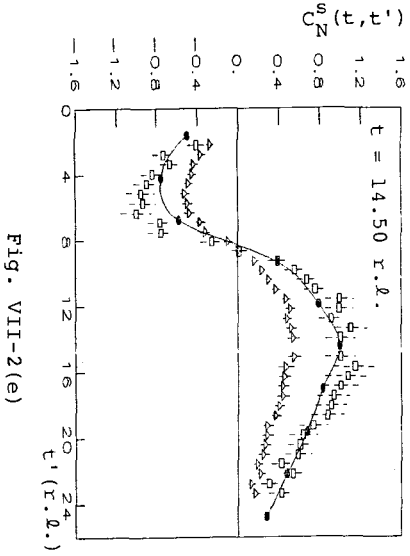

Fig. VII-2(e)

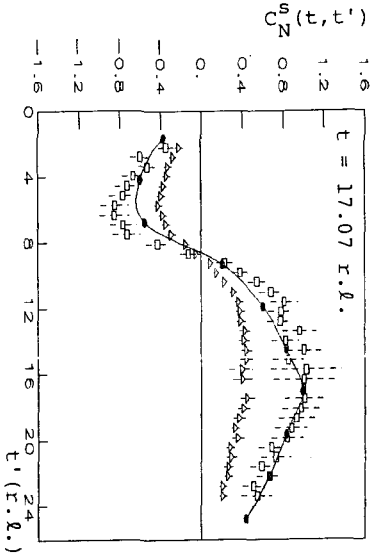

Fig. VII-2(f)

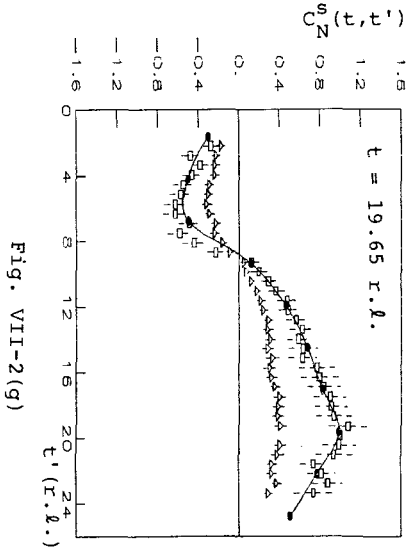

Fig. VII-2(g)

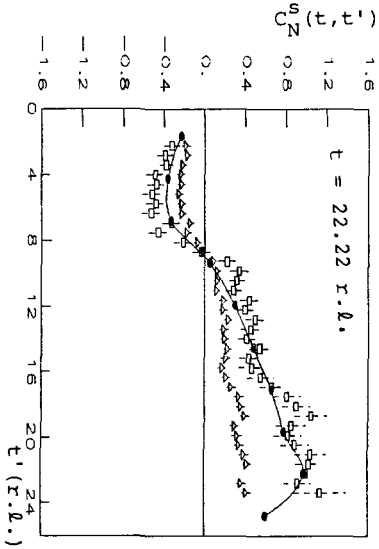

Fig. VII-2(h)

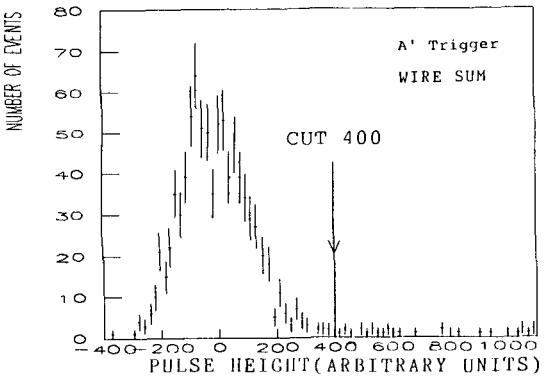

Fig. C-1(a)

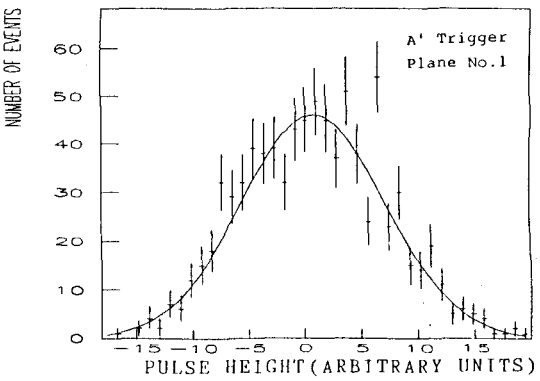

Fig. C-2(a)

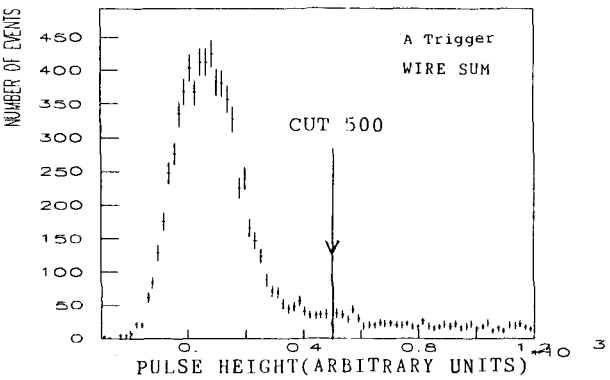

Fig. C-1(b)

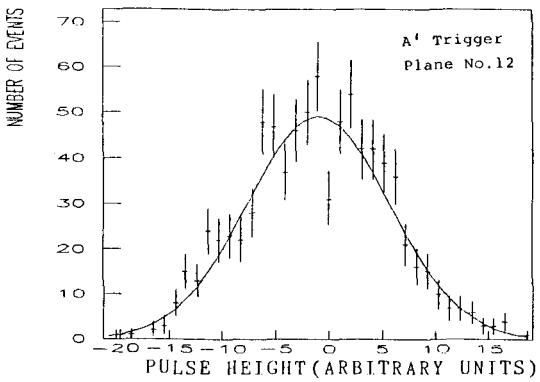

Fig. C-2(b)

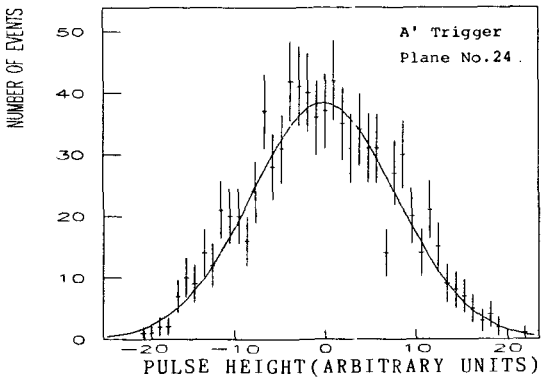

Fig. C-2(c)

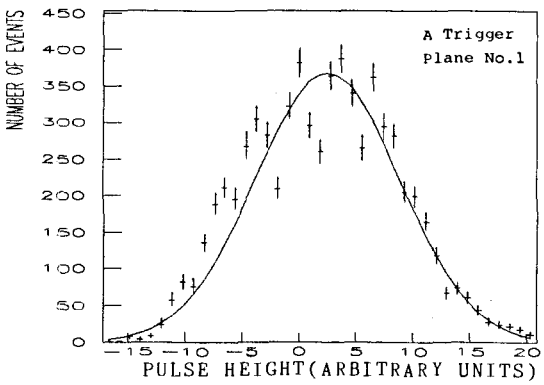

Fig. C-3(a)

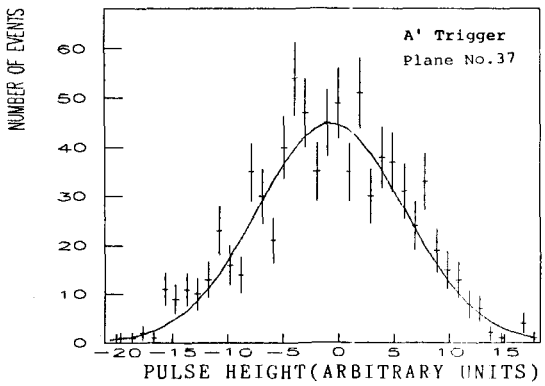

Fig. C-2(d)

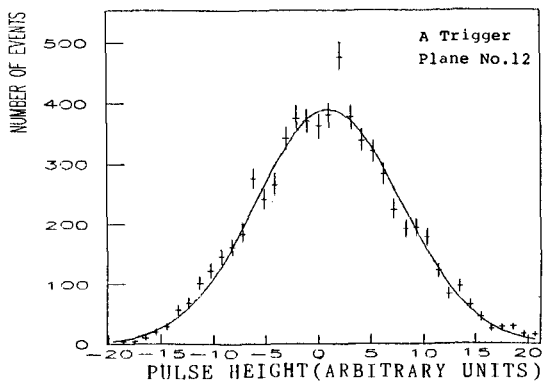

Fig. C-3(b)

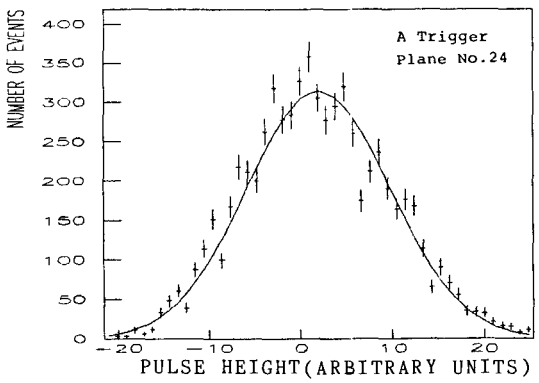

Fig. C-3(c)

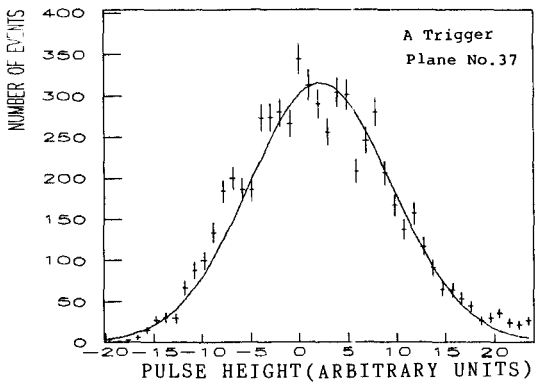

Fig. C-3(d)